Author:
Godden, Paul James

Title:
Turbulent buoyant fluid flows in confined regions

Turbulent Buoyant Fluid Flows In Confined Regions

Paul James Godden

A dissertation submitted to the University of Bristol in accordance with the requirements of the degree of Doctor of Philosophy in the Faculty of Science.

Department of Applied Mathematics, March 2000

(52,020 words)

Abstract

Experimental and theoretical investigations were carried out upon a fluid mechanical system. The system comprised two turbulent buoyant fluid flows propagating in a confined region. These flows originated via sources which input fluid of an initially contrasting density to the original ambient fluid. The novel feature of the fluid sources was the fact that they possessed an associated flux of mass. This was found to have significant effects upon the behaviour of the system. The physics of these effects had not been previously investigated for a dual-plume filling-box system.

The fundamental system was studied in the steady-state regime for which the overall properties of the system had converged to equilibrium. A number of variations upon this basic configuration were modelled theoretically. The resulting expressions were solved numerically to determine certain global parameters. A theoretical analysis was used to explain the physics of system. The theory was shown to agree with the numerical predictions. Applications and novel extensions of the fundamental model were studied and discussed. The transient time regime of the canonical system was also investigated both experimentally and numerically.

Acknowledgements

Many thanks to everyone who had to put up with me during the final stages of this work. In particular, great thanks go to Dr's. Richard Porter, Andrew Hogg, Darren Mason, Michael Patterson and Charlie Bird for a lot of support and essential advice. I would like to thank, for both academic support and advice, Dr Sean Collins and Professor Howell Peregrine. A special thanks to Emeritus Professor Philip Drazin, for long-standing support, advice and some of the best anecdotes I've ever heard. Phillip is a true scholar whose support I have been very grateful for. Also, to Professor Howell Peregrine, much gratitude for generous support and encouragement as my internal examiner. Finally, a sincere thanks to my Ph.D. supervisor, Professor A.W. Woods. Without his vital guidance, I would have relinquished this project before it had even begun.

Finally, I wish to extend my gratitude to the University of Bristol for funding this work via a University Scholarship.

Dedication

To my mother, without whom I would have given all this up long ago. This is for you, with all my love.

Author's Declaration

The work described in this dissertation was carried out in the School of Mathematics, University of Bristol and has not been submitted for any other degree or diploma of any examining body. All the material described herein is the original work of the author, except where otherwise acknowledged.

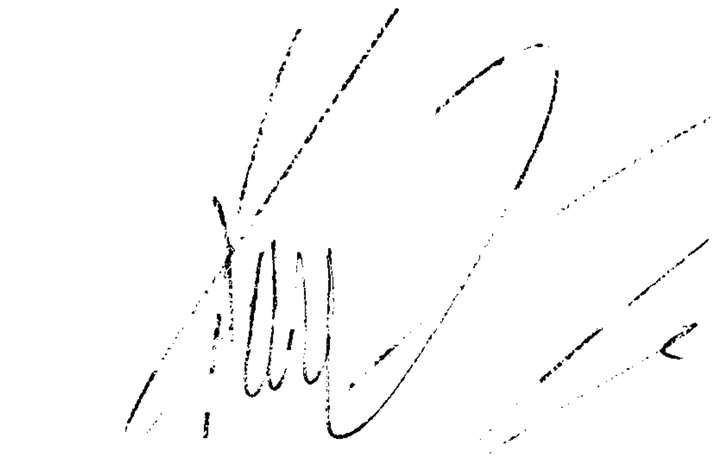

Paul James Godden

"Speak the speech, I pray you, as I pronounc'd it to you, trippingly on the tongue, but if you mouth it, as many of our players do, I had as live the town-crier spoke my lines. Nor do not saw the air too much with your hand, thus, but use all gently, for in the very torrent, tempest, and, as I may say, whirlwind of your passion, you must acquire and beget a temperance that may give it smoothness."

– William Shakespeare, *Hamlet*

Contents

List of Figures

Part I

Introduction

Chapter 1

Introduction

" Rivers are highways that move on,

and bear us where we wish to go. "

– Blaise Pascal.

1.1 Overview of the Thesis

Ventilation of enclosed regions is an important topic in many areas of engineering and industry. For example, ensuring adequate ventilation within a building is vital to maintain a comfortable environment for its inhabitants. This may be achieved by in-flows of relatively hot or cold air into the region where ventilation is desired. The air typically enters or leaves the building via openings whose physical dimensions are small compared to the dimensions of the building, such as doors and windows. Hence, this leads to air flows in the building which cause localised convection flows to develop. Further, the air which flows into the building typically has a different density

to the ambient fluid inside the enclosure. Consequently, the flows of air inside the building are turbulent in nature. Therefore, even in relatively simple situations, the ventilation flows can become extremely complex. We may model these flows successfully by using the theory of turbulent buoyant plumes. This theory is reviewed in section 1.2.

In this thesis, we examine a configuration consisting of two such fully-turbulent flows. This results in a complex, non-linear system. We investigate this system in detail, analysing how variations in the configuration of the fluid sources and the outflow vent may lead to the emergence of new physics. In turn, this leads to answers to fundamental questions, such as the effectiveness of using different types of hot air sources to warm a room. For example, we compare the relative efficiencies of a radiator and a point-like orifice.

During the course of the work, we assume that all of the fluid flows are incompressible. This is a valid assumption given the nature of the ventilation flows that we are studying. Further, it allows the new results to be applied to situations in geophysical and environmental fluid mechanics, where turbulent flows in confined regions often occur.

We begin by reviewing the literature relevant to the thesis. In the current work, the turbulent buoyant flows are modelled using plume theory. The flow of a plume in an unbounded environment was the first situation to be analysed, and we discuss this work first. We then consider the case for which the plume flows in a confined region. This situation is particularly relevant to the material in this thesis, since all the flows in the current work occur in a bounded domain. Next, we review the effect of initially stratified ambient fluid upon the overall dynamics of plume flows in confined regions. We continue by discussing fluid flows in buildings which are subject to natural

ventilation. In this type of system, the ventilation flows arise entirely due to buoyancy variations in the fluid: there is no air conditioning or other mechanical means to drive fluid into or out of the building. We then briefly describe some other applications of turbulent buoyant fluid flows in confined regions. These are concerned with geophysical situations. Finally, we briefly outline the contents of the rest of the thesis.

1.2 Turbulent Buoyant Convection In Unconfined Domains

In many situations of interest in geophysical, industrial and environmental fluid mechanics, fluid of constant density flows into a region containing ambient fluid of a contrasting density. We may define a Reynolds number for the intruding flow as

$$Re = \frac{uL}{\nu} \tag{1.1}$$

where u is a characteristic velocity of the intruding flow over a length scale L for a fluid of kinematic viscosity ν. When Re is sufficiently large, the flow is turbulent. A continuous release of fluid in this manner is referred to as a *turbulent plume.* There are numerous physical examples of such flows, and these include smoke from chimneys; volcanic eruption columns; hot air rising from a radiator; fluid flowing into a volcanic magma chamber; and industrial processes involving miscible fluids. It is of interest to note that although these flows are fully turbulent, careful observation reveals that they exhibit similar global features, the most prominent of which is the dominance of mixing in determining the overall dynamics of the flow. If there is no density contrast between the intruding fluid and the ambient, the flow is said to be a turbulent jet. Plumes may acquire jet-like characteristics

if their initial momentum flux is sufficiently large that momentum effects dominate over buoyancy in the initial stages of the flow. Such flows are sometimes referred to as buoyant jets or forced plumes.

An early analysis of turbulent plumes and jets assumed that the fluid motion occurred in a region of infinite extent (Morton et. al., 1956). The investigation concentrated upon the parameterisation of the turbulent mixing dynamics, which characterise both the local and global behaviour of the resulting flow. The proposition of Sir G.I. Taylor, which was investigated subsequently in great depth and over many different scales, is referred to as the entrainment hypothesis. This assumption is essentially a turbulent closure hypothesis, and leads to a mathematically tractable quantitative model of a turbulent buoyant plume. The fundamental basis for the entrainment hypothesis is the notion of averaged properties of the turbulent flow. This is considered over two regimes. Firstly, the model is time-averaged. In other words, the motion of the flow is considered for time scales much greater than the eddy turn-over time. Secondly, the model is spatially averaged over the effective cross-section of the turbulent plume. Following this approach, the entrainment hypothesis may be written as:

$$u_\epsilon = \epsilon u \tag{1.2}$$

where u_ϵ is a velocity representing the inflow of ambient fluid due to the action of turbulent eddies within the plume flow, ϵ is an empirical constant referred to as the entrainment coefficient, and u is the vertical plume velocity according to the time and spatial averages referred to above. Essentially, equation (1.2) expresses the fact that entrainment is due to turbulent eddies present in the plume. These eddies engulf and incorporate ambient fluid into the body of the turbulent flow. Hence, it may be assumed that the entrainment velocity u_ϵ scales with the vertical plume velocity. Consequently,

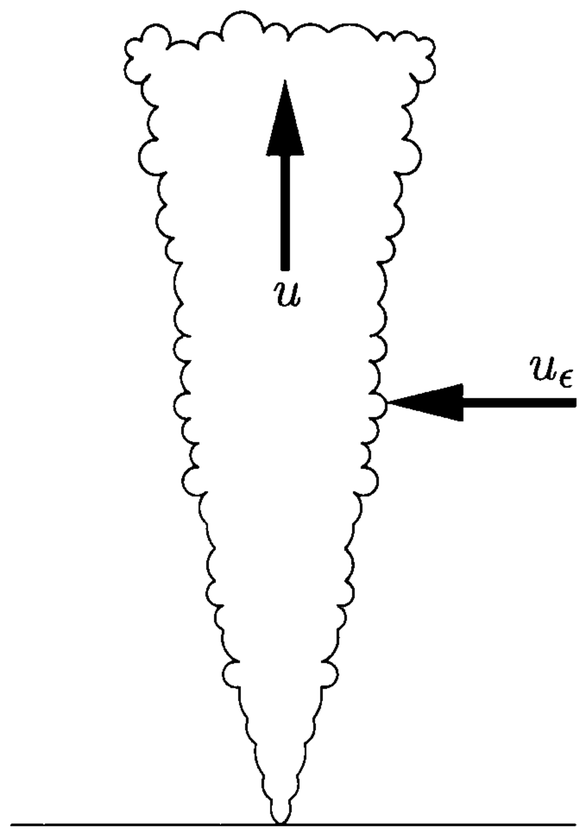

FIGURE 1.1: Depiction of the entrainment hypothesis for a self-similar plume propagating in a homogeneous environment of effectively infinite extent. The plume increases in both volume and density as a function of vertical distance from the source due to the entrainment of ambient fluid. Eventually, it reaches a vertical height for which its density is equal to the density of the ambient fluid. At this point, it will spread laterally. The assumption of similarity is valid up to this vertical distance.

the near-field time-averaged velocity of entrained fluid may be considered approximately horizontal. This simplification relates to the fact that the turbulent eddies which entrain the ambient fluid have an average vertical velocity. An important consequence of the entrainment assumption is that the resulting plume has a self-similar form at all heights in an unbounded domain. This situation is illustrated in figure 1.1, and we now describe the classical model which illustrates this.

The propagation of the plumes through the system occurs due to density contrasts between the plume fluid and the surrounding ambient fluid. These differences arise due to variations in some global property of the fluid, for example the salinity or temperature. In general, this fluid property C will

obey a conservation law, such as conservation of salinity or specific heat. We assume that variations in the conserved quantity C are small and so the density of the plume depends linearly on the value of C, namely $\Delta\rho = \beta\Delta C$, where β is the corresponding expansion coefficient for the fluid property. In this limit, the plumes are described by the Boussinesq approximation, in which all density variations are taken to be negligible except in the buoyancy terms. Hence, small changes in the conserved quantity ΔC lead to small changes in the density of the plume. These have the form $\Delta\rho = \rho_0\beta\Delta C$, where ρ is a reference density. Consequently, the behaviour and dynamics of a turbulent Boussinesq plume generated by an isolated axisymmetric source may be specified by three time and spatially averaged quantities. These are the specific mass flux, $\pi\rho_0 Q$; the momentum flux, $\pi\rho_0 M$; and a quantity derived from the conserved fluid property C. The latter is referred to as the buoyancy flux $\pi\rho_0 B$, defined as $B = g'Q$, where $g' = [g\Delta\rho]/\rho_0$ is the reduced gravitational acceleration, with $\Delta\rho$ the density contrast of the plume relative to the environment and ρ_0 a reference density. Hence, g' is the value of the effective acceleration due to gravity accounting for the presence of the denser ambient fluid. Morton et. al., (1956) defined these physical quantities according to

$$Q = 2\int_0^\infty wr\mathrm{d}r = wb^2 \tag{1.3}$$

$$M = 2\int_0^\infty w^2 r\mathrm{d}r = w^2\, b^2 \tag{1.4}$$

$$B = 2\int_0^\infty g'wr\mathrm{d}r = g'wb^2 \tag{1.5}$$

where $w(z)$ is the mean vertical velocity of the plume, z the vertical co-ordinate, r is the radial coordinate and $b(z)$ is the effective radius of the plume. The turbulent plume may then be completely specified, by a system of nonlinear ordinary differential equations (Morton et. al., 1956). The first

of these expresses that the rate of change of Q with vertical distance from the plume source occurs due to the entrainment process:

$$\frac{\mathrm{d}Q}{\mathrm{d}z} = 2\epsilon M^{1/2} = 2\epsilon b w \tag{1.6}$$

The second refers to the rate of change of the momentum flux of the plume as a function of vertical distance from the plume source. The form of the equation indicates that the plume is governed by the momentum flux due to the source, and the buoyancy force arising due to density contrasts between the source fluid and the ambient:

$$\frac{\mathrm{d}M}{\mathrm{d}z} = \frac{BQ}{M} = g' b^2 \tag{1.7}$$

To complete the model, we need to specify an expression for the rate of change of buoyancy with z. First, we write a relation for the rate of change of the conserved fluid quantity C with vertical distance from the plume source:

$$\frac{\mathrm{d}\left(C\,Q\right)}{\mathrm{d}z} = 2\epsilon M^{1/2} C_a \tag{1.8}$$

where C_a is value of C for the ambient fluid. We then have:

$$\frac{\mathrm{d}\left[\left(C - C_a\right) Q\right]}{\mathrm{d}z} = -Q\frac{\mathrm{d}C_a}{\mathrm{d}z} \tag{1.9}$$

Combining the above two expressions hence leads to the final differential equation of the plume model, namely:

$$\frac{\mathrm{d}B}{\mathrm{d}z} = -N^2 Q \tag{1.10}$$

N is the Brunt-Vaiasala frequency, defined according to

$$N^2 = -\left(\frac{g}{\rho_a}\right)\frac{\mathrm{d}\rho_a}{\mathrm{d}z} \tag{1.11}$$

and ρ_a is the density profile of the ambient fluid. The model of a turbulent buoyant plume flow consists of equations (1.8), (1.9) and (1.12).

In the case of an initially uniform ambient, N^2 vanishes. The system then admits similarity solutions such that

$$Q(z) = \frac{6\epsilon}{5}\left(\frac{9\epsilon B_0}{10}\right)^{1/3} z^{5/3} \tag{1.12}$$

$$M(z) = \left(\frac{9\epsilon B_0}{10}\right)^{2/3} z^{4/3} \tag{1.13}$$

$$B = B_0 \tag{1.14}$$

The self-similar solution has the same form at all points above the source. It is a special solution of the equations and requires an exact relationship between the fluxes of volume, momentum and buoyancy.

In an initially stratified ambient, however, the flow of the plume may be modified due to the presence of the background stratification. The consequence of this is that the plume flow will have a finite total height H. A scale for this may be obtained by dimensional arguments, and results in the expression

$$H = \lambda B_0^{1/4} N^{-3/4} \tag{1.15}$$

where B_0 is the initial plume buoyancy flux and λ is an empirical constant.

It may be noted that the entrainment mechanism is the fundamental physical process governing the flow of a turbulent buoyant plume. The theory of the turbulent entrainment process and its application to geophysical flows was surveyed by Turner (1986). In addition to the fundamental entrainment hypothesis represented by equation (1.2), Turner discussed the proposition that the total inflow at each position also depends upon the surface area and geometry of the flow and its fundamental form, such as a plume or jet. Hence, a detailed quantitative analysis of the entrainment processes for several types of flows was established. Turner (1986) also described the application of the theory of entrainment to turbulent penetrative convection. He concluded that the entrainment assumption is applicable over a

wide range of flows and scales.

We now continue by reviewing a significant development based upon the model due to Morton et. al. (1956).

1.3 Turbulent Buoyant Convection in a Confined Region

It is common for situations to arise in which the flow of the self-similar turbulent plume occurs in a confined region. An example of this is the intrusion of hot air into a cold room. These flows exhibit more complex behaviour than turbulent buoyant convection occurring in a region that is effectively infinite in extent. The turbulent mixing dynamics which characterise the behaviour of a plume have an even greater effect upon the form of the resulting flow when the environment is bounded. As the plume rises through the environment it entrains ambient fluid. When the plume arrives at the top of the container, it spreads out laterally to form a layer of relatively light fluid. This situation is illustrated in figure 1.2. The continuing plume now entrains fluid from this layer, and hence arrives at the top of the container progressively diluted. The plume then spreads laterally at the very top of the container. By continuity, the original layer is displaced downwards, and hence a return flow develops in the finite region. This process continues, and consequently a region of stratified fluid is produced. The mixed region is separated from the original ambient fluid by a density step referred to as the *first front*. This situation was first investigated by Baines & Turner (1969) for the case of a plume that originated from a source of buoyancy that possessed a zero associated mass flux. It is commonly referred to as a *filling-box*. Certain key assumptions were applied in the model. Firstly,

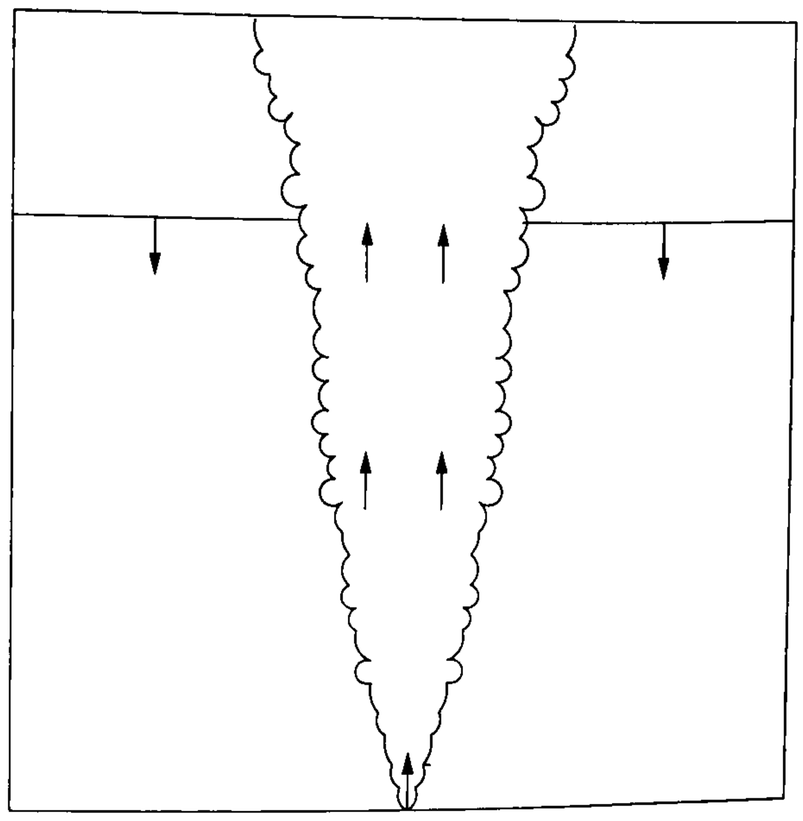

FIGURE 1.2: A filling-box flowing driven by a single turbulent buoyant plume. In this case, the source is considered to possess a zero associated mass flux. The first front. depicted as a uniform horizontal line, propagates vertically downwards through the container.

the flow of the plume was such that the entrainment assumption in the fundamental form of equation (1.2) may be applied. This required the plume to be free of the influence of the vertical boundaries during propagation through the container. Secondly, it was assumed that the relatively light fluid layer formed at the top of the container as the fluid supplied at $z = H$ spreads out, and forms a well-defined stratified layer through which there is negligible vertical mixing. Hence, it becomes part of the non-turbulent environment. Baines & Turner (1969) produced large-time asymptotic solutions for a point source in an environment of constant cross-section. From the model of a turbulent buoyant plume, specified by equations (1.8), (1.9) and (1.12), they arrived at a solution for the location of the first front z at

a time t. In dimensional variables, this expression was found to be

$$t = \left(\frac{5}{4\epsilon}\right)\left(\frac{5\pi}{18\epsilon}\right)^{1/2} R^2 H^{-2/3} B_0^{1/3} \left[\left(\frac{H}{z}\right)^{2/3} - 1\right] \tag{1.16}$$

where H is the vertical height of the confined region and πR^2 is its cross-sectional area, and B_0 is the buoyancy flux of the plume at the source.

Baines & Turner (1969) also discussed various extensions to the filling-box model. Corresponding solutions were obtained for the case of a filling-box system driven by a line plume, and also a variation which introduced a second source of pure buoyancy with zero associated mass flux. This source was located on the upper horizontal boundary, and produced a downward-propagating plume of relatively dense fluid. A steady-state solution was also obtained for this configuration. Finally, Baines & Turner (1969) discussed the extension of the filling-box system to the case of non-regular containers.

The model of Baines & Turner (1969) was re-formulated by Manins (1979). In this system, the turbulent buoyant flow was generated by a line source located at the lower boundary in such a manner that the resulting plume propagated along one of the vertical walls of the container. This situation is depicted in figure 1.3. The model was generalised to include the effect of radiation of heat from one of the horizontal boundaries. In this situation, the temperature difference between the vertical boundary and the ambient caused a plume-like flow to originate close to the boundary. The filling-box process was hence driven by this flow. The quantitative analysis started from first principles, with the model derived starting from the Navier-Stokes equations. Several conditions were imposed upon the model to ensure its validity. Firstly, the Prandtl number $\nu/\chi = O(1)$ or greater, where ν is the kinematic viscosity of the fluid and χ is the molecular diffusivity. This criterion ensures that diffusion of buoyancy does not dominate over fluid advection. The aspect ratio of the confined region $L/H > 1.2$,

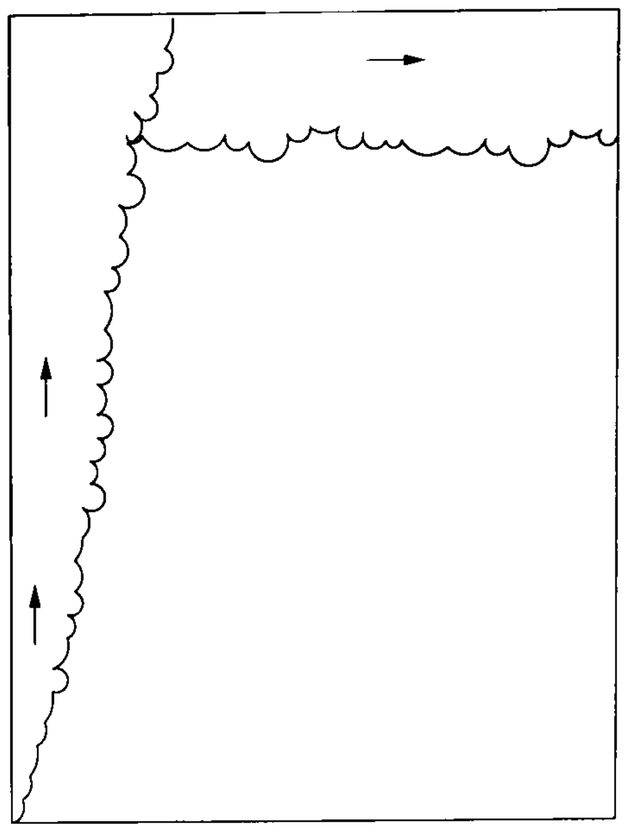

FIGURE 1.3: The modified filling-box system of Manins (1979). The flow is driven by the line source located at the base of the left-hand vertical boundary.

where L is the horizontal length of the container and H the vertical height. The aspect ratio is then sufficiently large to ensure that the plume flow has self-similar form. Hence, the unmodified entrainment assumption in the form of equation (1.2) may be applied to the turbulent flow. Finally, two restrictions were placed upon the range of the Grashof number, defined as

$$R^2 = \left(\frac{\epsilon^{2/3} B_0^{1/3} H}{\nu} \right)^2 \tag{1.17}$$

where B_0 is the initial plume buoyancy flux and ϵ is the entrainment coefficient as per Morton et. al. (1956). It was required that $R \simeq L/H$ and $R >> 1/\alpha$. These conditions on R ensure that the source of buoyant convection is the dominant transport mechanism in the filling-box region, because they require that the plume is fully turbulent and thin in lateral extent. Further, these conditions ensured that the far-field effect of the radiative vertical boundary was negligible. In other words, the temperature contrast at the wall cause the plume flow to develop, but did not otherwise affect the buoyancy of the ambient. It was found that the system is steady to $O(\epsilon/A)$,

where A is the aspect ratio, and only the buoyancy was a linear function of time at every point in the large-time limit. The complete analysis was performed for a plume source which possessed zero associated mass flux. However, Manins (1979) allowed the filling-box system to be subject to a radiative condition applied to one of the horizontal boundaries. The condition upon the magnitude of the Grashof number restricted this effect to be of relatively small magnitude when compared to the turbulent buoyant convection arising due to the flow of the plume.

A substantial extension to the filling-box system was proposed by Germeles (1975). The process of liquefied natural gas being pumped into a storage tank was modelled following the method of Baines & Turner (1969). Although such flows are very common in many physical situations, this was the first major investigation to examine the effect of the addition of mass into a finite region via a turbulent plume. The model was also extended to consider sources that were inclined at an angle to the vertical. Analogous results were obtained for a plume that originated from a source that was not located at the centre of the tank. A numerical method was implemented to solve the problem, which we will now briefly outline.

First, we introduce three dimensionless variables. δ is the normalised density profile, scaled upon the input density of the plume fluid; ξ is the dimensionless vertical distance from the plume source, normalised with the height of the container; and τ is dimensionless time, scaled with the total filling-box time.

It was proposed that the normalised ambient density profile δ may be represented at the dimensionless time τ by the function

$$\delta = \sum_{i=1}^{n} \delta_i \left[S\left(\xi - \xi_{i-1}\right) - S\left(\xi - \xi_i\right) \right] \tag{1.18}$$

where S is the unit step defined by

$$S(\xi - \xi_i) = \begin{cases} 0 & \text{for} \quad \xi < \xi_i \\ 1 & \text{for} \quad \xi \geq \xi_i \end{cases} \tag{1.19}$$

The plume equations were numerically integrated by a Runge-Kutta method, and the values of the fluxes of mass, momentum and buoyancy were calculated at the very top of the container. Then, in the dimensionless time interval $\Delta\tau$, the normalised interfaces ξ_i of the so-called 'staircase' profile were moved downwards to new positions ξ_I. The procedure was then repeated so that the density profile throughout the tank could be evaluated.

In addition to the asymptotic solution derived by Baines & Turner (1969), an approximate analytic expression for the time-dependent density profile in a filling-box flow was calculated by Worster & Huppert (1982). This result was shown to be in good agreement with a complete numerical integration of the governing equations utilising the method of Germeles (1975). The analytic expression was found to be useful in situations where the asymptotic solution calculated by Baines & Turner (1969) is not applicable. Worster & Huppert (1982) cited an example of this situation, namely when double-diffusive effects are significant in the confined region. In this case, the stratified region may break down into discrete well-mixed layers, and this in turn can significantly affect the subsequent plume behavior. The key step in the calculation was based upon the approximation that the density of fluid behind the first front changed at a rate that was virtually independent of position. The implementation of the model required the value of the dimensionless buoyancy flux $\hat{B}$, normalised with the initial plume buoyancy flux, to be known at the dimensionless heights $\hat{\xi} = \hat{\xi}_0$ and $\hat{\xi} = 1$. $\hat{B}$ was then approximated to be linear between those points. This was equivalent to assuming that the rate of change with time of the density

of the fluid above the first front was independent of position to leading order in $\hat{\xi}_0$. The density profile could then be evaluated.

The introduction of a source with non-zero associated mass flux, by Germeles (1975), was a significant modification to the original filling-box model of Baines & Turner (1969). However, this was not the only situation in which the physics of the source itself was modified to create a novel flow situation. The investigation of Killworth & Turner (1982) considered a source that produced an unsteady buoyant plume. The time-scale of these variations was typically small compared with the filling-box time. It was found that the final asymptotic state is independent of the oscillating buoyancy source. Killworth & Turner (1982) introduced a key step in their model to account for the possible effect of unstable interior stratification. Since the interior time scales were long compared with those in the plume, convective overturn was treated by a method due to Bryan (1969): if at any time the buoyancy distribution in the interior became statically unstable, the buoyancy in this area was averaged vertically to simulate the mixing due to convection. This averaging was then repeated, so that buoyancy was conserved, until a stable or neutrally stable condition resulted. The dimensionless equations of the problem were numerically integrated by using a predictor-corrector method. In conclusion, Killworth & Turner (1982) found that steady-state or long-time filling box models may be applied without modification to physical situations with rapidly or seasonally varying buoyancy sources, such as bottom-water formation in high latitudes.

The investigations discussed so far have considered flows which possess a single component of buoyancy. McDougall (1983) investigated the situation in which double-diffusive effects had a significant influence upon the dynamics of the filling-box flow. The study examined flows in both confined

and unbounded environments. McDougall (1983) examined two cases. In the first, the double-diffusive effects occurred in the same direction as the buoyancy. Hence, the flow of the turbulent plume was enhanced. In the second case, the buoyancy was diminished because the double-diffusive effects occurred in the opposite sense to the buoyant flow. Application of dimensional analysis gave good agreement for this second, counter-buoyant, case. When the double-diffusive plume flows in a confined region, the plume does not always reach the top of the container. Instead, it may intrude at intermediate heights. This implies the formation of double-diffusive interfaces. To understand this further, a quantitative measure of the importance of double-diffusive convection in relation to the normal filling-box mechanism was obtained in the experiments by using the measured density profile. It was found that this correlated well with a theoretically derived parameter B_ρ, which was defined as

$$B_\rho = \kappa \left[\frac{A(1 - R_f)}{R_\rho^N H^{20/9} B_0^{1/9} (R_\rho - 1)^{4/3}} \right] \tag{1.20}$$

where κ and N are constants dependent upon the physical nature of the two diffusive mechanisms, H is the vertical height of the plume source from the bottom of the container, A is the uniform cross-sectional area of the container, B_0 is the buoyancy flux at the plume source, R_f is ratio of the plume buoyancy flux to the buoyancy arising due to double-diffusivity and R_ρ is the density anomaly ratio. B_ρ represents the relative importance of double-diffusive convection to the filling-box mechanism.

Wells et. al. (1999) investigated a substantial modification to the original filling-box model of Baines & Turner (1969). The system was driven by turbulent buoyant convection originating from two distinct sources. The first source produced an axisymmetric plume, in an identical manner to the

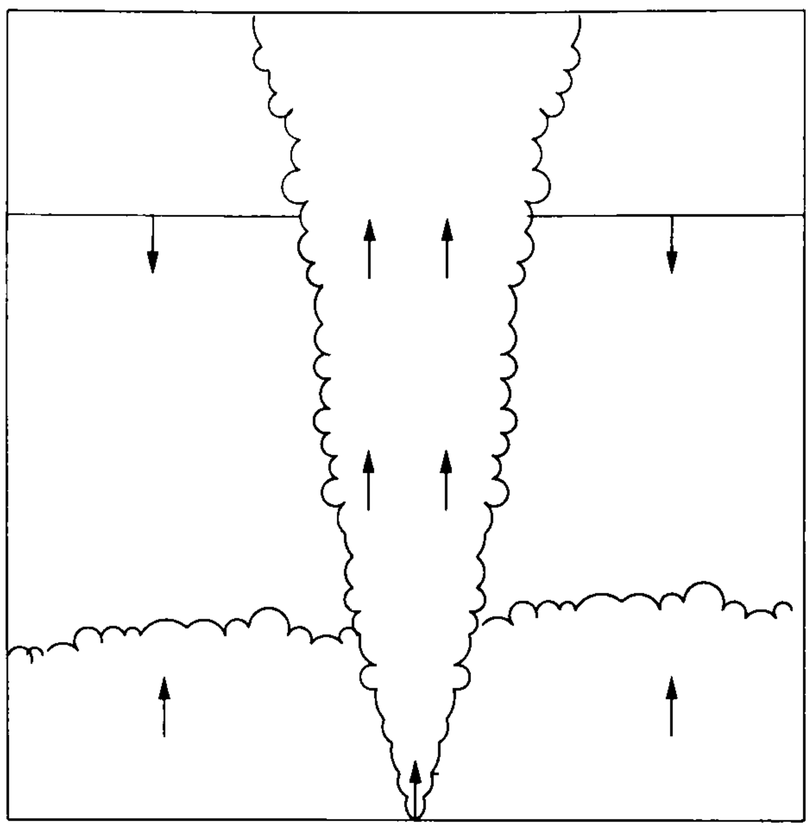

FIGURE 1.4: The filling-box system of Wells et. al. (1999). The ascending plume drives a return flow in an identical manner to the original filling-box system of Baines & Turner (1969). The additional turbulent buoyant convection arises due to the relatively hot temperature of the entire lower boundary.

original filling-box system. The second flow arose due to the effect of heating the lower horizontal boundary. This is illustrated in figure 1.4. Two cases of the system were studied. In the first case, the system comprised an ascending plume and a positively-buoyant distributed source originating due to heating of the lower horizontal boundary. In the second case, the plume propagated vertically downwards through the system. The distributed source was located at the lower boundary.

The analysis of the system was subject to an assumption that the heated lower boundary supplied a buoyancy flux uniformly across its horizontal extent. Wells et. al. (1999) subsequently showed that the long-term form of the density profile in the container was dependent upon a dimensionless

parameter R, defined by

$$R = \frac{B}{F} \tag{1.21}$$

where B is the buoyancy flux of the flow originating from the distributed source and F is the buoyancy flux associated with the turbulent plume.

Wells et. al. (1999) also found that when the plume is negatively buoyant, the form of the stratification resulting from the filling-box processes is also dependent upon the value of R. However, in this case they found that for $R < -1$, the stratification was unstable, and subsequently overturned. The model was then applied to the problem of identifying the density structure that may occur due to thermal convection in enclosed seas.

1.4 The Effect of Ambient Stratification Upon the Filling Box Flow

1.4.1 Two-Layered Stratification

A new extension to the canonical filling-box model was proposed by Baines (1975). The investigation was motivated by a desire to produce a more realistic model of heat transfer in the lower regions of the atmospheric boundary layer. Consequently, the effects of turbulent penetrative convection were introduced into the system. Hence, the free surface that represented the upper boundary of the Baines & Turner (1969) model was replaced with an overlaying layer of relatively light fluid. The rate of entrainment through the end of a plume which impinged upon the density interface was investigated both theoretically and experimentally. The entrainment flux into the plume was found to be a function of the local width of the layer and the velocity and width of the plume, and this led directly to the proposition that the Froude number is the fundamental parameter in quantifying the mixing dynamics

of such a flow. Previous work performed by Linden (1973), upon turbulent entrainment, was extended and applied to the impingement problem.

In order to improve understanding of the entrainment mechanism, Linden (1973) proposed a model of a vortex ring interacting with a sharp density interface. It was found that the vortex ring engulfed ambient fluid as it propagated through the density step. The interaction was considered to be a good approximation to a typical turbulent eddy driving the entrainment process. In performing the experiments and also in the subsequent analysis, Linden (1973) applied some restrictions upon the system, namely that the Froude number based upon the density difference across the interface was less than unity. The value of Fr for the flow in question was defined as

$$Fr = \left(\frac{\rho_0}{\Delta\rho}\right)\left(\frac{u}{\sqrt{g\,l}}\right) \tag{1.22}$$

where u is a velocity scale and l a length scale for the intruding flow, ρ_0 a reference density and $\Delta\rho$ the density difference across the interface. The volume of fluid entrained by the vortex ring as it propagated past the interface was calculated and found to be proportional to the cube of Fr. This result was to form the basis of a large amount of later work upon the dynamics of interfacial mixing due to turbulent entrainment.

The work of Baines (1975) was later extended by Kumagai (1984). A more detailed theoretical discussion of the mixing dynamics of the flow was obtained. An experimental and theoretical study of the time evolution of a source in a confined two-layer region was devised. A downward propagating plume, originating from an input of relatively dense fluid, was used to drive the system. Initially, the plume became trapped in the upper fluid layer. This was duw to the change in density of the plume due to entrainment of relatively light ambient fluid. Hence, the plume did not posess enough buoyancy to flow through the interface. However, the plume im-

pinged upon the interface, and so entrained small amounts of fluid from the bottom layer. The dynamics therefore consisted of a filling-box flow combined with impingement and subsequent turbulent penetrative convection. The entrainment rate obtained from changes in the thickness of the upper fluid layer with time was found to be a function of the Froude number, as in previous work of Baines (1975). However, it was found that the rate of change was proportional to the cube of the Froude number at small values of Fr, but approached a finite limit as Fr increased. The dimensionless buoyancy flux across the interface also reached a maximum value of $\hat{B} = 0.168$, and decreased sharply at values of Fr less than this upper limit. Consequently, Kumagai showed that his calculations were in accordance with previous work. However, it was noted that the earlier results due to Baines (1975) were correct only at small values of Fr because they relied upon a constant-depth approximation. The model was applied as a more realistic description of convection in the atmospheric boundary layer.

The fundamental theory of both Kumagai (1984) and Baines (1975) was based upon work by Ball (1960), who studied atmospheric flows. Ball (1960) proposed that generation of turbulent kinetic energy in relatively dense atmospheric fluid resulted in the upward migration of an atmospheric inversion. This is a layer of fluid in which the sign of the temperature gradient is reversed. The resulting flow may be considered equivalent to a positively-buoyant turbulent plume. Ball (1960) suggested that the surplus turbulent kinetic energy was balanced by buoyancy forces in a region of *downward* transfer of heat in the upper part of the convection layer. This was referred to as a counter-gradient flux of heat.

This energetic argument which proposed that the dimensionless buoyancy flux cannot exceed unity, was discussed in the investigation by Kumagai

(1984). He evaluated the limit, and found it to be $\hat{B} = 0.41$ for his filling-box system.

1.4.2 Ambient Fluid with a Stratified Density Profile

The previous investigations of Baines (1975) and Kumagai (1984) considered only an overlaying layer of light fluid in the confined region. This was extended to a system initially consisting of a two-layer stable stratification by Cardoso & Woods (1993). Particular attention was paid to the dynamics of the mixing occurring in the filling-box flow. Initially, the plume was trapped in the lower fluid layer, but it impinged upon the interface and subsequently entrained light fluid from the upper layer. Hence, two fronts formed in the system, one propagating upwards and the other moving downwards. This system may be viewed as a completely new problem, rather than as an extension of the situation studied by Baines (1975).

The model proposed for the large-time behaviour is based upon an energetic formation which supposes that a constant fraction of the kinetic energy supplied by the plume, available for mixing across the interface, is converted into the potential energy of the convective layer at an efficiency of approximately 50%. This followed on from the original work upon mixing first introduced by Ball (1960), and is related to the theory of turbulent penetrative convection. A dimensionless entrainment rate E was defined as

$$E = C \left(\frac{\pi b^2}{A} \right) Ri^{-1} \tag{1.23}$$

where $C = (16/5)\,\epsilon f$, and f is a dimensionless constant indicating the fraction of kinetic energy converted to potential energy of the mixed layer, A is the cross-sectional area of the confined region and b is the effective plume radius. A discussion of the contrasting entrainment laws for different flow

regimes was also included. For large values of Ri, the entrainment process was proposed to be controlled by the wave-like response of the interface to bombardment by turbulent disturbances. In the regime of smaller Ri, entrainment is mainly caused by intrusions of large-scale turbulent disturbances into the region of lighter fluid and the associated capture of small portions of this fluid. The conclusion of the investigation was that the effect of smooth stratification upon the dynamics of the descending front is negligible.

The model of Baines et. al. (1990) was modified to account for the effects of an initially stratified ambient by Bloomfield & Kerr (1999). In this situation, the filling-box flow was driven by a turbulent *fountain.* This refers to an input of negatively buoyant fluid such that the flow is driven by the initial momentum only. A typical fountain flow is depicted in figure 1.8. It was found that the ascending fluid reached a maximum height before the flow reversed direction. After this height, the flow intruded either along the base of the container or at an intermediate height in the environment. This is in direct contrast to the case for which the ambient is unstratified. In this situation, the lateral intrusion always occurred along the lower boundary of the confined region.

Bloomfield & Kerr (1999) also determined expressions for the motion of the ascending and descending fronts which indicated the vertical extent of the mixed layer. They also considered changes to the environmental density profile and hence determined an expression for the rate at which the top of the fountain rises, subject to the effect of environmental stratification. The results were applied to two physical problems: replenishment of fluid in a volcanic magma chamber and the heating or cooling of a room.

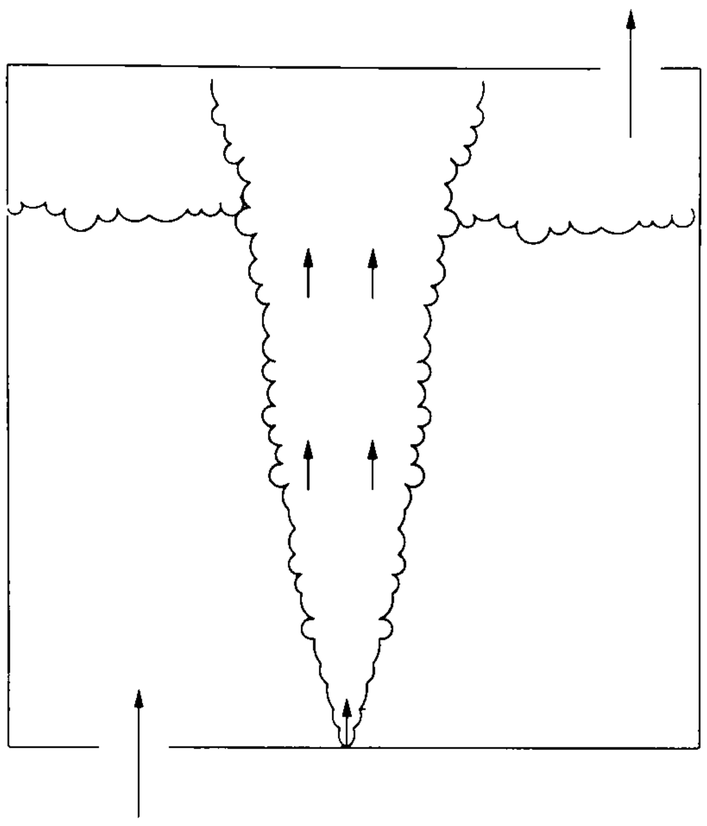

FIGURE 1.5: Natural ventilation in a uniform container. The filling box flow in this case is driven by a single turbulent buoyant plume which originates from a source which possesses a zero associated mass flux. The arrows indicate the direction of the buoyant flow and also the net direction of the subsequent displacement ventilation.

1.5 Natural Ventilation

The filling-box system was applied to model the dynamics of natural ventilation by Linden et. al. (1990). The investigation identified two different types of buoyancy-driven flow that may occur in the system. Mixing ventilation arises when fluid enters the confined region and mixes with environmental fluid. An example of such a flow is the intrusion of relatively cold air at some point into the room, which acts to effectively cool the ventilated space. Typically, this does not result in the ambient fluid becoming a well-mixed layer, but instead fluid in the environment takes the form of a weak vertical stratification. However, in true mixing ventilation, the space is well-mixed, and hence consists of a uniform density. This does assume that the inflow of cool air is at a high level, so that the incoming fluid mixes all of the ambient.

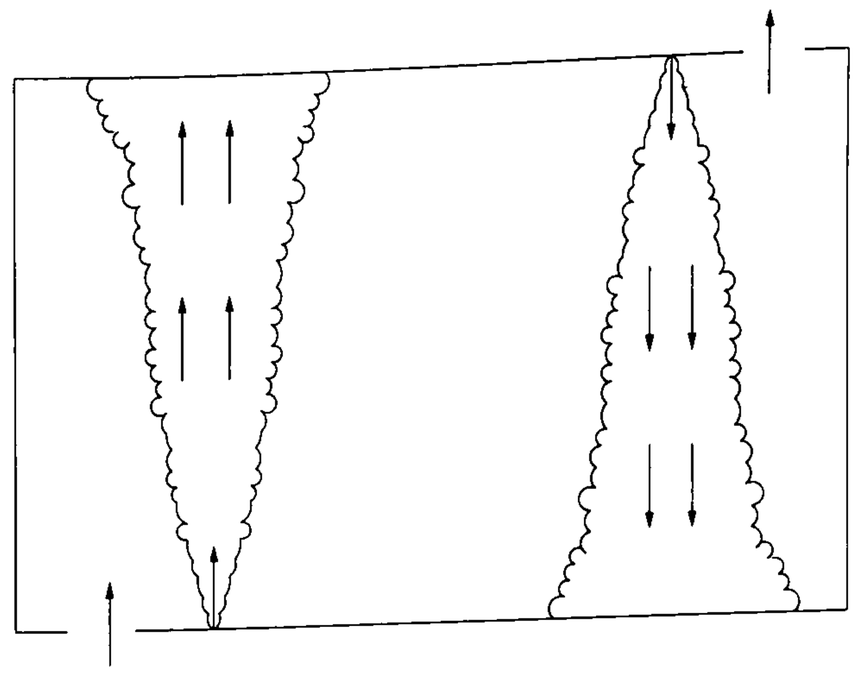

FIGURE 1.6: Natural ventilation in a bounded region. There are two turbulent plumes flowing in the container. The ascending plume originates due to input of relatively light fluid, the descending plume due to fluid that possesses a density greater than the ambient.

The second principle type of flow is referred to as displacement ventilation. This occurs when intruding fluid enters the container via sources located in the lower boundary. By continuity, relatively light fluid is displaced out of the confined region through sources located in the vicinity of the upper boundary.

The steady-state solution for the form of stratification within the container, as depicted in figure 1.6, was obtained. Linden et. al. (1990) found that the form of the equilibrium stratification within the space was dependent upon the volume of fluid entrained by the flow of the plume. The buoyancy flux associated with the plume source did not govern the location of the fluid interface. However, it did determine the density of the upper mixed region, and hence the resulting stratification of the ambient fluid.

The so-called 'emptying filling-box' model was then extended to consider a naturally-ventilated region subject to two independent buoyant flows by Cooper & Linden (1996). Two different configurations were studied for the system illustrated in figure 1.7. In the first case, both of the sources

were located in the lower boundary. The resulting turbulent plumes were positively-buoyant and hence upward-propagating. In the second situation, one of the plume sources was located in the upper boundary and supplied relatively dense fluid to the system. Consequently, this plume propagated vertically downwards through the container. In both situations. the height of the fluid interfaces was found to be a function of the height of the enclosure, the effective area of the enclosure openings, and the ratio of the initial buoyancy fluxes of the two plumes. This followed directly from dimensional analysis. Cooper & Linden (1996) proposed that the location of the fluid interfaces was dependent upon the total volume of fluid entrained by each of the plumes as they flowed from their respective sources to the fluid interface. This quantity was calculated by applying the model due to Kumagai (1984) for the volume of fluid entrained at a density step. The dynamics of the plume at the interface position was considered to be equivalent to a distributed plume whose source was situated at the fluid interface.

When the system was configured such that one of the plumes was downward-propagating and the other plume was upward-propagating, it was found that the resulting environmental stratification was dependent upon the ratio of the buoyancy fluxes associated with the plume sources. In the limit that the ratio of the source buoyancy fluxes was small, two distinct and well-mixed fluid layers formed. Large values of this ratio produced more complex patterns. Three-layer stratifications occurred, with two of the three well-mixed layers possessing a density less than the ambient fluid. The location of the fluid interfaces was primarily determined by the volume fluxes associated with the flow of the plumes through the container. Hence, the magnitude of ambient fluid entrained by the plumes as they propagated the vertical distance of the confined region was again found to be a key factor in the

overall dynamics of the system.

The model was also extended to cover an arbitrary number of positive sources of buoyancy in a naturally ventilated region by Linden & Cooper (1996). As in the previous analysis, the sources were considered to possess a zero associated mass flux. The approximation that the stratification within the region is neglected when evaluating the properties of each plume was applied in calculating the overall behaviour of the system. This is applicable when the the timescale for transient flow effects is much less than the filling box time. This approximation was shown to be satisfactory for a range of physical conditions. Experiments performed corroborated this. The approximation was again taken to be valid because the timescale of over which the experiment was performed was much greater then the filling box time. The result of a system comprising an arbitrary number of positively-buoyant ascending plumes was to produce a multi-layer stratification within the container. Each of the turbulent plumes terminates in one of the fluid layers. The plume with the smallest buoyancy flux is associated with the fluid layer closest to the floor of the room. Plumes that have a greater buoyancy flux may break through the stratification, and the plume with the largest buoyancy flux was therefore able to reach the topmost fluid layer. Consequently, the location of the lower interface was well-predicted by the model. This is important in physical applications of the theory.

1.6 Some Further Applications

The nature of the present work results in some very general theory. Hence, it is of value to briefly examine some further applications and extensions to the original filling-box model of Baines & Turner (1969). We note that the theory developed throughout the course of the present work is applicable to

the following models.

As a novel extension of the original filling-box model, the flow arising due to the intrusion of relatively dense fluid in a confined region was investigated by Baines et. al (1990). The original study of the flow which occurs as a result of the upward injection of relatively dense fluid was due to Morton (1959). He used the entrainment assumption to formulate a system of equations analogous to (1.6), (1.7) and (1.10) for a so-called turbulent fountain. The model was extended by Turner (1966), who performed experiments upon such flows in an unconfined region containing homogeneous ambient fluid. Baines et. al. (1990) then considered a filling-box flow in a confined region driven by a turbulent fountain. The situation is illustrated in figure 1.8. However, the fountain source possessed an associated mass flux, and consequently the level of the free surface increased with time.

A fountain-driven filling-box flow exhibits different features to the model of Baines & Turner (1969). The case of dense fluid injected vertically upwards into the region was considered. In a homogeneous environment, the downward-propagating fluid reaches the base of the tank where it spreads laterally as a thin layer (Baines et. al., 1990). The top of the layer represents a density step in the environment, analogously to the first front in a plume-driven filling-box, and this ascending front rises as ambient fluid from above it is entrained into the down-flow. As the layer increases in thickness, the dense fluid that has accumulated below the front is re-entrained back into the down-flow of the fountain. Consequently, all subsequent fluid arrives at the base of the tank even denser, and a weak, stable stratification is established in the region below the front. The presence of the dense layer reduces the density contrast between the source fluid and the ambient, and this causes the fountain to rise. However, the ascending front rises faster

than the fountain height, so that eventually, it overtakes the top of the fountain. After this point, the fountain only interacts with the stratified layer, and the ascent of the front is controlled only by the rate at which fluid mass enters the container via the fountain source.

In addition to the situations described in detail in this section, the filling-box system has also been applied to model convection and mixing in volcanic magma chambers by Turner & Campbell (1986), and also by Huppert & Turner (1981). Another investigation, by Turner & Gustafson (1978), utilised a filling-box subject to double-diffusive effects to model the massive sulphide deposits that occur when a dense gravity current of hot saline ore solution fills a depression on the sea floor. Such an application further illustrates the usefulness of the filling-box model.

1.7 The Present Work

Although there exists significant work upon turbulent buoyant fluid flows, as discussed above, there remain important questions not covered in the literature. One key area that has not been previously studied in detail forms the principle focus of the current work. This the situation for which two fluid flows of opposite buoyancy, in a confined region, originate from sources which possess associated fluxes of mass.

This represents a fundamental issue. For example, air conditioning systems supply a flux of both fluid mass and buoyancy. Industrial pollutants, such as chemical waste, also supply a flux of fluid mass into the rivers in which they are emptied. Another example is the accidental release of hazardous gases into factories and mine shafts. The flux of mass associated with the intruding flow may be a key factor in understanding how to vent dangerous fluids safely out of the confined region into which they flow.

Our aim in the present work therefore is to model the dynamics of a dual-flow filling-box driven by sources which supply both buoyancy and a significant flux of fluid mass. The system is depicted in figure 1.7. An outflow vent is provided to vent fluid mass from the container. We assume throughout the current work that the turbulent plumes flow in such a manner that they are free of the influence of the vertical boundaries of the container. Hence, we may apply the self-similar model of Morton et. al. (1956), and consequently apply plume theory to describe the fluid flows within the confined region. However, as noted before, the dual-plume filling-box represents a complex non-linear system with a wide range of novel behaviour. We thus focus on the understanding of the physics of the system and how the results may be applied to answer a variety of important questions.

The majority of the work which follows deals with the steady-state analysis of the dual-plume filling-box systems. The fundamental model, which contains the essential physics, is investigated in Part I. In Chapter 2 a model is presented which is used to predict global values of the system. Numerical solutions are computed and subsequently discussed. The results are compared with a theoretical analysis based upon plume entrainment. An application of the system to ventilation of a building is presented and discussed. Guided by the numerical solutions, the key effects which the finite mass flux has upon the dual-plume flow system are identified.

In order to test the basic steady-state model, we present in chapter 3 some new results from a set of laboratory experiments. In these experiments, we examine the mixing and flow produced by two opposing point sources of buoyancy and compare the results with the fundamental model. A simple modification to the fundamental system, applied via vertical displacements of the fluid sources, is derived. The modification allowed a greater amount

of experimental data to be obtained. The solutions of this system are then compared with experiment for the location of the fluid interface. The agreement was found to be good.

Part II comprises three further steady-state systems, each of which retain the basic feature of the model described in chapter 2; namely, a system driven by two opposing turbulent buoyant fluid flows which possess associated fluxes of mass. However, each of the systems comprises novel features which leads to new physics.

Chapter 4 extends the work of the previous chapter by examining new source configurations. The physical ramifications of a dual-plume filling-box system driven by plumes originating from line sources are discussed. The new system is modelled in the steady-state case, and the resulting expressions are solved numerically. Hybrid systems, comprising one line plume and one axisymmetric plume, are then introduced. The corresponding numerical solutions are then compared to both the fundamental system and the dual line-plume filling-box.

In Chapter 5 a second mass sink is introduced. The second outflow vent is located in the base of the container. We examine the consequences of this with a view to understanding the conditions that cause the confined region to be subject to a natural ventilation flow. A simple argument is presented to show which of two possible regimes the ventilation will occur. Each of the possible methods is modelled and solved numerically. The results are compared and discussed. A simple model involving the effect of external wind upon the subsequent development of the ventilation flow is discussed and solved. Conclusions are drawn for the steady-state models derived in the chapter.

Part III returns to the fundamental model of Part I. However, in this

case the analysis, theory and experiments are performed for the unsteady flow regime. The time-dependence is modelled in Chapter 6, and a numerical scheme is implemented to obtain solutions of the transient system. The model is shown to reduce to the steady-state when $t \to \infty$. The numerical results are shown to be in good agreement with a number of analogue experiments. The limitations of the numerical technique are also discussed.

Finally, some overall conclusions and deductions are drawn and discussed in Chapter 7.

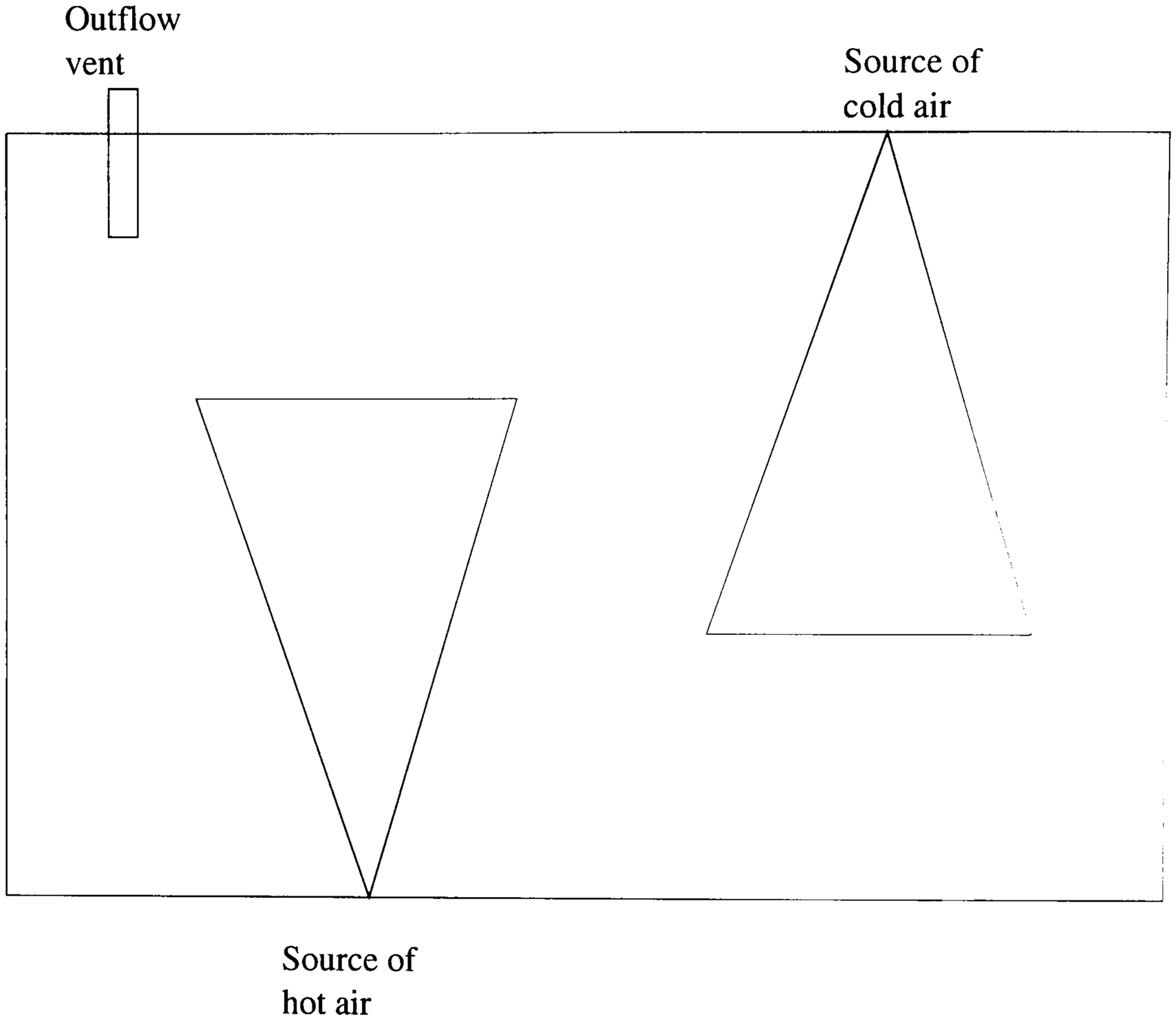

FIGURE 1.7: Illustration of the dual-plume filling-box system that is central to the present work. The outflow vent is required because each of the plume sources possesses a significant associated mass flux.

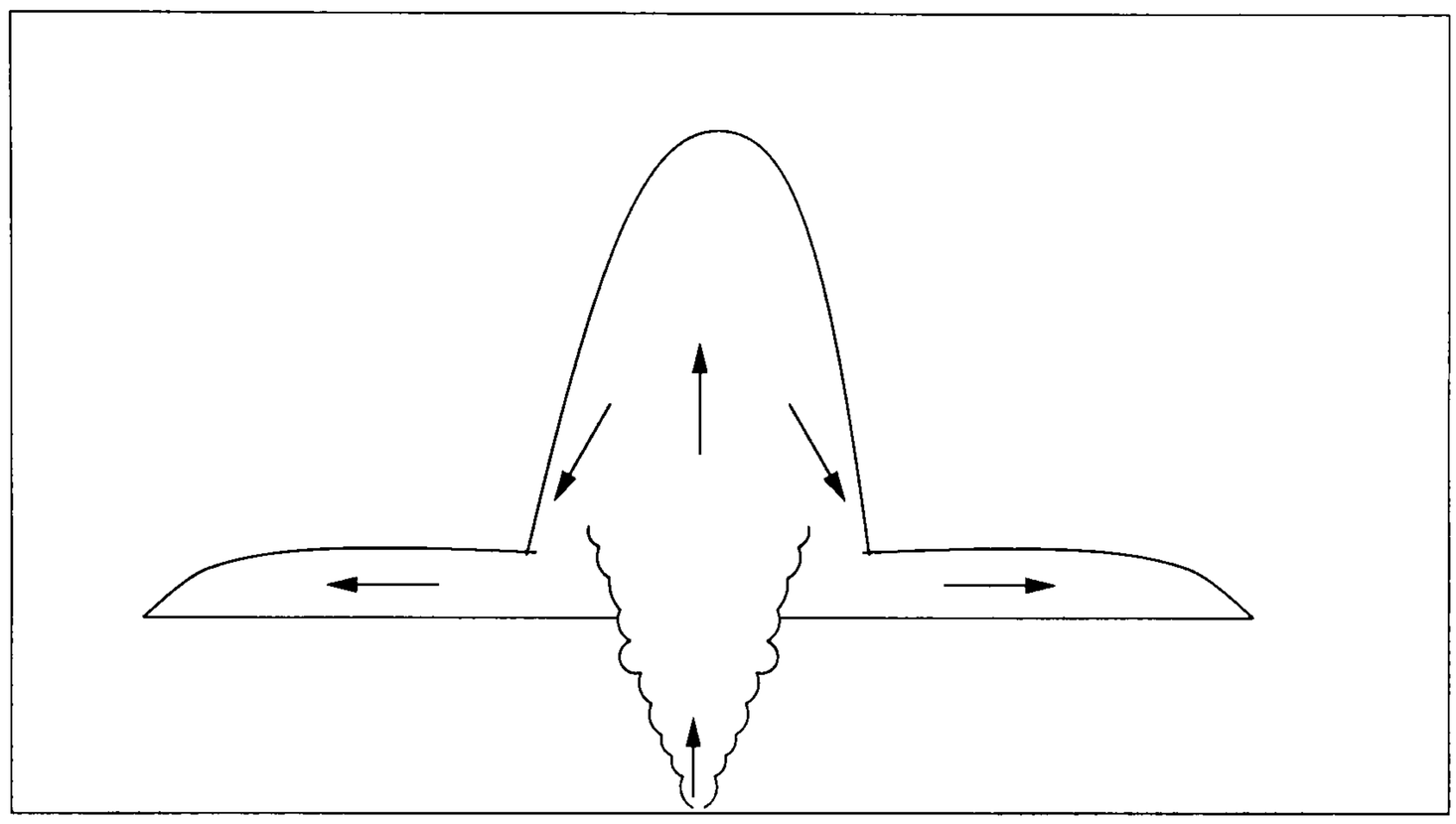

FIGURE 1.8: The turbulent fountain flow that occurs due to the injection of dense fluid vertically upwards into an unconfined region. The flow reaches a certain height at which its vertical velocity vanishes. The dense fluid then falls vertically downwards. The density of the descending fluid has been diluted due to the entrainment mechanism. However, it may possesses a density greater than the surrounding ambient fluid. The height at which the fluid intrudes laterally is dependent upon the stratification present in the ambient fluid.

Part II

The Fundamental Steady-State Model

Chapter 2

Theory

"Everything has been figured out, except how to live."

– Jean-Paul Sartre

2.1 Equilibrium Steady State for the Dual-Plume Filling Box

In this chapter we derive a model for the steady-state equilibrium of the dual-plume filling-box system. The model is comprised of two parts. Consideration of fundamental physical quantities associated with the system leads to a set of conservation laws. These are described in §2.2. In section 2.2.1, we complete the model by quantifying the internal mixing dynamics that characterise the overall behaviour of the system.

Numerical solutions of the model are then computed for two regimes. The special case for which the mass fluxes associated with the plume sources are equal is examined first in section 2.3.1. The two most important param-

eters are the dimensionless mass fluxes associated with the plume sources. These are referred to as R and S, for the top and bottom source respectively. Note that we present the appropriate normalisation in §2.2. A key result concerns the value of R required such that the system comprises a single, well-mixed fluid layer. A theoretical analysis is then presented, which predicts the single-layer system occurs for precisely the same value of R obtained numerically. The analysis of the numerical results is then extended to the more general case of $R \neq S$. This is described in §2.3.2, where the theoretical analysis from the previous section is generalised to the case of sources with unequal associated initial mass fluxes.

In §2.4 we examine the consequences of a small modification to the system, namely the case in which the mass outflow is located a distance below the upper vertical boundary.

A direct application of the model is presented in §2.5. This involves the calculation of the two-layer temperature stratification in a room subject to simultaneous heating and cooling. Finally, we discuss the physics of the steady-state system and draw some overall conclusions in §2.6.

2.2 A model of two opposite-buoyancy plumes in a finite region

We make the assumption that the system has evolved through a transient stage and hence evolved to steady-state equilibrium. This occurs over a time scale T, which we refer to as the convergence time. Another time scale of importance is the filling-box time τ. By dimensional analysis, we have

$$\tau \sim \frac{AH}{Q_0} \tag{2.1}$$

namely, the time for which all the ambient fluid in a container of cross-sectional area A and depth H has been mixed through a plume of initial volume flux Q_0. We note that, in general, $T >> \tau$. This is discussed further in Chapter 6.

In steady-state, the dual-plume system consists of a two-layer stratification separated by a well-defined interface. Such a state is reached in a timescale of $O\ (T)$, which is the timescale over which the experiments, presented in the next Chapter, are performed. For the system to achieve, and consequently remain, in steady-state equilibrium, there are two physical effects that occur. Firstly, the return flows associated with the two plumes will have met at some point in the container. Hence, the system consists of two layers separated by a well-defined interface. Secondly, the density of each layer remains constant in steady-state. This is a key point which warrants further discussion.

Let us consider, for example, the flow of the ascending plume when the system is in equilibrium. As the ascending plume flows through the lower layer, it acts principally as a buoyancy sink, entraining ambient fluid. However, when it reaches the interface, we suppose that its density has changed sufficiently due to the entrainment process that it now possesses a density *equal* to the upper fluid layer. Hence, the physical effect of the ascending plume as it flows through the upper layer is to *mix* ambient fluid. Hence, the above proposition implies that the motion of the ascending plume in the upper layer is to cause the fluid to be approximately well-mixed. The experimental work, detailed in Chapters 3 and 6, corroborates this well-mixed assumption. Hence, to leading-order, we assume that each of the fluid layers are well-mixed in steady-state equilibrium. Further, we note that the above assumption follows from the respective expressions for the

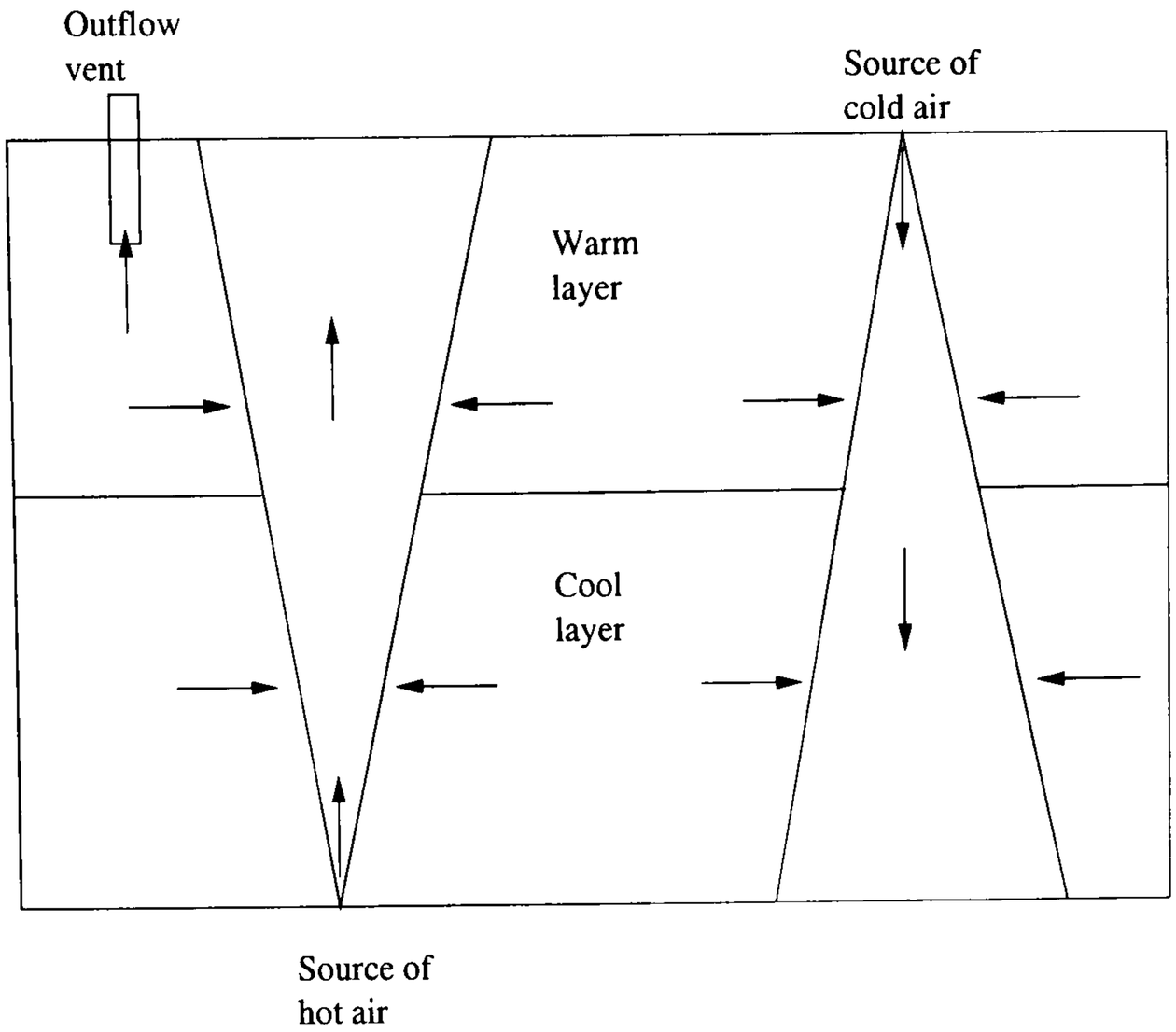

FIGURE 2.1: Illustration of the dual-plume system In this situation, the plumes are depicted as arising due to inflows of relatively hot and cold air. A distinct interface separates the two well-mixed fluid layers.

conservation of total buoyancy flux of each plume. These are represented by equations (2.8) and (2.9).

Consequently, when $t \geq T$, we may assume that both of the fluid layers are well-mixed to leading order. The time required to converge to the steady-state solution depends upon the initial conditions. If the system starts with static initial conditions, namely the initial configuration is identical to the final equilibrium state, the system remains in steady state and does not evolve. Otherwise, the system typically takes a time comparable to T to reach the steady-state. The system is illustrated in figure 2.1, with the plumes depicted as turbulent flows of relatively hot and cold air.

We begin to model the steady-state system by considering the conserva-

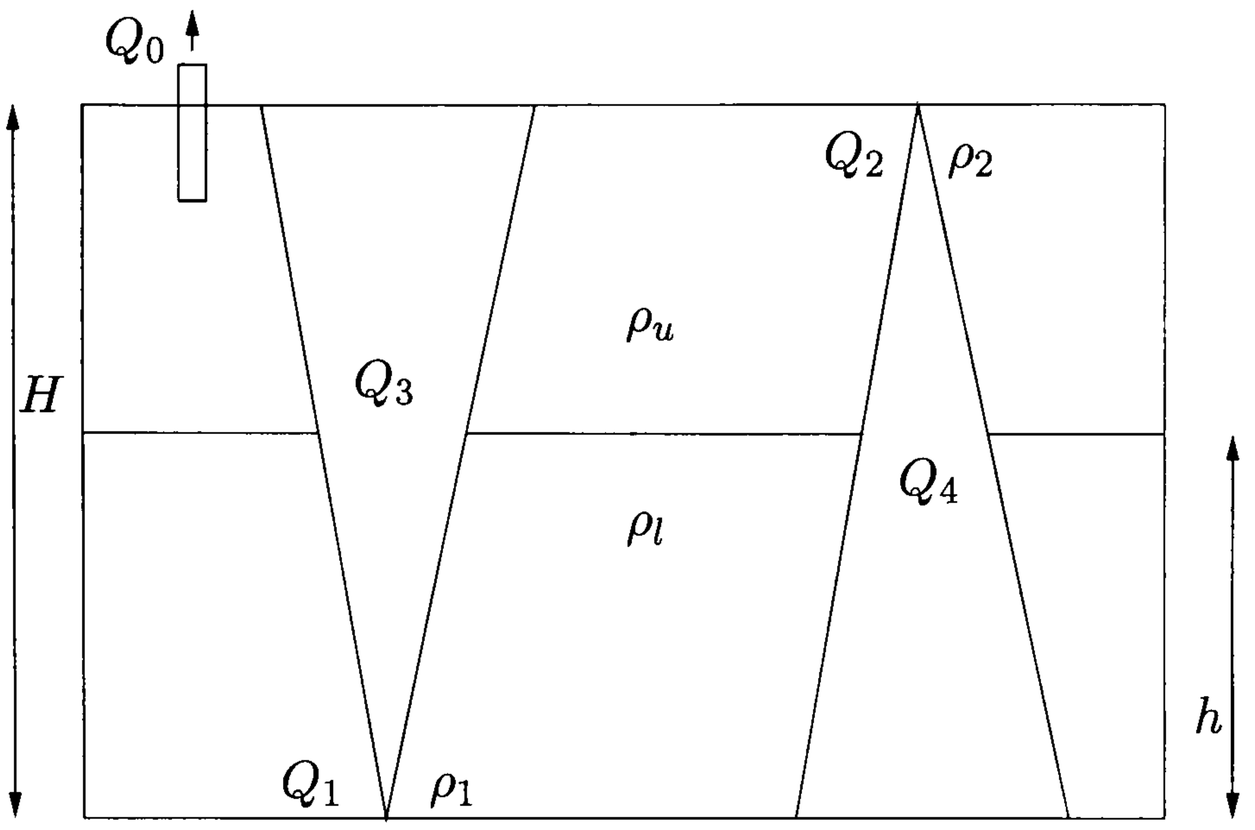

FIGURE 2.2: Depiction of the defining parameters utilised in the mathematical formulation of the dual-plume filling box system.

tion of quantities within the container. Therefore, without loss of generality, we may take $\rho = \rho(C)$. Figure 2.2 shows the labels attached to each parameter.

Global conservation of mass implies that

$$Q_1 + Q_2 = Q_0 \tag{2.2}$$

and global conservation of the conserved quantity C, a property associated with the buoyancy of the fluid, may be written as:

$$Q_1\rho_1 + Q_2\rho_2 = Q_0\rho_0 \tag{2.3}$$

where Q_1 and Q_2 are the initial mass fluxes of the ascending and descending plumes respectively. If we denote the flux associated with the ascending plume across the interface as Q_3, and the flux across the interface due to the descending plume as Q_4, then conservation of mass in the lower layer gives

$$Q_1 + Q_4 = Q_3 \tag{2.4}$$

while conservation of C is given by

$$Q_1\rho_1 + Q_4\rho_4 = Q_3\rho_3 \tag{2.5}$$

Since both the upper and lower layers are well-mixed, we may write similar conservation relations for the lower layer. Mass conservation gives:

$$Q_2 + Q_3 = Q_0 + Q_4 \tag{2.6}$$

and application of conservation of the conserved property C gives:

$$Q_2\rho_2 + Q_3\rho_3 = Q_0\rho_u + Q_4\rho_4 \tag{2.7}$$

While the ascending plume is flowing through the lower layer, the buoyancy flux of the plume is conserved. This follows from the steady-state condition that the total flux of buoyant fluid entering the container equals the total flux of buoyant fluid leaving the system via the outflow vent. This leads to the relation

$$Q_1\left(\rho_1 - \rho_l\right) = Q_3\left(\rho_3 - \rho_l\right) \tag{2.8}$$

For the descending plume flowing through the upper fluid layer, the buoyancy flux is also conserved. Hence, we may apply an identical argument to yield

$$Q_2\left(\rho_2 - \rho_u\right) = Q_4\left(\rho_4 - \rho_u\right) \tag{2.9}$$

The net mass flux across the interface is given by an identical expression to equation (2.4):

$$Q_3 = Q_4 + Q_1 \tag{2.10}$$

We now derive a result for the eventual density associated with each of the plumes. This condition arises as a consequence of the steady-state condition referred to above. As the plumes flow through the fluid layer in which they originate to the interface, they become diluted due to entrainment of ambient

fluid. When they propagate through the interface, they possess a density equal to the fluid layer that they arrive in. This is because, in steady-state, the density of each fluid layer does not change.

Hence, the ascending plume entrains fluid from the lower layer such that at $z = h$, the density of the ascending plume is equal to the density of the upper layer. Therefore, the ascending plume replaces the upper-layer fluid entrained by the descending plume. Further, in the upper layer, say, the ascending plume mixes the ambient fluid. This acts to cause the ambient fluid to become approximately well-mixed. The descending plume has a similar effect upon the lower layer. Consequently, upon combining (2.5) and (2.8), we have

$$\rho_4 = \rho_l \tag{2.11}$$

upon using equation (2.4). The same argument may be applied to the upper fluid layer, and so upon combining (2.7) and (2.9), we find:

$$\rho_3 = \rho_u \tag{2.12}$$

We now proceed to find explicit expressions for the upper and lower layer densities. Using equation (2.4) in equation (2.8) gives:

$$Q_1\rho_1 - Q_3\rho_3 = \rho_l\left(Q_1 - Q_3\right) = -Q_4\rho_l \tag{2.13}$$

and hence

$$\rho_l = \frac{Q_3\rho_3 - Q_1\rho_1}{Q_4} \tag{2.14}$$

Taking equation (2.6) in equation (2.9) gives:

$$Q_2\rho_2 - Q_4\rho_4 = \rho_u\left(Q_0 - Q_3\right) \tag{2.15}$$

and with some further algebraic manipulation, we have

$$\rho_u = \frac{Q_2\rho_2 - Q_4\rho_4}{Q_1 + Q_2 - Q_3} \tag{2.16}$$

The density equivalence relations then lead to

$$\rho_l = \frac{Q_3\rho_u - Q_1\rho_1}{Q_4} \tag{2.17}$$

$$\rho_u = \frac{Q_2\rho_2 - Q_4\rho_l}{Q_1 + Q_2 - Q_3} \tag{2.18}$$

We now eliminate ρ_u from (2.17) and ρ_l from (2.18) respectively to obtain

$$\rho_u = \frac{Q_1\rho_1 + Q_2\rho_2}{Q_1 + Q_2} \tag{2.19}$$

and

$$\rho_l = \frac{\rho_1 Q_1 (Q_4 - Q_2) + Q_2\rho_2 (Q_4 + Q_1)}{(Q_1 + Q_2) Q_4} \tag{2.20}$$

We expect the system to be stably stratified in steady state, by definition. Hence, we require that $\rho_u < \rho_l$. To verify this, we use equations (2.19) and (2.20):

$$\left(\frac{Q_4 - Q_2}{Q_4}Q_1 + \frac{Q_4 + Q_1}{Q_4}Q_2\right) > Q_1\rho_1 + Q_2\rho_2 \tag{2.21}$$

and

$$\frac{Q_4 - Q_2}{Q_4} < 1 \tag{2.22}$$

$$\frac{Q_4 + Q_1}{Q_4} > 1 \tag{2.23}$$

We therefore need:

$$\left(\frac{Q_4 + Q_1}{Q_4} - 1\right) Q_2\rho_2 > \left(1 - \frac{Q_4 - Q_2}{Q_4}\right) Q_1\rho_1 \tag{2.24}$$

Hence, if $\rho_2 > \rho_1$, then we deduce that $\rho_u < \rho_l$, as required. We conclude that, in steady-state, the dual plume system is always stably stratified. If this were not the case, the possibility would exist of an unstable stratification, and hence an overturning of the two fluid layers.

2.2.1 Plume-driven mixing dynamics

Equations (2.20) and (2.21) specify the upper- and lower-layer densities as functions of the input mass fluxes Q_1 and Q_2, the input densities ρ_1 and ρ_2 and the interfacial mass fluxes Q_3 and Q_4. In order to complete the model to determine the behaviour of the system, and to obtain an explicit expression for the location of the interface, we need to examine the internal mixing processes that occur within the container. These mixing processes arise entirely as a consequence of the propagation of the turbulent buoyant plumes through the confined region.

We therefore need to quantify Q_3 and Q_4. However, the behaviour of a plume which originates from a source possessing a relatively strong associated mass flux as it flows across the interface is complex. For a given buoyancy flux and mass flux there exists a unique momentum flux such that the plume is in so-called pure plume balance, as given by the self-similar solutions of Chapter 1. For other source conditions the flow has a excess or deficit of momentum at the source in comparison to a pure buoyant plume. As a result there will be a transition zone as this additional momentum is dissipated due to entrainment of ambient fluid, and the flow asymptotes to the form of a pure buoyant plume. This axisymmetric pure plume has a so-called *virtual origin* which is defined for the self-similar solution as that point for which the mass and momentum flux would be zero. For simplicity in this work, we assume that the fluid which issues from the actual source is in pure plume balance so that calculation of the location of the virtual origin is relatively straightforward. However, in Chapter 3, where we present some experiments, we provide a further discussion of this effect.

We therefore make the assumption that between the source and the interface position, the plume asymptotes to the classic self-similar form (Morton

et. al., 1956). We may hence derive relatively simple expressions for the interfacial mass fluxes. For the case of a self-similar plume, the solution of the equation representing the specific mass flux has the form (Morton et. al., 1956)

$$Q = \lambda B^{1/3} z^{5/3} \tag{2.25}$$

as a function of the plume buoyancy flux at a vertical distance z from the plume source, with λ an empirical constant (Turner, 1973). The buoyancy flux is defined as

$$B = Qg\beta\left(\rho_p - \rho_e\right) \tag{2.26}$$

where ρ_p and ρ_e are the plume and environment densities respectively. We may define the virtual origins, y_l and y_u, of the ascending and descending plumes respectively, in terms of the buoyancy fluxes at the plume sources, B_1 and B_2, as follows

$$y_l = \left(\frac{Q_1^3}{\lambda^3 B_1}\right)^{\frac{1}{5}} \tag{2.27}$$

$$y_u = \left(\frac{Q_2^3}{\lambda^3 B_2}\right)^{\frac{1}{5}} \tag{2.28}$$

The interfacial volume fluxes are then given in terms of a corresponding virtual origin by:

$$Q_3 = \lambda^{3/2}\left[\frac{g\beta\left(\rho_l - \rho_1\right)}{\rho_o}\right]^{\frac{1}{2}}\left(h_l + y_l\right)^{\frac{5}{2}} \tag{2.29}$$

$$Q_4 = \lambda^{3/2}\left[\frac{g\beta\left(\rho_2 - \rho_u\right)}{\rho_o}\right]^{\frac{1}{2}}\left(h_l + y_u\right)^{\frac{5}{2}} \tag{2.30}$$

We now introduce dimensionless parameters to represent the physical quantities in the system. We denote normalised variables with a caret. The interface position, h, and the densities are scaled according to

$$\hat{h} = \frac{h}{H} \tag{2.31}$$

where H is the vertical height of the container. We define dimensionless fluid densities associated with the system according to the relation

$$\hat{\rho} = \frac{\rho_i - \rho_1}{\rho_2 - \rho_1} \tag{2.32}$$

An appropriate scale for the mass flux is then chosen. We consider a reference plume with input mass flux Q_p defined by

$$Q_p = \lambda^{\frac{3}{2}} \left[\frac{g\beta\left(\rho_2 - \rho_1\right)}{\rho_0}\right]^{\frac{1}{2}} H^{\frac{5}{2}} \tag{2.33}$$

Hence, Q_p defines a plume with a maximal density contrast flowing the total vertical extent of the container. We may then scale the source mass fluxes by this quantity to give

$$R = \frac{Q_1}{Q_p} \tag{2.34}$$

$$S = \frac{Q_2}{Q_p} \tag{2.35}$$

R and S are quantities which represent the normalised magnitudes of the mass flux associated with the ascending and descending sources respectively. In the limit $R << 1$, $S << 1$, the initial specific momentum flux and the initial volume flux of each plume are in the same balance as plume which has risen from a point source of buoyancy alone. This is the case studied by Baines & Turner (1969). The dimensionless interfacial mass fluxes now take the form

$$\hat{Q}_3 = \frac{Q_3}{Q_p} = \hat{\rho}_l^{\frac{1}{2}} \left(\hat{h} + \hat{h}_l\right)^{\frac{5}{2}} \tag{2.36}$$

$$\hat{Q}_4 = \left(1 - \hat{\rho}_u\right)^{\frac{1}{2}} \left(1 - \hat{h} + \hat{h}_u\right)^{\frac{5}{2}} \tag{2.37}$$

Where $\hat{h}_u$ and $\hat{h}_l$ are the virtual origins associated with the ascending plume and the descending plume respectively. Hence, the interfacial mass fluxes are functions of $\hat{h}$, the native fluid layer density and their respective virtual origin. We therefore need an expression for the location of the interface

and the plume virtual origins. The ascending plume input mass flux, Q_1, is defined as

$$Q_1 = \lambda^{\frac{3}{2}} \left[\frac{g\beta\left(\rho_l - \rho_1\right)}{\rho_o}\right]^{\frac{1}{2}} \left(h_l\right)^{\frac{5}{2}} \tag{2.38}$$

so that, upon scaling by Q_p, we have:

$$R = \hat{\rho}_l^{\frac{1}{2}} \hat{h}_l^{\frac{5}{2}} \tag{2.39}$$

and similarly for Q_2:

$$S = \left(1 - \hat{\rho}_u\right)^{\frac{1}{2}} \hat{h}_u^{\frac{5}{2}} \tag{2.40}$$

Using equations (2.40) and the normalised form of the expression for the density of the upper-layer fluid, we may now express the descending plume virtual origin in terms of the input mass fluxes:

$$S = \left[1 - \frac{S}{R+S}\right]^{\frac{1}{2}} \hat{h}_u^{\frac{5}{2}} \tag{2.41}$$

and hence

$$\hat{h}_u = S^{\frac{2}{5}} \left(\frac{R+S}{R}\right)^{\frac{1}{5}} \tag{2.42}$$

Upon using equation (2.4), we may derive the expression for the ascending plume virtual origin:

$$\hat{\rho}_l^{\frac{1}{2}} \left(\hat{h} + \hat{h}_l\right)^{\frac{5}{2}} = R + \left(1 - \hat{\rho}_u\right)^{\frac{1}{2}} \left(1 - \hat{h} + \hat{h}_u\right)^{\frac{5}{2}} \tag{2.43}$$

Invoking the previous scalings, the layer densities become:

$$\hat{\rho}_u = \frac{S}{R+S} \tag{2.44}$$

$$\hat{\rho}_l = \left(\frac{S}{R+S}\right) \left[\frac{R + \left(\frac{R}{R+S}\right)^{\frac{1}{2}} \left(1 - \hat{h} + \hat{h}_u\right)^{\frac{5}{2}}}{\left(\frac{R}{R+S}\right)^{\frac{1}{2}} \left(1 - \hat{h} + \hat{h}_u\right)^{\frac{5}{2}}}\right] \tag{2.45}$$

and so we may therefore obtain an expression for the ascending plume virtual origin:

$$\hat{h}_l = \left(\frac{R}{S}\right)^{\frac{2}{5}} \left[\frac{(R+S)\left(\frac{R}{R+S}\right)^{\frac{1}{2}} \left(1 - \hat{h} + S^{\frac{2}{5}} \left(\frac{R+S}{S}\right)^{\frac{1}{5}}\right)^{\frac{5}{2}}}{R + \left(\frac{R}{R+S}\right)^{\frac{1}{2}} \left(1 - \hat{h} + S^{\frac{2}{5}} \left(\frac{R+S}{S}\right)^{\frac{1}{5}}\right)^{\frac{5}{2}}}\right]^{\frac{1}{5}} \tag{2.46}$$

Manipulation of equation (39) results in the following expression for the virtual origin associated with the ascending plume:

$$\hat{h}_l = \left(\frac{R}{\hat{\rho}_l^{\frac{1}{2}}} \right)^{\frac{2}{5}} \tag{2.47}$$

We now have an expression relating the interface position with the plume input mass fluxes:

$$\hat{h} - \left[\gamma \left(1 - \frac{S}{R+S} \right)^{\frac{1}{2}} + R \right]^{\frac{2}{5}}$$
$$\cdot \frac{1}{S}^{\frac{1}{5}} \left[\frac{\gamma (R+S) \left(\frac{R}{R+S} \right)^{\frac{1}{2}}}{R + \gamma \left(\frac{R}{R+S} \right)^{\frac{1}{2}}} \right]^{\frac{1}{5}} + \hat{h}_l = 0 \tag{2.48}$$

where

$$\gamma = \left[1 - \hat{h} + S^{\frac{2}{5}} \left(\frac{R+S}{S} \right)^{\frac{1}{5}} \right]^{\frac{5}{2}} \tag{2.49}$$

Before obtaining numerical solutions of this expression, we may perform some algebra to test the consistency of the relation. Firstly, we wish to confirm that in the limit of sources with vanishingly small mass fluxes that the system tends to the zero associated mass flux case of Baines & Turner (1969). To do this, we examine the expression for $\hat{h}_l = 0$ and $S\,, R << 1$. We arrive at:

$$h - \left[\left(\frac{1}{2} \right)^{1/2} \left(1 - h + 2^{1/5}\, S^{2/5} \right)^{5/2} + S \right]^{2/5}$$
$$\cdot \left(\frac{1}{S} \right)^{1/5} \left[\frac{2S\ (1/2)^{1/2} \left(1 - h + 2^{1/5}\, S^{2/5} \right)^{5/2}}{S + \left(1 - h + 2^{1/5}\, S^{2/5} \right)^{5/2}} \right]^{1/5} = 0 \tag{2.50}$$

This expression simplifies to

$$h - \left[(1-h)^{5/2} \right]^{2/5} = 0 \tag{2.51}$$

Therefore:

$$h = \frac{1}{2} \tag{2.52}$$

and so in the limit of sources with vanishingly small associated mass fluxes, the model tends to the solution obtained by Baines & Turner (1969). Before embarking upon a discussion of the solutions of equation (2.48) above, we note that the derivation of the model presented in this section is for the case whereby the outflow vent is located in the upper fluid layer. Unless indicated otherwise, this is the situation in which the results of the next section have been obtained. However, we note that by applying the transformations

$$\hat{h} \to H - h \tag{2.53}$$

$$R \to S \tag{2.54}$$

$$S \to R \tag{2.55}$$

we arrive at the respective equations for the case when the outflow vent is located in the lower fluid layer.

2.3 Numerical Calculations

Equation (2.48) specifies the interface position in terms of the dimensionless initial mass fluxes associated with the fluid sources. We solve this expression numerically to calculate the interface position for varying values of R and S. To proceed, we examine first the special case for which $R = S$. We then consider the more general situation where the initial mass fluxes associated with the fluid sources are unequal in magnitude.

2.3.1 The Equal-Magnitude Case

We commence by examining the steady-state system when the plume sources possess equal-magnitude associated mass fluxes. Firstly, we examine the system in the limit $R \to 0$. We then consider the situation where R increases

in magnitude, away from the small-mass flux case. Finally, we look at the situation for which $R >> 1$. This introduces a key feature: a system which exhibits a single, well-mixed fluid layer. This is a novel result that has not been studied in any previous research. In section 2.3.3, we present a simple but powerful theoretical argument to explain the physics of this effect. Further, we show that the theory is in exact agreement with the numerical solution.

2.3.2 The Limit of Small Mass Fluxes: $R = S \to 0$

We begin by briefly reviewing the results of Baines & Turner (1969), who studied a dual-plume filling-box system driven by sources which possessed zero associated mass fluxes. We do this because in the limit $R \to 0$, the model derived in section 2.2 of the current work should reduce to the Baines & Turner (1969) case.

They found that two distinct fluid layers formed with the interface between the layers located at $\hat{h} = H/2$, where H is the height of the container. The upper and lower layer densities had values of $\overline{\rho} + \Delta\rho_0$ and $\overline{\rho} - \Delta\rho_0$ respectively, where Δ is the difference in density between the plume and its initial layer, ρ_0 is a reference density and $\overline{\rho}$ is defined in terms of the source input densities. We therefore expect that the principle effect of the provision of sources which supply a flux of mass as well as buoyancy is to move the location of the interface away from $H/2$.

Hence, when $R << 1$, we expect that $\hat{h} \sim 0.5$. The numerical solution of equation (2.48) is shown in figure 2.3. This is a curve depicting the location of the fluid interface as a function of R, the mass flux associated with the ascending plume. Note that the abscissa is displayed on a logarithmic scale. There are two points of principal interest about the solution curve in figure

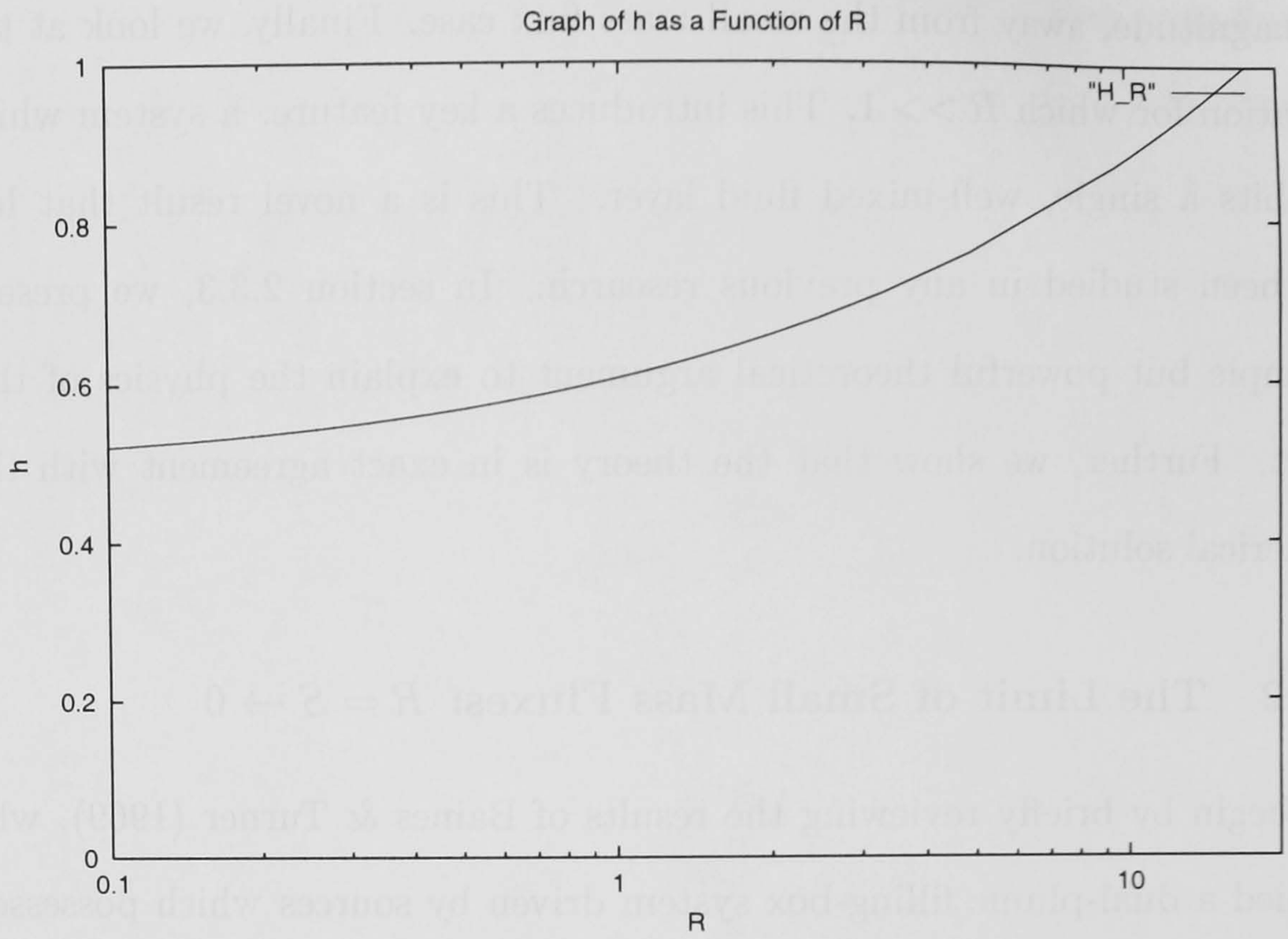

FIGURE 2.3: Location of the fluid interface as a function of the normalised mass flux associated with the ascending plume. The curve shows the interface location in the situation of both of the plume sources possessing equal initial mass fluxes. When $R = 17.3$, $\hat{h} = 1$. We refer to this as the critical value of R.

2.3. The first is that when $R << 1$, the value of $\hat{h} \to 0.5$. Hence, in the limit of sources with relatively small initial associated mass fluxes, the model in the present work does indeed reduce to the zero-associated mass flux case studied by Baines & Turner (1969). This is a very important observation, since it implies that the new results presented in this work represent are compatible, in the limit of sources such that $R \to 0$, with the previous research in this area. The second point to note about the curve in figure 2.3 is that it increases monotonically as R increases. We discuss this further in the next section.

Figure 2.4 is a graph of $\hat{\rho}_l$ as a function of R obtained by numerical solution of equations (2.45) and (2.48). We note that when $R = 0.1$, $\hat{\rho}_l \sim 0.6$.

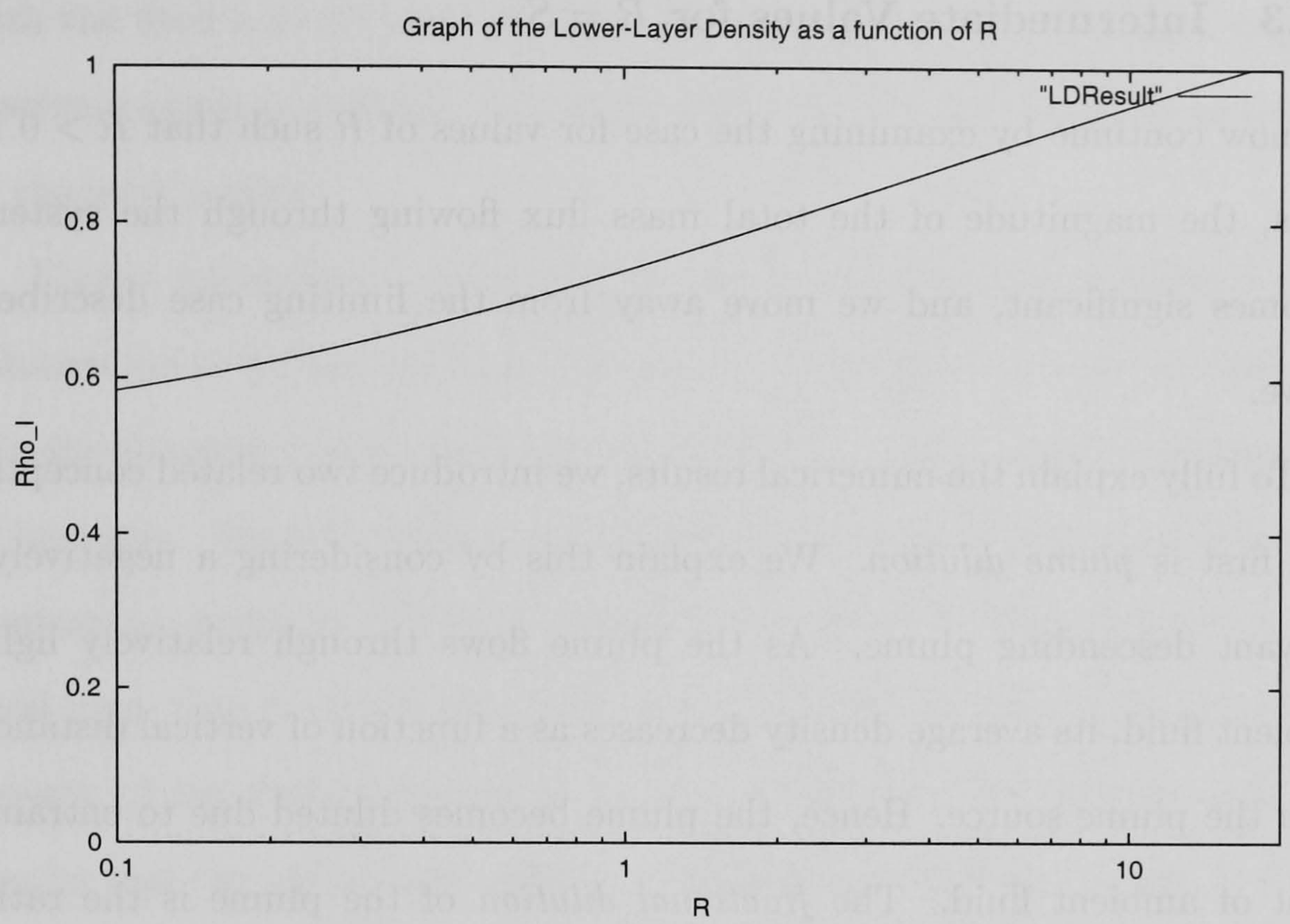

FIGURE 2.4: Density of the lower fluid layer as a function of mass flux associated with the ascending plume in the case of equal initial mass fluxes.

Further, from equation (2.44), we find that when $R = S$ the expression has the constant value

$$\hat{\rho}_u = \frac{1}{2} \tag{2.56}$$

This is a remarkable result. It states that when the mass fluxes associated with the fluid sources are equal in value, the density of the upper fluid layer is *independent* of R and S. This is a key result with very important implications in the applying the model to ventilation of buildings. This is discussed further in §2.4.

Therefore, we see that in the limit $R \to 0$, the difference in density between the upper and lower fluid layers is small, but $\hat{\rho}_l > \hat{\rho}_u$. This is again consistent with the results in Baines & Turner (1969).

2.3.3 Intermediate Values for $R = S$

We now continue by examining the case for values of R such that $R > 0.1$. Thus, the magnitude of the total mass flux flowing through the system becomes significant, and we move away from the limiting case described above.

To fully explain the numerical results, we introduce two related concepts. The first is *plume dilution*. We explain this by considering a negatively-buoyant descending plume. As the plume flows through relatively light ambient fluid, its average density decreases as a function of vertical distance from the plume source. Hence, the plume becomes diluted due to entrainment of ambient fluid. The *fractional dilution* of the plume is the ratio of the total plume dilution to the initial mass flux of the plume flow. We will subsequently use these concepts to elaborate upon the physics of the dual-plume filling-box system.

The first departure from the case of Baines & Turner (1969) is the relocation of the fluid interface. We expect this to occur because of the location of the outflow vent, which during this discussion we consider to be in the upper fluid layer. Because of this inherent asymmetry in the system, mass continuity dictates a net up-flow occurs in the container. The relative magnitude of this up-flow is dependent upon the mass of fluid flowing into the system via the plume sources. Global conservation of mass implies that when there is a large mass of fluid entering the confined region via the sources, the net up-flow will be large. The location of the fluid interface is therefore displaced vertically upwards. We may confirm this prediction by examining figure 2.3. The effect upon the system of increase in R is depicted pictorially in figures 2.4 and 2.5. As noted previously, the interface location $\hat{h}$ is a monotonically increasing function of R. We also note that if the mass fluxes associated

with the fluid sources becomes large enough, the interface vanishes and the system comprises a single, well-mixed fluid layer. We discuss this situation in the next section.

Figure 2.4 shows $\hat{\rho}_l$ as a function of R. In a similar manner to the solution curve for the interface location as a function of R, we see that the density associated with the lower fluid layer also monotonically increases as R increases. We may explain this as follows. Firstly, following on from the assumption made in §2.2 that each plume possesses a density equal to the fluid layer that it terminates in, we note that the lower layer density is the density of the descending plume at $\hat{z} = \hat{h}$. Further, we already have the results that the upper layer density is independent of R and S and that the depth of the upper fluid layer decreases as R and S increase. Hence, the descending plume is less diluted with fluid from the upper layer when the upper layer is less deep. Further, the fractional dilution of the descending plume decreases as its source mass flux increases. From these facts, we may deduce that the density of the lower fluid layer increases as the plume mass flux increases. This is shown in figure 2.6.

In conclusion, we note that a principle effect of the addition of mass to the steady-state system is to cause the fluid interface to be located above $H/2$. This has the additional effect of increasing the density of the lower fluid layer. The reason for the interface to be located closer to the top of the container as the source mass flxues increase is due to the mass sink being located in the upper fluid layer. This creates an asymmetry in the system, because it implies that there will always be a net up-flow in the confined region. As the total flux of fluid mass flowing through the finite region increases, the net up-flow also increases. Hence, the asymmetry in the system becomes more pronounced.

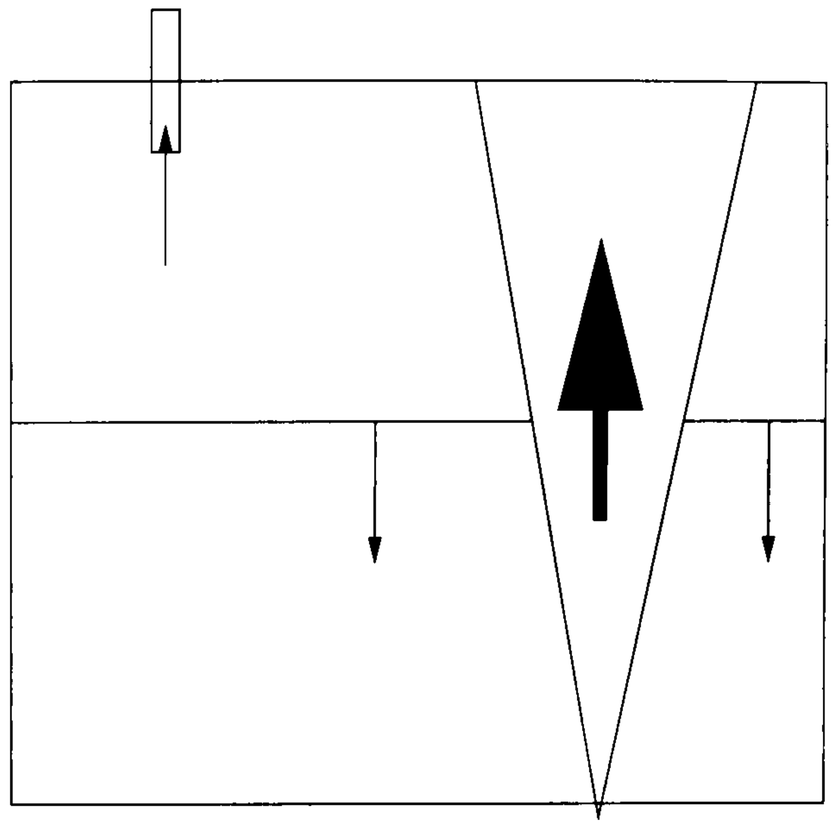

FIGURE 2.5: Illustration of the contribution to the net flow in the system due to the ascending plume. A entrainment flux, greater than the initial mass flux, arrives in the upper layer. A large proportion of this flux leaves the system via the mass sink. Hence, the downward return flow is relatively weak.

2.3.4 The Single-Layer System for $R = S$

In the previous sections, examination of figure 2.3 implied that there exists a value of R for which the system comprised a single, well-mixed fluid layer. We refer to this as the *critical value* of R. Evaluation of the critical value is essential if the single-layer system is to useful in applications. Hence, in this section, we describe a theoretical prediction for the critical value of R. Further, we show that this is in exact agreement with the numerical solution presented in figure 2.3.

We may define the dimensionless fractional plume dilution $\hat{D}$ as follows:

$$\hat{D} = \frac{\left[Q\left(\hat{h}_i + H\right) - Q\left(\hat{h}_i\right)\right]}{Q\left(\hat{h}_i\right)} \tag{2.57}$$

Equation (2.56) therefore represents the total volume of ambient fluid entrained by the plume after it has flowed a distance H, less its source mass

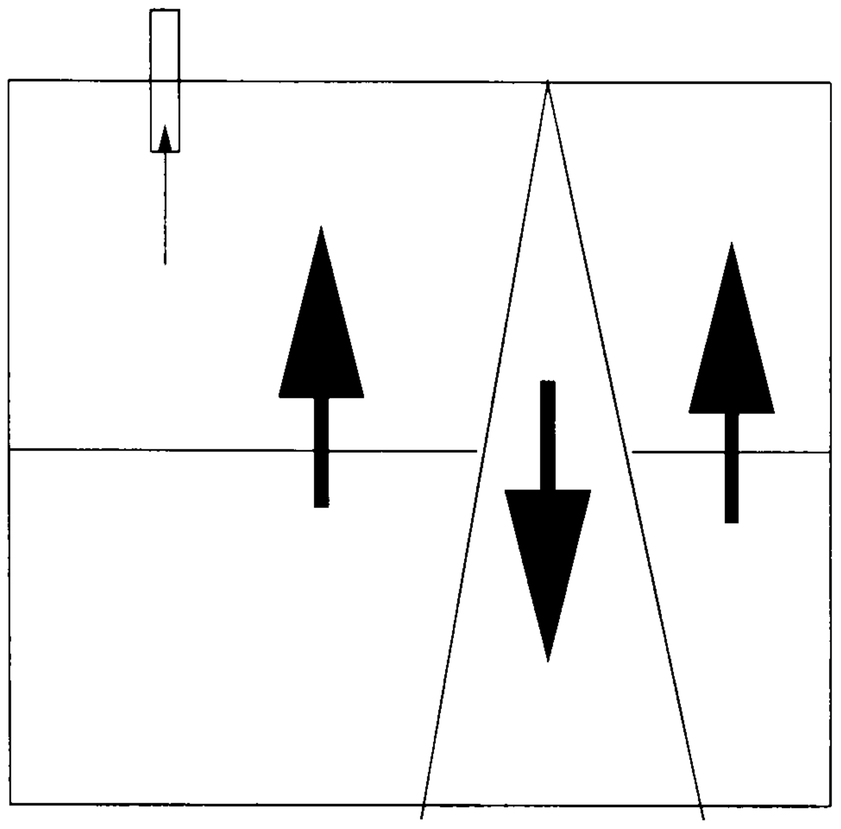

FIGURE 2.6: Diagram illustrating the contribution to the net up-flow in the system that manifests due to the entrainment flux associated with the descending plume. The resulting up-flow is strong due to the relatively large volume flux arriving in the lower layer.

flux, divided by its source mass flux.

Figures 2.5 and 2.6 depict how the net return flow in the container, which originates due to the plumes, is affected by $\hat{D}$. Note that for simplicity, the figures refer to only one of the two plumes in the dual-plume system.

When $\hat{D} > 1$, the system comprises a two-layer stratification. This occurs because the ascending plume has a relatively large net entrainment flux compared with its initial mass flux. Hence, the ascending plume generates a relatively large return flow at the upper horizontal boundary. However, when $\hat{D} < 1$, there exists a single, well-mixed fluid layer. This is because the ascending plume entrains a relatively small amount of ambient fluid as it flows through the container. Consequently, the return flow at the upper boundary is relatively small. Hence, all the fluid associated with the ascending plume vents through the mass sink. The result is that the system only

has a single, well-mixed fluid layer.

Therefore, to find the critical value of R, namely the minimum value of R such that the system comprises a single layer, we examine the limiting case of $\hat{D} \to 1$. Hence, we have:

$$1 = \frac{\left(\hat{h}_l + 1\right)^{5/2} - \hat{h}_l^{5/2}}{\hat{h}_l^{5/2}} \tag{2.58}$$

After some algebra, we arrive at the expression

$$\hat{h}_l = \left(\frac{1}{2^{2/5} - 1}\right) \tag{2.59}$$

Now, from equation (2.4.7):

$$\hat{h}_l = \left(\frac{R}{\hat{\rho}_l^{1/2}}\right)^{2/5} \tag{2.60}$$

However, when there is only a single fluid layer, the density of the lower layer is equal to the input density of the descending plume. Hence, $\hat{\rho}_l = 1$, and so we have

$$\hat{h}_l = R^{2/5} \tag{2.61}$$

Substituting for R in the above expression, we have:

$$R = \left(\frac{1}{2^{2/5} - 1}\right)^{5/2} = 17.32 \tag{2.62}$$

This is exactly the same critical value of R predicted by the numerical solution.

2.3.5 The Unequal-Magnitude Case

We now continue by considering the more general case, for which $R \neq S$. This situation introduces a new asymmetry in the system, since it follows that one of the mass fluxes associated with the fluid sources may be much greater in magnitude than the other.

We therefore introduce a dimensionless parameter, $R*$, to indicate the relative magnitude of the asymmetry between the sources. We define this variable according to:

$$R* = \frac{R}{R+S} \tag{2.63}$$

In the next two sections, we examine the numerical results by considering separately the two limiting cases of $R* \to 0$ and $R* \to 1$. These correspond to $S >> R$ and $R >> S$, the two situations for which the asymmetry in the mass fluxes is greatest in magnitude.

We note also that when $R \neq S$, the fractional dilutions of each plume will not be equal in magnitude. This in contrast to the equal-magnitude case described previously. However, we will show that the relative magnitudes of the fractional plume dilutions are again the key to understanding the behaviour of the system.

Before discussing the details of the three possible situations, we also note that the density associated with the upper-layer fluid is no longer independent of R and S, as in the equal-magnitude case. Equation (2.44) specifies $\hat{\rho}_u = S/(R+S)$, and hence the upper-layer density is a function of the mass fluxes associated with the fluid sources only.

2.3.6 $R* \to 0$: Weak Ascending Plume, Strong Descending Plume

First, we examine the case for $R* \to 0$. In this situation, the initial mass flux associated with the descending plume is much greater than the flux of mass associated with the ascending plume. This implies that the all of the entrained fluid flux associated with the ascending plume will vent via the mass sink. In this case, the system should comprise a single fluid layer.

Figure 2.7 shows solution curves for the location of the fluid interface

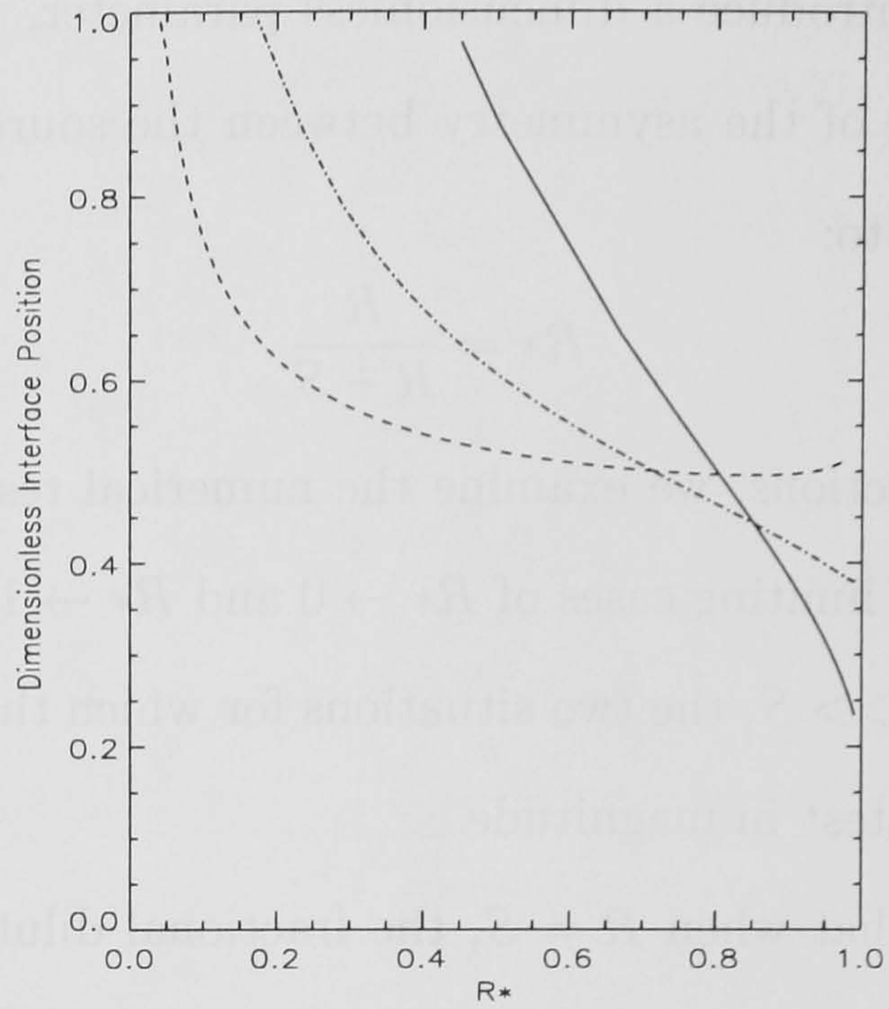

FIGURE 2.7: Location of the fluid interface as a function of $R*$ in the case of sources possessing unequal initial mass fluxes. The curves are plotted for three constant values of R, namely: — —, $R = 0.1$; — - — - —, $R = 1.0$; ——, $R = 10.0$.

as a function of $R*$ for the three constant values of $R = 0.1, 1.0, 10.0$. We note that for $R* \to 0$, the system does indeed consist of a single fluid layer. However, as the value of R increases, the corresponding critical value of $R*$ also increases. This is apparent from inspection of figure x, where $R*_{crit} \simeq 0.01$ for $R = 0.1$. For the case $R = 10.0$, however, $R*_{crit} \simeq 0.45$.

One of the important results that we wish to explain is how the value of these critical points depend upon the value of R. We begin by examining the case $R = 0.1$, for which the mass flux associated with the ascending plume is relatively small. This implies that the magnitude of $\hat{D}$ for the ascending plume is relatively large, and hence the return flow associated with ascending plume is also large in magnitude. Hence, the system consists of a single layer only as $R \to 0$, when the entrainment flux associated with

the ascending plume is very small. As soon as this becomes significant in magnitude, the return flow associated with the ascending plume is sufficient to cause the system to form two fluid layers.

Conversely, in the case of $R = 10.0$, $\hat{D}_R$ is relatively small. In this situation, the magnitude of the return flow associated with the descending plume is relatively large, and hence the critical point occurs for $R* = 0.5$.

Figure 2.8 shows the density of the lower fluid layer as a function of $R*$. We note that when the room consists of a single, well-mixed fluid layer, the density of the ambient fluid is equal to the input density of the descending plume. Hence, we expect that in the limit $R* \to 0$, the density of the lower fluid layer $\to 1$ for all values of R. Each of the curves in the figure show this behaviour.

2.3.7 $R* \to 1$: Strong Ascending Plume, Weak Descending Plume

We now analyse figure 2.7 for the case of $R* \to 1$. Each of the three curves imply that as the value of R increases, the interface is located progressively closer to the lower horizontal boundary. One of the key questions that which we wish to answer is: can the fluid interface ever reach the floor, or does it just form a shallow lower layer?

To answer this, we examine the fractional dilution associated with each of the plumes. We recall the definition of the fractional plume dilution, $\hat{D}$, from section 2.3.4:

$$\hat{D} = \frac{\left[Q\left(\hat{h}_i + H\right) - Q\left(\hat{h}_i\right)\right]}{Q\left(\hat{h}_i\right)} \tag{2.64}$$

Therefore, as R increases, $\hat{D}_R$ decreases. Conversely, as S decreases, $\hat{D}_S$ increases. Since $\hat{Q}_0 = R+S$, all of the mass flux associated with the ascending plume leaves via the vent. $\hat{D}_R$ is relatively small, since R is relatively large.

Therefore, a relatively large amount of the net entrained flux associated with the ascending plume also leaves the confined region via the mass sink. However, the net entrained flux of the descending plume is large compared with its source mass flux, because $\hat{D}_S$ is relatively large. This implies that there is always a return flow associated with the descending plume, even when $R >> S$. Consequently, the fluid interface never reaches the base of the confined region when the outflow vent is located in the ceiling. This result has important consequences when applied to hazardous gas releases in buildings. For example, suppose that a fire in an adjacent room causes relatively dense smoke-filled air to leak into a potentially-occupied enclosure. If a window, say, is opened in the upper part of this room (perhaps a skylight located in the ceiling, for example), and fresh air is pumped into the enclosure, this strategy is insufficient to completely vent all of the smoke from the room. Further, the layer of diluted smoke will occur at the base of the confined region, potentially affecting inhabitants if the room is very tall.

We now examine figure 2.8 for the case $R* \to 1$. Firstly, we expect that as $R >> S$, $\hat{\rho}_l \to 0$, with $\hat{\rho}_l > \hat{\rho}_u$. We explain this as follows.

As $R*$ increases, $\hat{h}$ decreases, and so the ascending plume has a less deep lower layer to flow through. This implies that it entrains less fluid from the lower layer as $R*$ increases. Hence, the ascending plume arrives at the interface less diluted. Conversely, the density of the descending plume will decrease as $R*$ increases. However, since $\hat{\rho}_u \to 0$, the density of the lower fluid layer will also decrease as $R*$ increases. This is the behaviour shown for all values of R in figure 2.8.

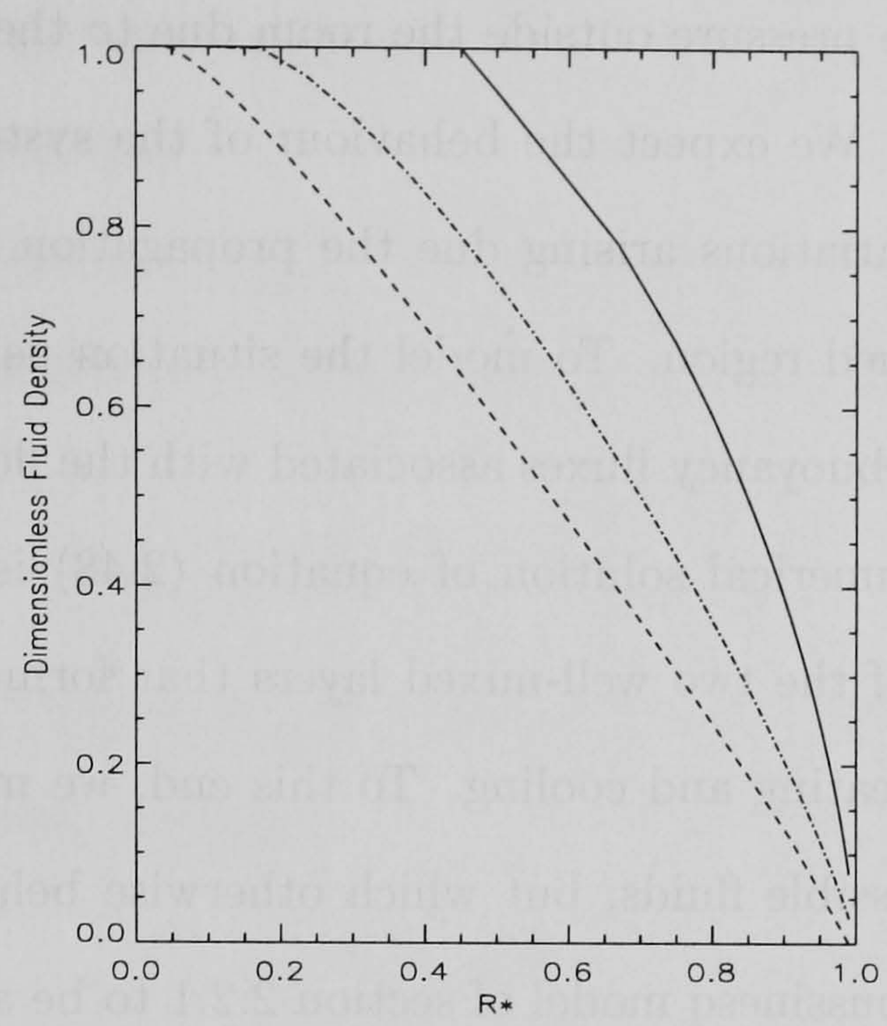

FIGURE 2.8: Density of the lower fluid layer in the unequal-magnitude case. The curves are plotted for the same three values of R, namely: — —, $R = 0.1$; — - — - —, $R = 1.0$; ——, $R = 10.0$.

2.4 Application: Heating and Cooling of a Finite Enclosure

In this section, we describe a direct application of the steady-state dual-plume filling-box model. We consider a large room subject to certain flow conditions. The first of these is air conditioning, represented in the model by a flux of relatively cold fluid. The room also contains a source of heating, represented by an upward-propagating relatively hot flow of fluid. Finally, the room also has an open window, which is considered to be a single-directional mass sink. Physically, we state this assumption as neglecting the effect of wind external to the ventilated region. Hence, fluid in the confined region leaves via the mass sink, but external fluid does not flow into the room through the window. This is valid if the pressure inside the container

is greater than the pressure outside the room due to the presence of external ambient fluid. We expect the behaviour of the system to be governed by temperature variations arising due the propagation of the two plumes through the confined region. To model the situation using this theory, we need to define the buoyancy fluxes associated with the flows of hot and cold air. Then, the numerical solution of equation (2.48) is used to calculate the temperature of the two well-mixed layers that form in a room subject to simultaneous heating and cooling. To this end, we model the intruding flows as incompressible fluids, but which otherwise behave as ideal gases. This allows the Boussinesq model of section 2.2.1 to be applied with loss of generalisation. To determine the buoyancy fluxes of the flows, we begin by using the equation of state for an ideal gas, namely:

$$P = \rho R T \tag{2.65}$$

where R is the molar gas constant. For a small change in temperature ΔT, the corresponding change in density, at constant vaolume and pressure, is given by

$$\Delta\rho = -\left(\frac{P}{RT^2}\right)\Delta T \tag{2.66}$$

Following the derivation of the equation specifying the location of the interface as a function of the mass fluxes associated with the plume sources. we may therefore apply equations (2.43), (2.44) and (2.48) of section 2.2 and evaluate the location of the fluid interface and the respective densities of the two well-mixed layers.

We may define the buoyancy at the sources respectively as

$$B_1 = g\left(\frac{\Delta T_1}{T_0}\right) \tag{2.67}$$

and

$$B_2 = g\left(\frac{\Delta T_2}{T_0}\right) \tag{2.68}$$

because the conserved fluid property in this case is heat flux, and where T_0 is a reference temperature.

We then define a scale for the mass flux associated with the propagation of the two turbulent plumes. This is analogous to equation (2.33), and is defined as

$$Q_p = \lambda^{\frac{3}{2}} \left[\frac{g\,(T_1 - T_2)}{T_0}\right]^{\frac{1}{2}} H^{\frac{5}{2}} \tag{2.69}$$

and we introduce a parameter with which to convert the fluid temperature into dimensionless form, namely

$$\hat{T}_i = \frac{T_i - T_1}{T_2 - T_1} \tag{2.70}$$

We may apply the equilibrium steady-state model for several physically-realistic values of the temperature associated with the intruding fluid and the mass fluxes associated with each the plume sources. We find numerical solutions for five different cubic rooms. The first, room A, has a height of 3 m. Each subsequent room has a height one metre greater than the previous one.

We now proceed by evaluating R and S. Taking $\rho_0 = 1\,\mathrm{kg\,m^{-3}}$, the temperatures associated with the system to be $T_0 = 290\,\mathrm{K}$, $T_1 = 295\,\mathrm{K}$ and $T_2 = 285\,\mathrm{K}$, and so $Q_p = 0.108\,\mathrm{m^3\,s^{-1}}$. Assuming values of $Q_1 = 5 \times 10^{-3}\,\mathrm{m^3\,s^{-1}}$ and $Q_2 = 1 \times 10^{-3}\,\mathrm{m^3\,s^{-1}}$, and $\beta = 4.2 \times 10^{-5}$, we have

Room	Total mass flux	Q_p	Normalised source mass flux
A	$2.4 \times 10^{-3}\,\mathrm{m^3\,s^{-1}}$	$0.108\,\mathrm{m^3\,s^{-1}}$	1.1×10^{-2}
B	$2.4 \times 10^{-3}\,\mathrm{m^3\,s^{-1}}$	$0.221\,\mathrm{m^3\,s^{-1}}$	5.4×10^{-3}
C	$3.47 \times 10^{-3}\,\mathrm{m^3\,s^{-1}}$	$0.387\,\mathrm{m^3\,s^{-1}}$	4.5×10^{-3}
D	$5.00 \times 10^{-3}\,\mathrm{m^3\,s^{-1}}$	$0.610\,\mathrm{m^3\,s^{-1}}$	4.1×10^{-3}
E	$6.81 \times 10^{-3}\,\mathrm{m^3\,s^{-1}}$	$0.897\,\mathrm{m^3\,s^{-1}}$	3.8×10^{-3}

In the case of room A, the lower fluid layer has a temperature of 293.03 K and the interface is located at 1.52 m. In the case of room E, the lower layer temperature is 292.57 K and the interface is located at 3.30 m.

The following table shows the results for each room in the case of sources which possess equal associated mass fluxes.

Room:	$\hat{h}$	$\hat{\rho}_l$
A	0.503	0.512
B	0.502	0.512
C	0.501	0.510
D	0.501	0.509
E	0.501	0.508

In the case of sources which possess unequal associated mass fluxes, such that $R = Q_0/4$, and $S = 3Q_0/4$, we have:

Room A: $\hat{h} = 0.506$, $\hat{\rho}_l = 0.803$.

Room B: $\hat{h} = 0.472$, $\hat{\rho}_l = 0.757$.

We may now evaluate the temperatures in the upper and lower layers. Proceeding analogously to section 2.2, we have $\hat{T}_u = 0.192$ and $\hat{T}_l = 0.929$. Returning to dimensional variables, we find:

$$h = 1.54\text{m} \tag{2.71}$$

$$T_u = 293.1\text{K} \tag{2.72}$$

$$T_l = 285.7\text{K} \tag{2.73}$$

Consequently, the interface is located near the middle of the room. This is consistent with the explanation of the unequal-magnitude case discussed in section 2.3.5, because although the sources are of comparable strength, the

total flux of mass flowing through the room is relatively small. The principle effect of the sources of heating and cooling is to introduce a temperature contrast of $7K$, which occurs across a sharp front.

Faber & Kell (1987) discuss the practical applications of air conditioning in detail. The Health and Safety at Work Act, 1974, recommends that a minimum of 4.7 litre s^{-1} of outside air be provided, per person, to meet the requirements of the act. The London Building (Constructional) By-laws 1972 specify that if a room may not be naturally ventilated, mechanical ventilation of a minimum of $22\,m^3$ per hour per person, or $5\,m^3$ per hour per square metre, whichever is greater, is required

To examine the implications of the latter of these conditions, we apply the model of Chapter 2, and evaluate the steady-state configuration for rooms of different sizes. We make the assumption that the enclosed regions are cubic in shape, and that there are four occupants in each case. The conditions are summarised in the following table:

Room	Height	Ventilation required due to room size
A	3 m	$1.25 \times 10^{-2}\,kg\,m^{-3}$
B	4 m	$2.22 \times 10^{-2}\,kg\,m^{-3}$
C	5 m	$3.47 \times 10^{-2}\,kg\,m^{-3}$
D	6 m	$5.00 \times 10^{-2}\,kg\,m^{-3}$
E	7 m	$6.81 \times 10^{-2}\,kg\,m^{-3}$

Hence, for case A and case B, we use the condition requiring $22\,m^3$ per hour per person, namely $2.4 \times 10^{-2}\,m^3\,s^{-1}$. Hence, we may see that following the guidelines in this case produces two fluid layers of approximately equal

depth. This implies that the fluid interface has a height of at least 1.5 metres, and this is sufficient to allow the relatively hot upper layer to be located above the level of the occupants.

2.5 Conclusions

A model has been formulated for the equilibrium steady-state regime of a system comprising two sources of buoyancy possessing non-zero associated mass fluxes. The model illustrates the importance of the turbulent mixing dynamics upon the global properties of this system. It predicts that two distinct fluid layers form, separated by a well-defined fluid interface. These two layers may be approximated as well-mixed to leading order, and the theoretical model predicts their respective densities and the location of the interface.

Additionally, the effects of the flux of mass flowing through the system are examined in detail, and compared with the case for which the sources possessed zero associated mass flux, which was studied by Baines & Turner (1969). It was found that the system always converges to a stably-stratified configuration, regardless of the mass fluxes associated with the plume sources, as long as the assumptions used in deriving the model are sustained. There is a strong inherent asymmetry present in the system due to the location of the outflow vent. This is apparent even in the case whereby the sources provide equal input mass fluxes to the system. In this case, the principle effect of mass entering the confined region is to displace the fluid interface so that it is located closer to the upper boundary of the container. This subsequently affects the dilution of the plumes as they propagate from their respective sources to the interface location. The descending plume, for example, will flow a shorter vertical distance through a region with a

relatively large density contrast when the fluid interface is located close to the top of the confined region. A notable result is that when the two sources possess equal associated mass fluxes, the upper layer attains a constant density equal to the average of the source input densities. This is independent both of the location of the fluid interface and also the input mass fluxes themselves. The lower-layer density, however, is strongly dependent upon the location of the fluid interface as well as the mass fluxes associated with the plume sources.

One of the most important consequences is the success of both the numerical solution and the analysis of the physics in predicting the circumstances under which initial conditions cause the system to comprise a single fluid layer. In this situation, there is no interface. The region of fluid inside the box is well-mixed to leading order and has an overall density comparable to the input density of the descending plume. This is of great use in many physically relevant scenarios, for example the flushing of a toxic gas leak from the interior of a factory. A detailed application and calculation was presented for the situation of simultaneously heating and venting a room.

Chapter 3

Experiment

"But here there is no light,

Save what from heaven is with the breezes blown,

Through verdurous glooms and winding mossy ways."

– Keats, *"Ode to a Nightingale"*

3.1 Introduction

In this chapter we present some experimental results relating to the steady-state dual-plume filling box system. Our aim is to substantiate both the validity and the predictions of the theoretical model.

In order to test the theory presented in chapter 2, we first consider the experimental configuration for the analogue salt-bath experiments. The magnitudes of the initial mass fluxes associated with the plume sources in the laboratory have a limited range of values which produce turbulent buoyant plume flows in the tanks used in the experiments. Firstly, relatively small

values of R and S give rise to plumes which have a relatively large zone of flow establishment. This is defined as the lengthscale over which the flow has adjusted to be in pure plume balance. Further, plumes with very large values of R and S give rise to flows that are dominated by their initial momentum flux. In this situation, the plumes may have a zone of flow establishment Comparable to the vertical height of the container. Neither of these extremes are well-represented by the assumptions used to derive the fundamental model of Chapter 2. Hence, there is a limited range of values of R and S which lie in-between the two extreme cases described above. Consequently, the range of values that $\hat{h}$ may take, and the subsequent values of $\hat{\rho}_l$, are relatively small. We may test experimentally the predictions of the model of the fundamental system, but not over the entire range of parameter space represented by the numerical solutions.

It is clearly important to gather sufficient experimental data in order to test the theoretical predictions appropriately. The suitable parameter ranges for the values of R and S are discussed further in §3.1.1. A modification to the fundamental model of Chapter 2 was proposed in order to increase the amount of experimental data that could be gathered. This modification kept the essential physics of the original system unchanged. The modified steady-state model is described in §3.2, and elaborated upon further in 3.2.1. In section 3.3, the experiments are discussed. A description of the experimental technique comprises §3.3.1, and some qualitative observations noted throughout the course of the experimental work are detailed in 3.3.2. The results of the experiments are presented in detail in §3.3.3, and the data for the location of the fluid interface for various values of R and S are compared with the corresponding numerical calculations. Finally, the conclusions of this Chapter are drawn and discussed in section 3.4.

3.1.1 Discussion of the Experimental Scales

It is also of importance to note that the construction of the plume sources is significant in ensuring that the resulting plume flows are within the range of mass fluxes representative of the turbulent buoyant plume flows assumed in the model of Chapter 2. If the aperture of the mass sources is too big, the resulting plume flow is distributed over a relatively large area. Such a flow does not conform to the original model due to Morton et. al. (1956), which assumed that the turbulent plume originated from a point source of buoyancy. Such a source is an idealisation, however, and is physically impossible when the resulting flow possesses a finite associated mass flux. However, if the orifice has a very small cross-sectional area, the resulting flow will have a significant jet length. Along this scale, the plume will be dominated by the momentum flux associated with the source conditions. Even for a moderate source of mass with a relatively small cross-sectional area, previous experimental observations indicate that the jet length may be of the order of several centimetres. An expression for the jet length, J, was defined initially by Morton (1959) according to:

$$J = \frac{M_0^{3/4}}{B_0^{1/2}} \tag{3.1}$$

where M_0 and B_0 are the initial fluxes of momentum and buoyancy respectively. In the set of experiments presented here, the values of the jet lengths associated with the turbulent plumes was found to be between $J \sim 1.5 - 2.5\,\mathrm{cm}$.

There also exists a range of values of the associated mass fluxes which approximate a plume flow which is fully turbulent but not dominated by the initial momentum flux at the fluid source. In such a case, the plume flow rapidly adjusts to a self-similar, but fully-developed, turbulent flow

within a relatively small vertical distance from the fluid source. It is plumes originating from such source conditions that may be well represented by the theory of Chapter 2. The experimental results in the present Chapter relate to these source conditions.

We note, however, that restrictions in the values of R and S in the experimental configuration also affect the range of values that may be taken by the densities associated with each fluid layer. This is because the density associated with each fluid layer is a function of R and S, as specified by equations (2.44) and (2.45) of Chapter 2. Therefore, if the assumptions of Chapter 2 cannot be applied to the dimensionless values of the mass fluxes associated with the plume sources, the fluid flows in the experiments will not be accurate representations of the corresponding experimental quantities.

For very large values of the initial source mass fluxes, the plume flows are completely dominated by the vertical component of their initial momentum flux. These effects were observed to be significant enough that the construction of the plume sources still resulted in flows that had a large jet length. In this circumstance, the resulting plumes were of such dimensions that interaction with the vertical boundaries of the container and also with each other, were unavoidable. The flow regime represented by these values is incompatible with the assumptions made in the model of Chapter 2. Experiments were therefore not performed for values representing these source conditions. We may derive an expression to determine whether the plume flow is free of the influence of the vertical boundaries of the container. From the similarity solution of Morton et. al. (1956), we have:

$$Q = \lambda B_0^{1/3} z^{5/3} \tag{3.2}$$

and for the effective radius $b(z)$ as a function of vertical distance from the

source, we have:

$$b(z) = \left(\frac{6\,\epsilon}{5}\right) z \tag{3.3}$$

Combining these two expressions, after some algebra, yields:

$$b(H) = \left(\frac{6\,\epsilon}{5}\right) \left[\frac{Q(H)}{\lambda B_0^{1/3}}\right]^{3/5} \tag{3.4}$$

and so, when $b(H) << L$, where L is the horizontal lengthscale of the confined region, the plume will be free of the influence of the vertical boundaries of the container $\forall\, z$. In terms of the dual-plume filling-box system, this is modified to

$$b_{asc}(z = H) + b_{desc}(z = 0) << L \tag{3.5}$$

so as to consider the effect of both plumes. Over the course of all the experimental work, two different tanks were used. For each tank, $H = 30.0\,\text{cm}$, while the physical height of the containers was $35\,\text{cm}$. All the experimental data presented here was obtained by using a tank for which $L = 44\,\text{cm}$.

3.2 Vertically-Displaced Sources

We desire to obtain a wide range of experimental data in order to test the fundamental model of Chapter 2. Hence, to overcome the restriction of the limited range of values of the initial mass fluxes associated with the fluid sources, it was decided to introduce two perturbations to the fundamental model.

We consider the situation whereby the plume sources are located a vertical distance above and below the lower and upper boundaries respectively. This configuration is depicted in figure 3.1.

A priori, we expect that displacing the fluid sources will cause the interface to be located at a different position compared to the fundamental

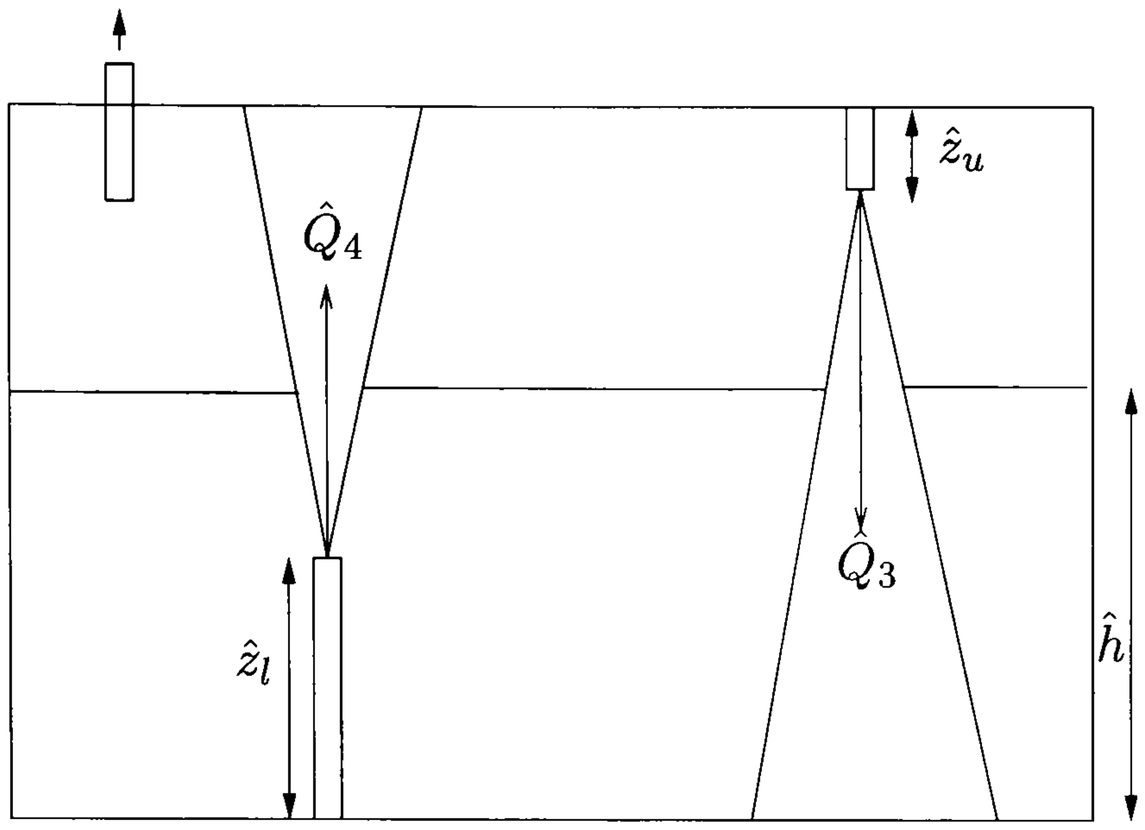

FIGURE 3.1: Illustration of the dual-plume filling-box system with fluid sources displaced from each boundary. $\hat{z}_u$ and $\hat{z}_l$ are defined as shown on the diagram.

system. If the mass fluxes of the plume sources are equal in magnitude, then we expect that the interface is located at the midpoint between them. We incorporate these perturbations into the model by proposing that the principal effect of displacing the sources is to reduce the flux of ambient fluid entrained by the plume as it flows the vertical distance from source to boundary relative to the undisplaced case. Hence, in dimensional form, the volume fluxes of the ascending and descending plumes now have the respective forms:

$$Q_1 = \lambda B_1^{1/3} (h + h_l)^{5/3} \tag{3.6}$$

$$Q_2 = \lambda B_2^{1/3} (H - h + h_u)^{5/3} \tag{3.7}$$

where λ is an empirical constant, B_1 and B_2 are the initial buoyancy fluxes of each plume, h is the vertical distance from the lower boundary, H is the height of the container, and h_l and h_u are the virtual origin terms for the ascending and descending plumes respectively. Normalising as per before,

we have:

$$R = \hat{\rho}_l^{1/2} \hat{h}_l^{5/2} \tag{3.8}$$

$$S = (1 - \hat{\rho}_u)^{1/2} \hat{h}_u^{5/2} \tag{3.9}$$

while the interfacial volume fluxes become

$$\hat{Q}_3 = \hat{\rho}_l^{1/2} \left(\hat{h} + \hat{h}_l - \hat{z}_l \right)^{5/2} \tag{3.10}$$

$$\hat{Q}_4 = \left(1 - \hat{\rho}_u^{1/2} \right) \left(1 - \hat{h} + \hat{h}_u - \hat{z}_u \right)^{5/2} \tag{3.11}$$

Proceeding in a similar manner to Chapter 2, we may use the local conservation equation

$$\hat{Q}_3 = \hat{Q}_4 + R \tag{3.12}$$

to derive an expression for the location of the interface as a function of R and S. If we now introduce a parameter γ, defined according to

$$\gamma = \left(\frac{R}{R+S} \right)^{1/2} \left(1 - \hat{h} + \hat{h}_u - \hat{z}_u \right)^{5/2} \tag{3.13}$$

then equation for the density of fluid associated may now be written as

$$\hat{\rho}_l = \left(\frac{S}{R+S} \right) \left[\frac{R + (1 - \hat{\rho}_u)^{1/2} \left(1 - \hat{h} + \hat{h}_u - \hat{z}_u \right)^{5/2}}{(1 - \hat{\rho}_u)^{1/2} \left(1 - \hat{h} + \hat{h}_u - \hat{z}_u \right)^{5/2}} \right] \tag{3.14}$$

Hence, we may express equation (2.48) in terms of the dimensionless mass fluxes associated with the plume sources and the respective source displacements:

$$\hat{h} = \left[(R+\gamma)^{2/5} - R^{2/5} \right] \left[\left(\frac{R}{R+S} \right)^{1/2} \left(\frac{\gamma}{R+\gamma} \right) \right]^{2/5} + \hat{z}_l \tag{3.15}$$

3.3 Experimental Method

In order to understand the global dynamics of the dual-plume filling box, a series of analogue laboratory experiments were performed. The purpose

of these was twofold. Firstly, observation of the experiments led to the development of physical insight into the behaviour of the system. Secondly, recorded measurements allowed verification of the mathematical model that was derived following the experimental observations. We describe the experimental method in the following section, and in §3.3.2, we comment upon the qualitative observations gained during the course of the experimental work. The empirical results are then presented in 3.3.3.

3.3.1 Description of the Experimental Technique

The experiments were performed using a rectangular glass tank of dimensions 30cm by 30cm by 46cm. A series of test experiments were performed in this container for a wide variety of source mass fluxes. This allowed a range of mass fluxes to be established for which the resulting plume flows were observed to correspond with the assumptions discussed in section 3.2.1. This ensured that the tank was of sufficient volume such that the vertical boundaries did not influence the flow of the turbulent plumes for the proposed range of mass fluxes associated with the fluid sources. These prelimenary experiments consisted of a filling-box flow driven by a single source of buoyancy with an associated flux of mass.

The single-plume filling-box experiments also served another important purpose. In the early stages of the experimental work, ball-bearing flow-meters were used to control the mass flux of fluid supplied to the confined region via the each source. However, the flow-meters were found to be unsatisfactory for the flow rates utilised in the experiments. Hence, the single-plume experiments were used to calibrate two Flowstat electrical pumps. Further, the experiments were repeated for both sources to ensure that their construction was adequate enough to minimise any experimental error.

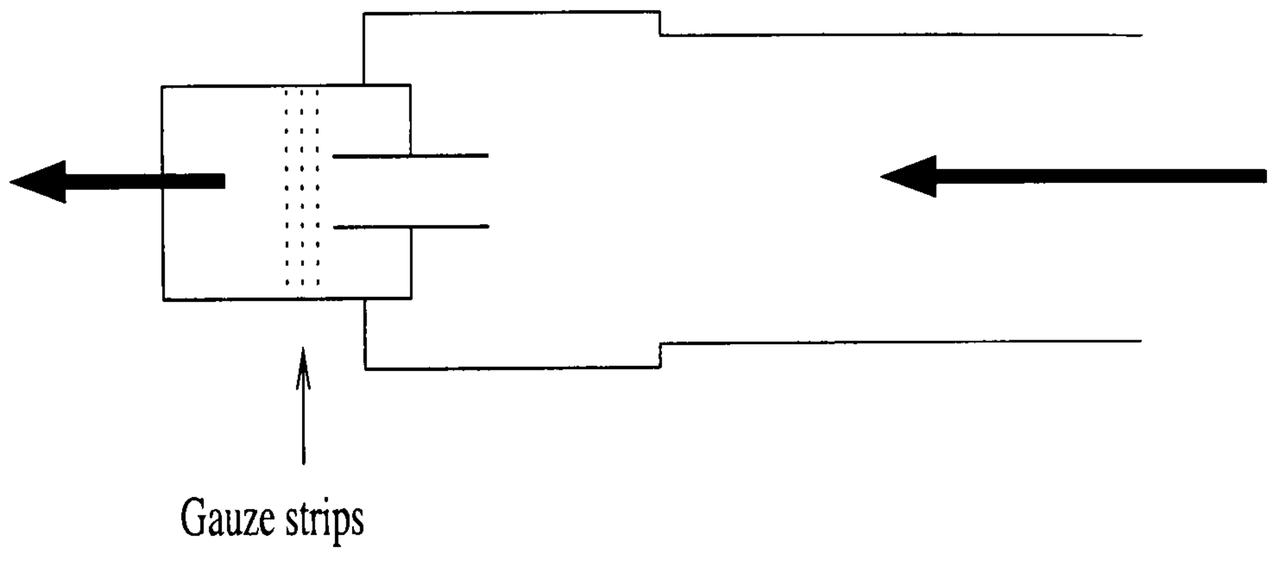

FIGURE 3.2: Schematic illustrating the basic construction of the fluid sources used in the experiments. Arrow indicate the direction of flow through the source, with the exit nozzle located on the left. Note the location of the gauze strips. These are positioned to induce the flow to become turbulent if the volume flux is relatively small.

The buoyant fluids used to create the plumes were driven by two electrical pumps. Density contrasts were created using pure salt to produce aqueous saline solutions. The fluid was dyed using industrial food dye to increase clarity of observation, and visualised using a shadowgraph in conjunction with a video camera. The outflow vent consisted of a siphon connected to a large external reservoir. The plumes were generated via buoyant fluid flowing into custom-built sources. Principally, the sources were designed to reduce the jet-like characteristics associated with plume flows which possessed a large initial mass flux. Their construction is illustrated in figure 3.2. Further, the experimental set-up is depicted in figure x.

The ambient density profile was measured during the experiment by withdrawing small samples of environmental fluid from fixed points within the container. The salinity of these samples was measured using a temperature-compensated refractometer. Great care was taken to minimise disturbances to both the plumes and the fluid interface during the measurement process. This was achieved by using a custom-built frame to suspend the sampling

tubes at the required position within the container. Fluid samples were then carefully withdrawn from the flow field by using a small amount of external suction. This was established by the use of pipettes.

The fluid sampling was repeated at regular time intervals. The location of the fluid interface was measured at each time interval prior to withdrawing fluid. The data for the evolution of the density profile is presented in Chapter 7.

3.3.2 Experimental Observations

The evolution from the initial conditions to steady-state progressed through several distinct stages. The transition to equilibrium was observed to be dependent upon both the initial conditions and the mass fluxes associated with the fluid sources. In this section, however, we are concerned only with experimental results relating to the final equilibrium state. Hence, we will briefly describe the time-dependent stages, delaying a more detailed discussion until Chapter 6. Further, we note that we describe a simple experiment here, leaving a detailed discussion of other possibilities until Chapter 6.

Upon starting the experiment, a turbulent buoyant plume flow originated from each of the fluid sources. The plumes subsequently flowed a vertical distance $\hat{H}$. At this point, each of the turbulent flows encountered the opposite horizontal boundary of the confined region. By continuity, therefore, a return flow associated with each incident plume formed at the upper and lower boundaries of the container.

The return flows were initially formed by a complex flow situation. For the purpose of the following description we refer to the ascending plume only, noting that the other return flow arose in an identical manner. A

short time after the experiment was started, the ascending plume flowed a vertical distance H from it source. At this point, the plume met the upper boundary of the container. Mass conservation indicates that the plume flow will intrude laterally along the horizontal extent of the upper boundary. Hence, two laterally spreading flows propagated away from the point at which the plume encountered the top of the container. These two spreading flows had the form of gravity currents which flowed until they reached the vertical boundaries of the container. At this point, a thin layer of buoyant fluid had formed just below the upper boundary of the confined region.

The mixed regions that formed were initially turbulent in nature, and did not exhibit stable interfaces. However, this wave-like motion settled quite swiftly, leaving the regions with a well-defined density step. The first fronts then propagated uniformly away from the horizontal boundary. Eventually, the two filling-box fronts met at some point within the container. At this time, the system consisted of two well-mixed fluid layers, separated by a well-defined fluid interface. This was the first key step in the establishment of a steady-state configuration. Once the fronts met, the interface location did not change. However, the density associated with each of the well-mixed layers continued to develop until the equilibrium values were reached.

3.3.3 Experimental Results

Experiments were thus performed to build up a picture of the density evolution in the system and the location of the fluid interface when the fluid sources were vertically displaced from their respective boundaries.

Figures (3.6) $-$ $-$(3.8) are photographs of various stages of the experiments.

Figure 3.6 shows a comparison between the theoretically determined lo-

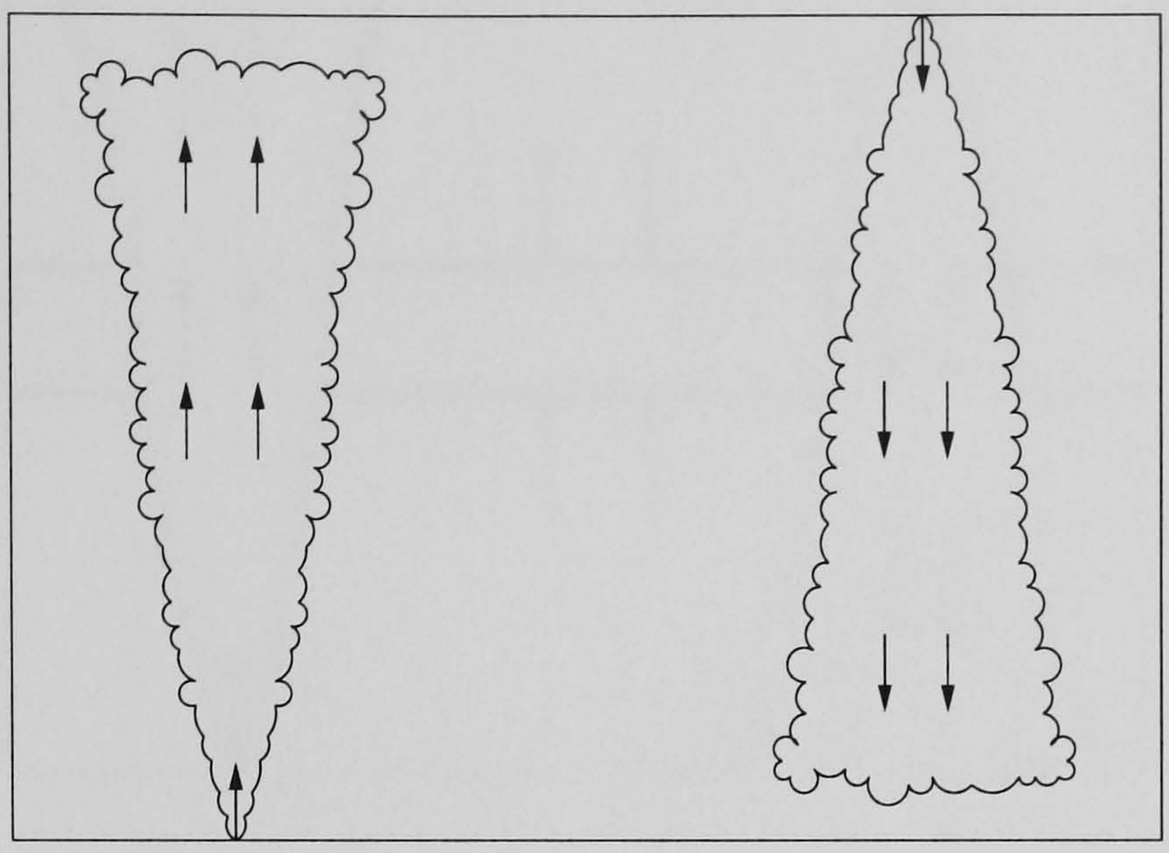

Figure 3.3: Illustration depicting an experiment a short time after initiation. The two turbulent buoyant plumes flow towards the opposite boundaries of the container.

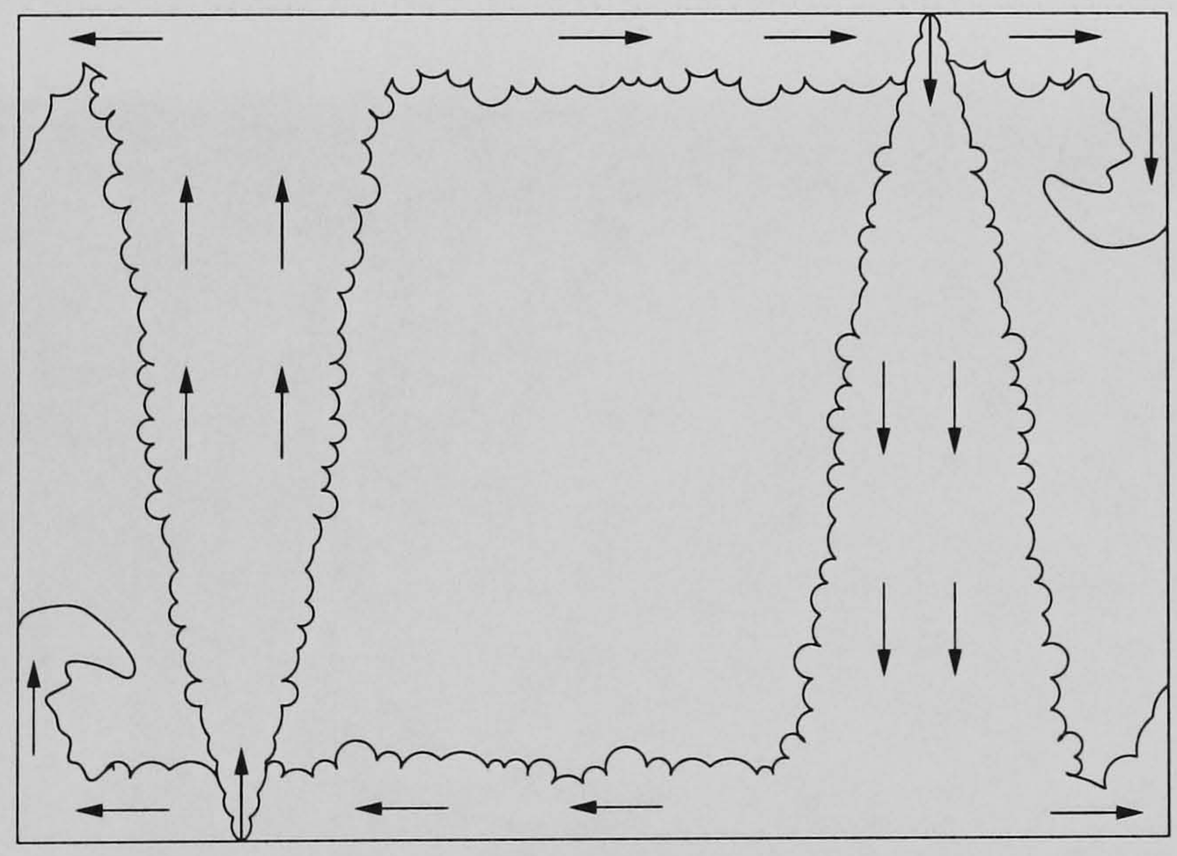

Figure 3.4: Depiction of the system after a small time. The turbulent plumes have reached the vertical extent of the container. The subsequent lateral spread of fluid forms two gravity currents which flow horizontally along the upper and lower boundary of the confined region.

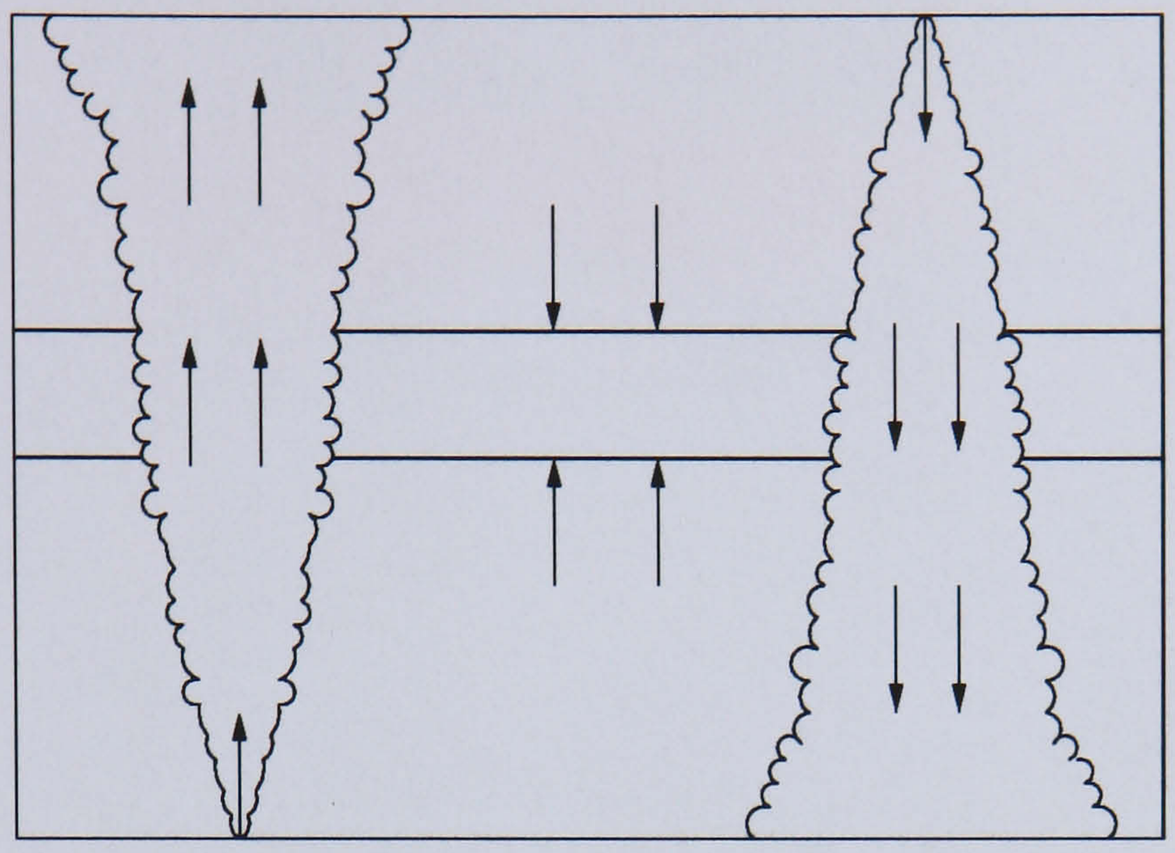

Figure 3.5: Illustration of the subsequent transient stage. The turbulence present in the two mixed regions has dissipated as they have increased in depth. The density steps associated with each of the filling box fronts are distinct and laminar. The two fronts propagate through the confined region towards the centre of the container.

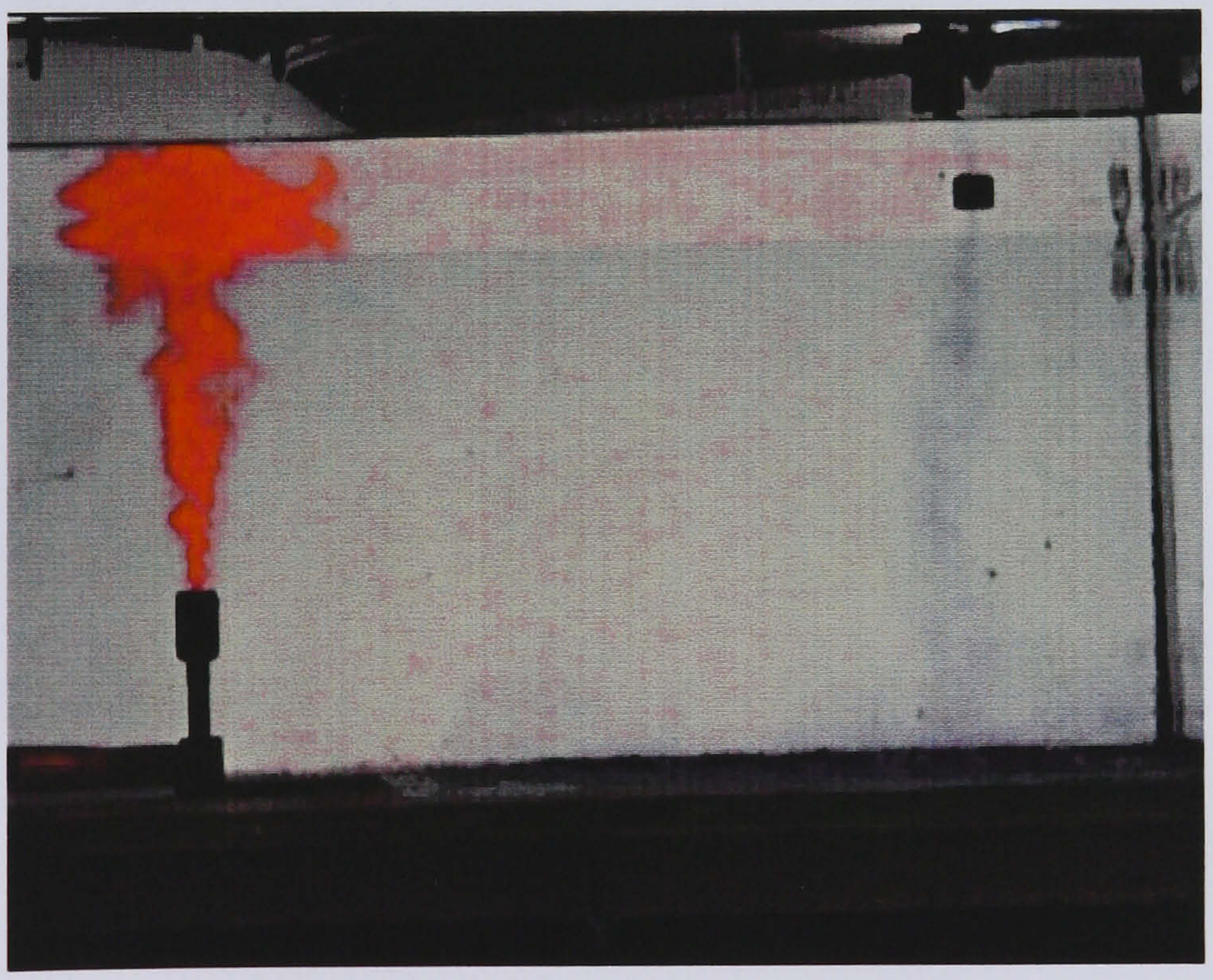

FIGURE 3.6: Photograph of the early state of a dual-plume experiment.

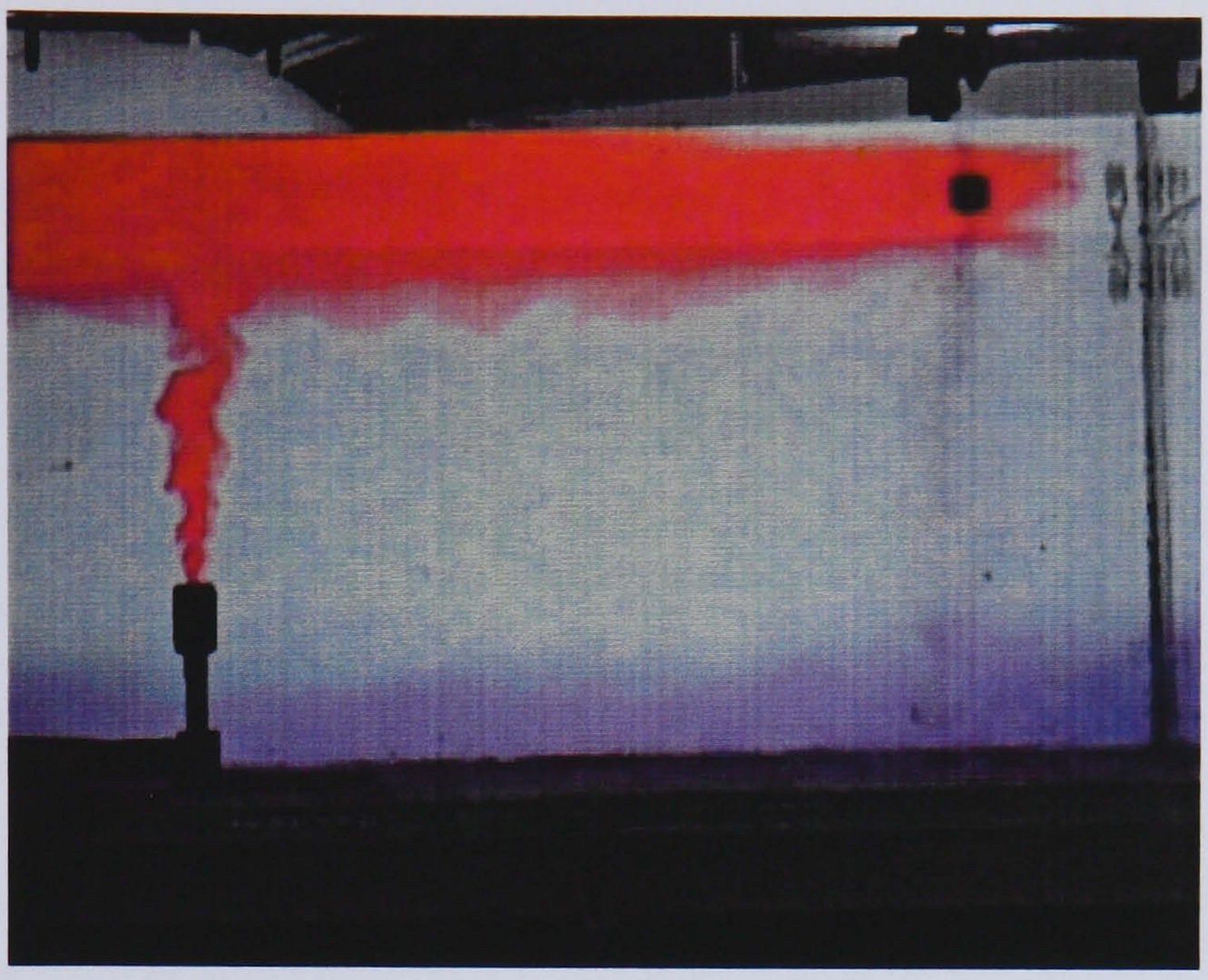

FIGURE 3.7: Photograph depicting the experiment after the two mixed layers have formed.

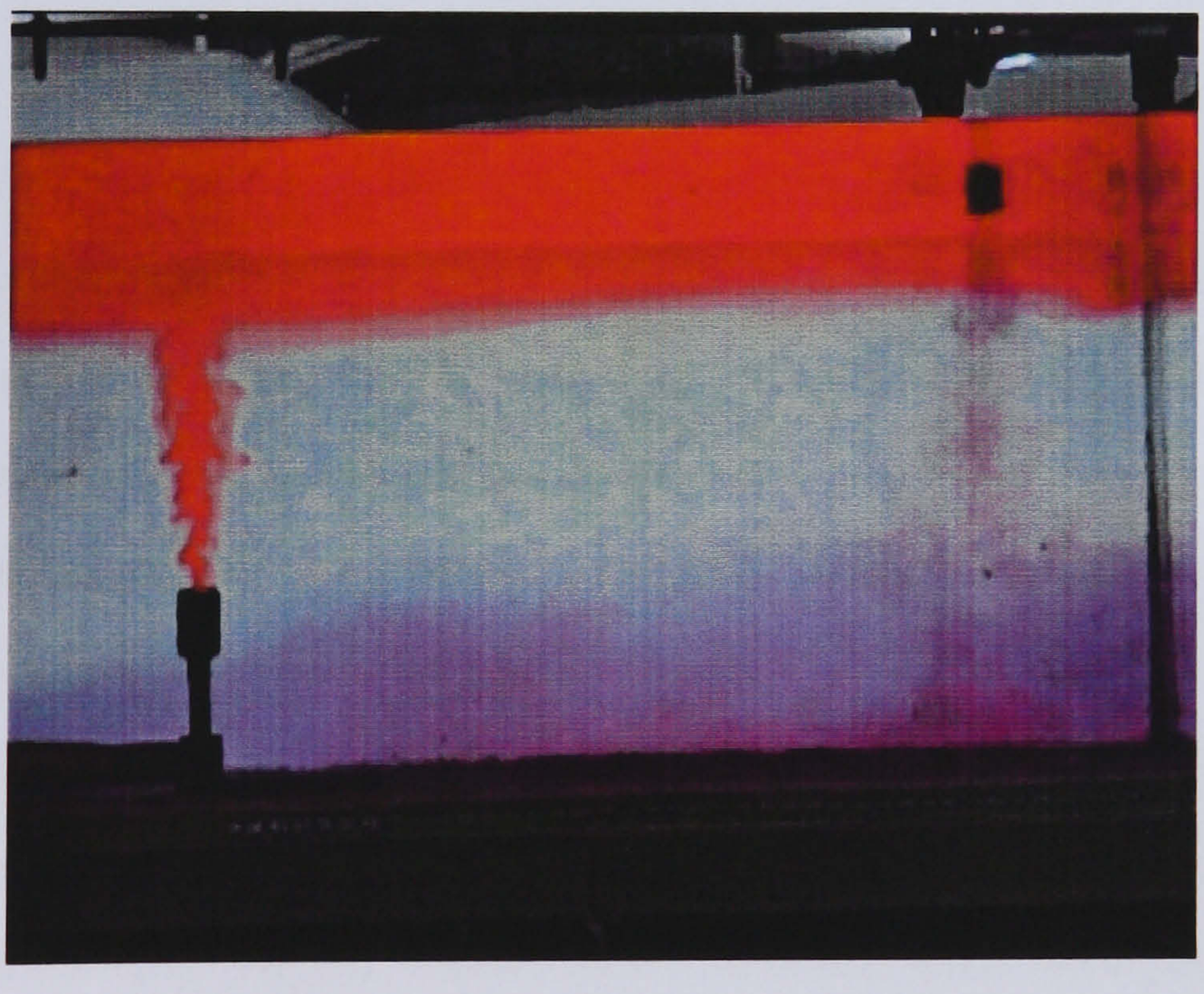

FIGURE 3.8: Photograph showing an experiment for which the layers are close to convergence.

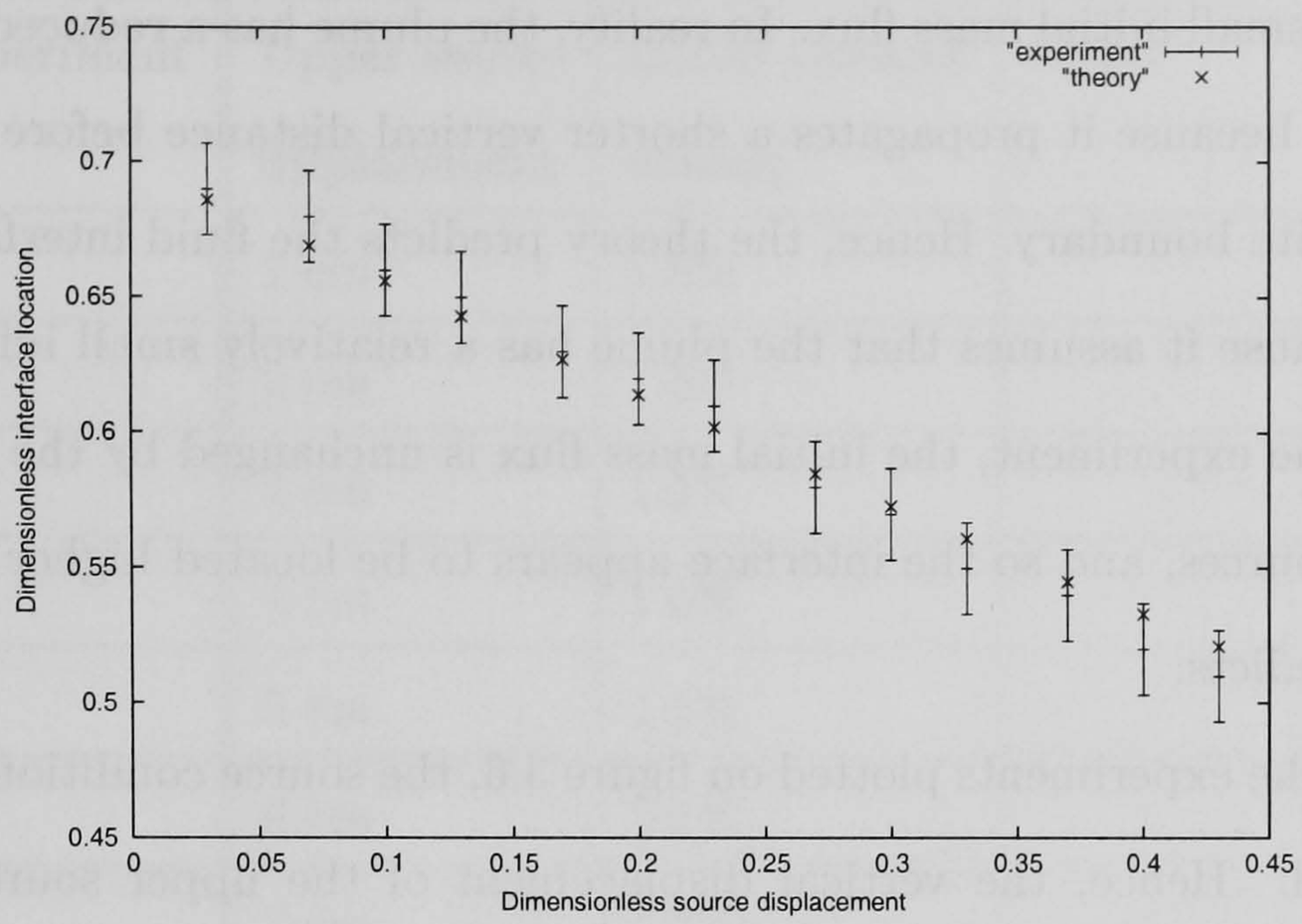

FIGURE 3.9: Numerical solution for the interface location as a function of the normalised mass fluxes associated with the plume sources and their respective dimensionless vertical displacements as compared with a series of analogue experiments. In this case, $\hat{z}_u$ is varied while $\hat{z}_l$ remains constant. Further, $R = S$ in all cases.

cation of the fluid interface and the experimental results. There is good agreement between the results. However, there appears to be a slight fluctuation in the correlation around the point $\hat{z}_u = 0.2$. This may be seen by noting that for $\hat{z}_u < 0.2$, the theoretical values are located slightly below the experimental results, but slightly above them for $\hat{z}_u > 0.2$. This is partially due to the discrepancy introduced by the mass sink being located a distance below the upper boundary. This effect is relatively small, because the lower source displacement is also relatively small in the course of the experiments. Essentially, the theory considers the displaced source to be equivalent to a plume with a large virtual origin. Hence, a source that is displaced by a relatively large vertical distance is equivalent to a source which has been originates from a point a large distance in front of its real origin. Hence, the theory predicts that each source has a reduced volume flux because it has a

relatively small initial mass flux. In reality, the plume has a reduced entrainment flux because it propagates a shorter vertical distance before reaching the opposite boundary. Hence, the theory predicts the fluid interface to be lower because it assumes that the plume has a relatively small initial mass flux. In the experiment, the initial mass flux is unchanged by the displacement of sources, and so the interface appears to be located higher than the theory predicts.

In all the experiments plotted on figure 3.6, the source conditions remain unchanged. Hence, the vertical displacement of the upper source is the only variable. The mass fluxes associated with each of the plume sources were $Q = 0.175\,\text{litres}\,\text{min}^{-1}$, while the initial ambient fluid had a density of $\rho_0 = 1015\,\text{kg}\,\text{m}^{-3}$. The fluid entering via the lower source had a density of $\rho_1 = 1010\,\text{kg}\,\text{m}^{-3}$, and the fluid from upper source $\rho_1 = 1030\,\text{kg}\,\text{m}^{-3}$. These values give a mass flux scale as $Q_p = 4.47 \times 10^{-6}\,\text{m}^3\,\text{s}^{-1}$. Applying these scale, we have $R = S = 0.653$.

The experiments that were performed are listed in the following table:

Experiment	Upper source displacement	Initial ambient density	Notes
A1	1 cm	1.5%	
A2	2 cm	1.5%	
A3	3 cm	1.5%	
A4	4 cm	1.5%	
A5	5 cm	1.5%	
A6	6 cm	1.5%	
A7	7 cm	1.5%	
A8	8 cm	1.5%	
A9	9 cm	1.5%	
A10	10 cm	1.5%	
A11	11 cm	1.5%	
A12	12 cm	1.5%	
A13	13 cm	1.5%	
B1	1 cm	4%	
C1	1 cm	1.5%	Mass sink in lower layer
CC1	12 cm	1.5%	Mass sink in lower layer
D1	17.5 cm	1.5%	Sources in same horizontal plane

3.4 Conclusions

A simple theory has been developed to model the situation whereby the sources of mass and buoyancy are displaced from their respective boundaries

in the interior of the confined region. The theory provides a simple method of estimating the position of the fluid interface, which should be located halfway between the sources if the mass fluxes associated with the sources are equal in magnitude.

Experiments were performed to measure the location of the fluid interface for the dual-plume filling box with vertically-displaced sources for various values of R and S. It was observed that a sharp fluid interface always formed, and hence there were two distinct fluid layers. However, in the case of fluid sources being displaced a large distance from their respective boundaries, the fluid layers ceased to be well-mixed. The strength of the resulting stratification was also found to be related to the displacement distance. In all cases, the experiments converged to a two-layer configuration, within which the stratification was weak compared to the overall two-layer state.

The experimental data was found to be in good agreement with numerical solution of the displaced-source dual-plume filling-box model derived in section 3.2.

Part III

Further Steady-State Models

Chapter 4

Configurations Involving Line Sources

"Some circumstantial evidence is very strong,

as when you find a trout in milk."

– Henry David Thoreau.

4.1 Introduction

In Chapter 2, we presented an equilibrium steady-state model for a dual-plume filling-box system. This system was driven by a pair of opposing buoyancy sources. These sources produced plume flows that were axisymmetric. However, the research of Morton et. al. (1956) also considered another type of turbulent buoyant plume flow that admitted self-similar solutions. These fluid flows originated from sources that were rectangular in shape, and were referred to as *line plumes*. They were modelled quantita-

tively, in a similar manner to the axisymmetric plumes, by applying a form of the entrainment hypothesis.

Models involving line plumes are useful in many applications. For example, the buoyant flow of hot air from a radiator is an example of a turbulent line plume. Gas leaks from fractured pipes and hydrothermal venting from fissures in the ocean floor are also modelled by considering the flows to originate from line sources.

In this chapter, we modify the source conditions of the dual-plume filling box system by replacing either one or both of the axisymmetric plume sources with a line source. The key result is, similarly to chapter 2, the condition that causes the interface to vanish and the system to consist of a single well-mixed fluid layer. Further, we are interested in how the line source modifies this occurrence. We also examine the parameter $\hat{L}$, defined as the aspect ratio of the line source, namely $L = L/W$. This is of fundamental importance, and we discuss quantitatively how varying $\hat{L}$ affects the behaviour of each of the dual-plume systems by modifying the ventilation flows. Hence, we examine different configurations of the steady-state system and compare the results. This leads to another new study involving the use of a hybrid dual-plume filling-box system, consisting of an axisymmetric source and a line source, to directly compare the mixing dynamics of the resulting flows. We are then able to answer a fundamental question: is it more effective to use line or axisymmetric sources if you wish to heat a room?

We begin, in §4.2, by considering a dual-line plume filling-box system. We briefly review the fundamental theory of line plumes in §4.2.1. The inherent asymmetry due to the location of the mass sink is retained in the system, enabling direct comparison with the model of chapter 2. The corre-

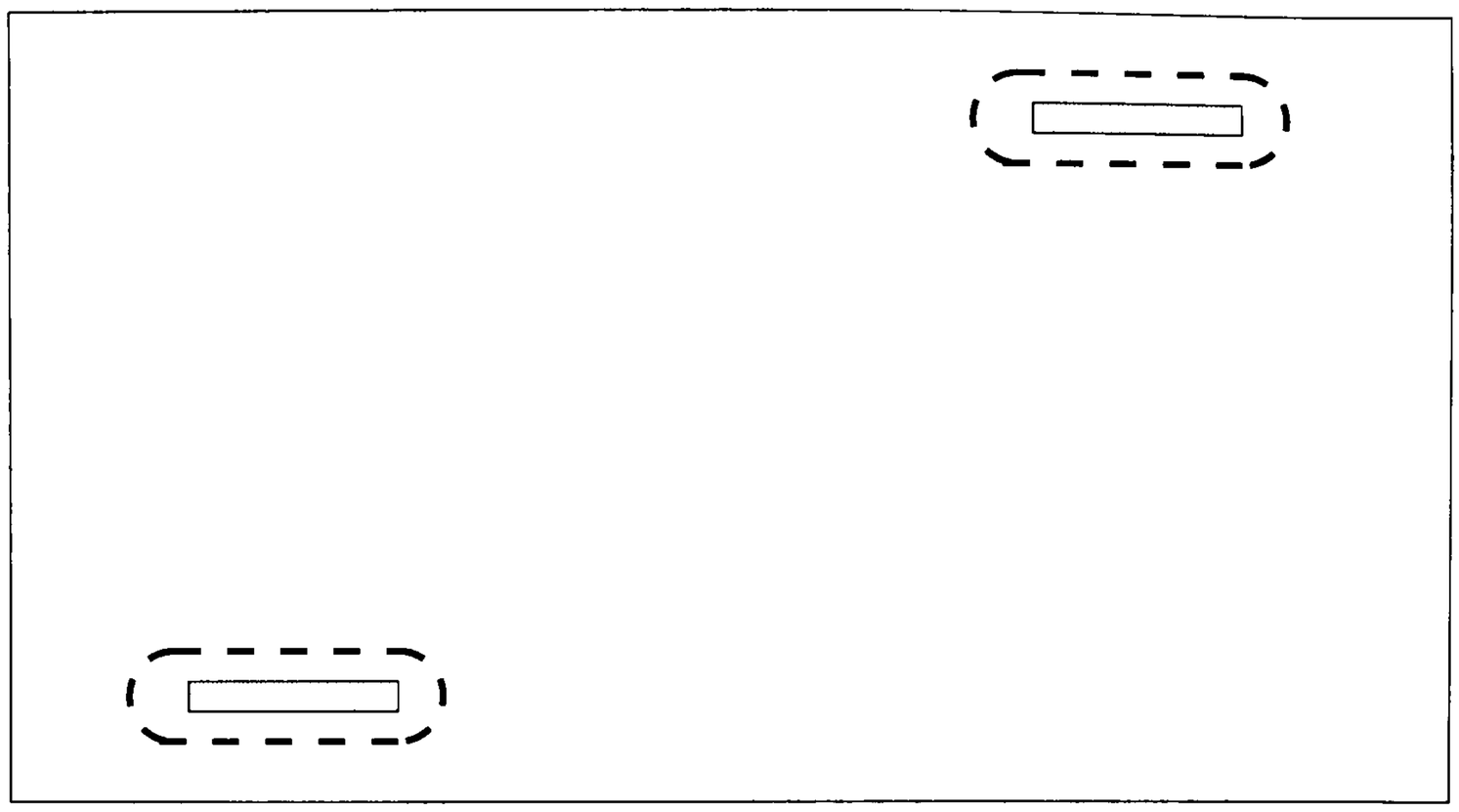

FIGURE 4.1: Diagram representing the location of the sources in the dual line-plume filling box. The figure represents an overhead perspective. The buoyant flow arising due to the temperature contrast between the source and the environmental fluid is depicted schematically by the shaded curves.

sponding numerical solutions for the dual-line plume system are presented in 4.2.3.

We then discuss hybrid models. By this, we refer to a dual-plume filling-box system consisting of a line plume and an axisymmetric plume. In §4.3. we study a hybrid system with an ascending line plume, and in section 4.4 a hybrid system with an ascending axisymmetric plume.

We end this chapter, in §4.5, by drawing some overall conclusions.

4.2 The Dual-Line Source Filling-Box System

4.2.1 Effectively Two-Dimensional Plume Sources

In this section, we briefly review the model of a turbulent buoyant line plume.

Following a similar approach to that for an axisymmetric plume (please refer to Chapter 1), by assuming an entrainment hypothesis, we arrive at a system of three ordinary differential equations:

$$\frac{\mathrm{d}Q}{\mathrm{d}z} = \frac{\epsilon M}{Q} \tag{4.1}$$

$$\frac{\mathrm{d}M}{\mathrm{d}z} = \frac{BQ}{M} \tag{4.2}$$

$$\frac{\mathrm{d}B}{\mathrm{d}z} = 0 \tag{4.3}$$

where the equations again represent conservation of the fluxes of volume, momentum and buoyancy per unit length. respectively. These quantities are specified by $Q = ub$, $M = u^2 b$ and $B = g' ub$ in terms of the mean vertical plume velocity u and the effective plume length b. Note that these expressions are for a uniform ambient, and so right-hand side of equation (4.3) vanishes. Dimensional analysis results in an expression for the mean plume velocity, namely

$$u \sim B_0^{1/3} \tag{4.4}$$

which is constant for a given initial buoyancy flux B_0. Further, direct substitution leads to

$$b = \epsilon z \tag{4.5}$$

and, consequently, we have

$$u = \left(\frac{B_0}{\epsilon}\right)^{\frac{1}{3}} \tag{4.6}$$

Analogously with the case of an axisymmetric plume, the equations representing the flow of a line plume have exact solutions in a homogeneous environment. The self-similar solution for the volume flux as a function of vertical distance from the plume source takes the form

$$Q = \lambda B^{1/3} z \tag{4.7}$$

where $\lambda \simeq 0.1$ (Turner, 1986). We now proceed to derive the equation for the interface location taking into account the modified expressions for the mass fluxes associated with the plume sources.

To model the configuration of the system as depicted in figure 4.1, we make the following assumptions. Firstly, we assume that the sources are positioned such that the two buoyant flows do not interact with each other as they propagate through the container. Also, we impose a constraint upon the physical location of the sources, namely that they are situated in such a manner that the consequent line plumes possess self-similarity as they propagate through the container. Figure 4.1 depicts a possible location of the two line sources. The shaded rectangles illustrate the sources positioned away from the influence of the boundaries of the container. In this case, the resulting flow is illustrated by the dashed lines. We assume that the source produces an effectively two-dimensional flow. We therefore expect that the region at the end of each radiator, indicated by the curved section of the dashed lines, has a negligible effect upon the overall dynamics of the resulting plume.

In the simplest configuration, we make the assumption that each of the two line plumes in the filling box system arise from sources of equal length. This constraint implies that the buoyancy flux per unit length associated with each of the plume sources will be equal. However, we expect that the horizontal length associated with each source will be of considerable importance in the overall dynamics of the resulting flow, assuming that each of the radiators provides the same total heat input.

In Chapter 2, it was found that the net entrained flux associated with each plume was the critical physical quantity that determined the behaviour of the system. Hence, we briefly compare the similarity solutions for the

volume fluxes of axisymmetric plumes with line plumes.

The volume flux as a function of vertical distance from the source for a self-similar line plume is given by the expression

$$Q_l = \lambda_L B_l^{1/3} z L \tag{4.8}$$

where L is the length of the line source and λ_L is an empirical constant associated with the turbulent buoyant line plume. Correspondingly, the solution for a plume originating from an axisymmetric source is

$$Q_a = \lambda_A B_a^{1/3} z^{5/3} \tag{4.9}$$

where λ_A is the empirical constant for a round plume. The effectively two-dimensional nature of the line plume implies that the the length of the source is a key parameter in determining the dynamics of the subsequent flow. For direct comparison with an axisymmetric plume, the total buoyancy flux associated with a flow originating from a line source is

$$B = B_l L \tag{4.10}$$

We may now examine the relative efficiency of each type of flow in ventilating a room. This is essentially due to the mixing dynamics associated with the flows as they propagate through the container. Hence, we introduce a parameter q, defined by

$$\frac{\bar{Q}_a}{\bar{Q}_l} = q \tag{4.11}$$

where the overline denotes the total volume flux possessed by the buoyant flow when it has propagated a vertical distance H. We note here that, given sufficient vertical freedom, the line plume will eventually asymptote to a form comparable with a corresponding round plume. Hence, at a vertical distance z from the source, the line plume will have an associated effective

width ϵz, and so the flow evolves according to

$$\frac{L}{z} > \epsilon \tag{4.12}$$

i.e.

$$\frac{L}{\epsilon z} \sim O(1) \tag{4.13}$$

Consequently, we may define a length scale z_c as the distance from their respective sources such that the line plume and the round plume possess identical associated volume fluxes. Therefore:

$$z_c \sim L\left(\frac{\lambda_1}{\lambda_2}\right)^{3/2} \tag{4.14}$$

Hence, z_c represents the vertical distance from the source such that a line plume of given associated mass flux asymptotes to possess the same flux of volume as an axisymmetric plume with an identical initial mass flux.

4.2.2 The Dual Line Plume Filling-box:

Derivation of the Model

We now proceed to formulate a model for the steady-state dual line-plume filling box system. We follow the same methodology as per the derivation of the model in Chapter 2. Hence, we will describe only briefly the details in this section.

The respective line source mass fluxes may be written in terms of the total source buoyancy fluxes as follows:

$$Q_1 = \lambda_L\left(\frac{B_1^{1/3}}{L_1}\right)z \tag{4.15}$$

$$Q_2 = \lambda_L\left(\frac{B_2^{1/3}}{L_2}\right)z \tag{4.16}$$

where B_1 and B_2 are the total buoyancy fluxes of the respective plume sources, L_1 and L_2 are the lengths of the respective plume sources and λ_L

is an empirical constant for the line plume. We now proceed to introduce scalings to transform the variables to dimensionless form. We select an appropriate scale for the mass fluxes associated with the plume sources, namely

$$Q_{pL} = \lambda_L^{3/2} \left[\frac{g\beta\,(\rho_2 - \rho_1)}{\rho_0}\right]^{1/2} H^{3/2} \tag{4.17}$$

where the dimensionless parameter $\hat{L}$ is defined as the ratio of the length of the line source to the vertical height of the confined region, namely $\hat{L} = L/H$. Further, we may define the volume fluxes associated with each of the turbulent buoyant line plumes as they propagate across the fluid interface. These quantities are defined according to

$$Q_3 = \lambda_L \left[\frac{g\beta\,(\rho_l - \rho_1)}{\rho_0}\right]^{1/3} (h_l + y_l) \tag{4.18}$$

$$Q_4 = \lambda_L \left[\frac{g\beta\,(\rho_2 - \rho_u)}{\rho_0}\right]^{1/3} (h_u + y_u) \tag{4.19}$$

where Q_3 is the interfacial volume flux associated with the ascending line plume, and Q_4 the corresponding quantity for the downward-propagating flow.

However, we note that from the self-similar solution for the volume flux associated with a line plume as a function of vertical distance from the source, namely

$$Q_l = \lambda_L \left(\frac{B}{L}\right)^{1/3} z \tag{4.20}$$

where B is now the *total* buoyancy flux at the plume source. We may re-arrange to yield:

$$Q_l = \lambda_L \left(\frac{g' Q_l}{L}\right)^{1/3} z \tag{4.21}$$

and hence:

$$Q_l = \lambda_L^{3/2} \left(\frac{g'}{L}\right)^{1/2} z^{3/2} \tag{4.22}$$

Therefore, in dimensional form, the interfacial mass fluxes Q_3 and Q_4 become

$$Q_3 = \lambda_L^{3/2} \left[\frac{g\beta\,(\rho_l - \rho_1)}{\rho_0\, L_1} \right]^{1/2} (h_l + y_l)^{3/2} \tag{4.23}$$

$$Q_4 = \lambda_L^{3/2} \left[\frac{g\beta\,(\rho_2 - \rho_u)}{\rho_0\, L_2} \right]^{1/2} (h_u + y_u)^{3/2} \tag{4.24}$$

In dimensionless form, these become:

$$\hat{Q}_3 = \left(\frac{\hat{\rho}_l}{\hat{L}_1} \right)^{1/2} \left(\hat{h} + \hat{h}_l \right)^{3/2} \tag{4.25}$$

$$\hat{Q}_4 = \left(\frac{1 - \hat{\rho}_u}{\hat{L}_2} \right)^{1/2} \left(1 - \hat{h} + \hat{h}_u \right)^{3/2} \tag{4.26}$$

where L_1 and L_2 are the lengths of the lower and upper line sources respectively.

We now consider the case for which $L_1 = L_2 = L$, say. The initial mass fluxes associated with each of the plume sources may also be normalised by scaling with equation (4.19). Hence, we have:

$$R = \frac{Q_1}{Q_{pL}} = \frac{\hat{\rho}_l^{1/2} \hat{h}_l^{3/2}}{\hat{L}} \tag{4.27}$$

$$S = \frac{Q_2}{Q_{pL}} = \left(\frac{R}{R+S} \right)^{1/2} \frac{\hat{h}_u^{3/2}}{\hat{L}} \tag{4.28}$$

and so the virtual origins associated with each of the plume sources are:

$$\hat{h}_u = \left[S\,\hat{L} \left(\frac{R+S}{R} \right)^{1/2} \right]^{2/3} \tag{4.29}$$

$$\hat{h}_l = \left(\frac{R\,\hat{L}}{\hat{\rho}_l^{1/2}} \right)^{2/3} \tag{4.30}$$

We now proceed by considering conservation of mass and buoyancy. Global conservation of mass remains unchanged from the case of chapter 2, and hence the expression for the dimensionless density of the upper fluid layer is given by

$$\hat{\rho}_u = \frac{S}{R+S} \tag{4.31}$$

We may now follow identical algebraic steps to equations (2.3) to (2.12), and similarly obtain the relations:

$$(4) - (7) \Rightarrow \rho_4 = \rho_l \tag{4.32}$$

$$(6) - (8) \Rightarrow \rho_3 = \rho_u \tag{4.33}$$

as expected.

We now proceed to find an explicit expressions for lower layer density. We follow the same process as per Chapter 2, and obtain

$$\hat{\rho}_l = \left(\frac{S}{R+S}\right)\left[\frac{\hat{L}\,R + (1-\hat{\rho}_u)^{1/2}\left(1-\hat{h}+\hat{h}_u\right)^{3/2}}{(1-\hat{\rho}_u)^{1/2}\left(1-\hat{h}+\hat{h}_u\right)^{3/2}}\right] \tag{4.34}$$

This is as expected, because the global conservation laws are unchanged in the case of the dual line-plume system. The internal mixing processes differ from the case of a system driven by a pair of axisymmetric plumes, however, and hence the local conservation laws are not the same as for the configuration described in chapter 2. The net flux of mass across the interface is given by

$$Q_3 = Q_4 + Q_1 \tag{4.35}$$

which in terms of dimensionless variables may be written as

$$\hat{L}\,R + (1-\hat{\rho}_u)^{1/2}\left(1-\hat{h}+\hat{h}_u\right)^{3/2} = \hat{\rho}_l^{1/2}\left(\hat{h}+\hat{h}_l\right)^{3/2} \tag{4.36}$$

Upon rearrangement of equation (4.36), we have an expression for the location of the fluid interface

$$\hat{h} = \left[\frac{\hat{L}\,R + (1-\hat{\rho}_u)^{1/2}\left(1-\hat{h}+\hat{h}_u\right)^{3/2}}{\hat{\rho}_l^{1/2}}\right]^{2/3} - \hat{h}_l \tag{4.37}$$

Manipulation of equation (4.37) leads to

$$\left[\left(\frac{1}{\hat{\rho}_l}\right)^{1/2}\frac{1}{\hat{L}}\right]^{2/3} = \left[\left(\frac{1}{1-\hat{\rho}_u}\right)^{1/2}\left(\frac{(1-\hat{\rho}_u)^{1/2}\left(1-\hat{h}+\hat{h}_u\right)^{3/2}\hat{L}}{R+(1-\hat{\rho}_u)^{1/2}\left(1-\hat{h}+\hat{h}_u\right)^{3/2}\hat{L}}\right)^{1/2}\frac{1}{\hat{L}}\right]^{2/3} \tag{4.38}$$

Therefore:

$$\hat{h} = \left[\frac{R + (1-\hat{\rho}_u)^{1/2}\left(1-\hat{h}+\hat{h}_u\right)^{3/2}\hat{L}}{\hat{\rho}_l^{1/2}\hat{L}}\right]^{2/3} - \left(\frac{R}{\hat{\rho}_l^{1/2}\hat{L}}\right)^{2/3} \tag{4.39}$$

If we now introduce a parameter γ, defined according to

$$\gamma = \left(\frac{R}{R+S}\right)^{1/2}\left(1-\hat{h}+\hat{h}_u\right)^{3/2} \tag{4.40}$$

then equation (4.38) may now be written as

$$\left[\left(\frac{1}{\hat{\rho}_l}\right)^{1/2}\frac{1}{\hat{L}}\right]^{2/3} = \left[\left(\frac{1}{1-\hat{\rho}_u}\right)^{1/2}\left(\frac{\gamma}{R+\gamma}\right)^{1/2}\frac{1}{\hat{L}}\right]^{2/3} \tag{4.41}$$

and

$$\left[\left(\frac{R}{\hat{\rho}_l}\right)^{1/2}\frac{1}{\hat{L}}\right]^{2/3} = R^{2/3}\left[\left(\frac{1}{1-\hat{\rho}_u}\right)^{1/2}\left(\frac{\gamma}{R+\gamma}\right)^{1/2}\frac{1}{\hat{L}}\right]^{2/3} \tag{4.42}$$

Hence, we may express equation (4.39) in terms of the dimensionless mass fluxes associated with the plume sources

$$\hat{h} = \left[\left(R+\gamma\hat{L}\right)^{2/3} - R^{2/3}\right]\left[\left(\frac{R}{R+S}\right)^{1/2}\left(\frac{\gamma\hat{L}}{R+\gamma\hat{L}}\right)\left(\frac{1}{\hat{L}}\right)\right]^{2/3} \tag{4.43}$$

Further, equation (4.43) is consistent with the analogous relation for the dual-axisymmetric plume filling-box model derived in chapter 2. Following the same steps yields a similar relation, namely:

$$\hat{h} = \left[(R+\gamma)^{2/5} - R^{2/5}\right]\left[\left(\frac{R}{R+S}\right)^{1/2}\left(\frac{\gamma}{R+\gamma}\right)\right]^{2/5} \tag{4.44}$$

4.2.3 Numerical Results for the Dual Line Plume System

We now present the numerical solution of equations 4.49 and 4.59, relations for the density of fluid associated with the lower layer and the location of the fluid interface, respectively. The results are presented for the equal-magnitude case of $R = S$. The more general situation, for which $R \neq S$, is discussed in section 4.26.

4.2.4 The Equal-Magnitude, Equal-Length Case: $R = S$, $\hat{L}_R = \hat{L}_S$

We begin by considering the simplest case, for which the magnitudes of the mass fluxes associated with the plume sources are equal, and the the aspect ratio of the line sources are also equal. Hence, $R = S$ and $\hat{L}_R = \hat{L}_S = \hat{L}$. We begin by considering $\hat{L} = 15$, which is a typical experimental value for the construction of a line plume.

Figure 4.3 shows the numerical solution of equation (4.44), with the corresponding graph of $\hat{h}$ as a function of R for the dual-axisymmetric filling-box system. The latter is duplicated from figure 2.3 of Chapter 2.

We note that the location of the fluid interface is a monotonic function of R for the dual-plume system, as it was for the model of Chapter 2. This follows directly from consideration of the fractional dilution, $\hat{D}$, of the dual-line plume configuration. However, in contrast to the model of Chapter 2, the line plume system exhibits different values for $\hat{h}$ as $R \to 0$ and also for the critical value R such that the system comprises a single fluid layer.

Firstly, we denote $\hat{D}_l$ and $\hat{D}_a$ as the fractional dilution associated with a line plume and am axisymmetric plume respectively. We assume that the mass flux associated with each source is equal, and we use the definition of $\hat{D}$ from equation (2.56) in Chapter 2. Consequently, we may explain the quantitative differences in figure 4.2 by comparing the fractional plume dilutions. For the line plume, this has the form

$$\hat{D}_l = \frac{\left(\hat{h} + \hat{H}\right)^{3/2} - \hat{h}^{3/2}}{\hat{h}^{3/2}} \tag{4.45}$$

Let us suppose that the virtual origins associated with an ascending line plume and an ascending axisymmetric plume are equal in magnitude. Further, the initial mass fluxes associated with each plume are equal, and each

of the plumes flows in ambient fluid of density $\hat{\rho}_0$. After the flows have progressed a vertical distance $\hat{H}$, equation (4.45) indicates that the line plume will have experienced a relatively smaller fractional dilution than the axisymmetric plume. Hence, the net entrained flux of the axisymmetric plume will be larger in magnitude. This is the key concept in explaining figure 4.2.

It follows that if the plume is driving a filling-box, the magnitude of the return flow will be greater for the plume which has the greater net entrained flux at the top of the container. For each value of R, the axisymmtric plume will therefore drive a return flow greater in magnitude than the line plume. In a dual-plume filling-box, where the mass sink is located in the upper layer, this governs the location of the fluid interface. This is because the return flow due to the ascending line plume will be weaker in magnitude than in the axisymmetric case. Therefore, the fluid interface will be located closer to the top of the container. This is the behaviour shown in figure 4.4.

It therefore follows that the dual-line plume system will consist of a single fluid layer at a smaller value of R than for the model of Chapter 2. Repeating the calculation of section 2.3.4, we find that $R_{crit} = 9.21$. This value is in excellent agreement with the numerical results.

Figure 4.4 shows the lower-layer density as a function of R. The numerical solutions are plotted for both the dual-line and dual-axisymmetric filling-box systems. We see that in both cases the density of the lower fluid layer approaches the input density of the descending plume as R increases. However, for the dual line-plume system, $\hat{\rho}_l \to 1$ for a relatively small value of R. However, this is consistent with the argument presented above. The lower-layer density is the density of the descending plume at the interface. As in Chapter 2, $\hat{\rho}_u = 0.5$. Further, as the upper fluid layer decreases in depth as R increases. This is the behaviour shown in figure 4.4. Therefore,

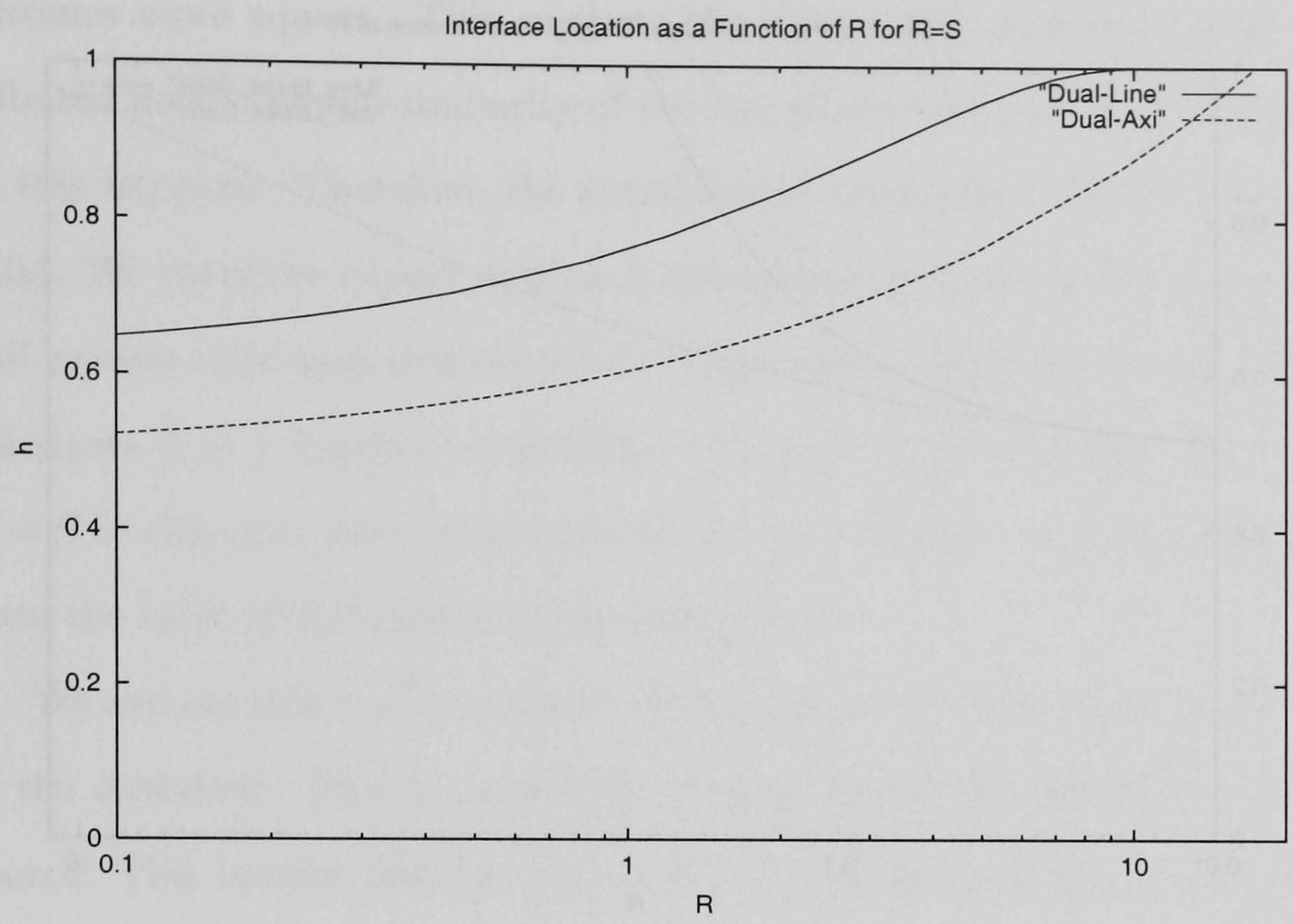

FIGURE 4.2: Location of the fluid interface as a function of the normalised mass flux associated with the ascending plume. The *dashed* curve refers to a dual-plume filling-box system driven by a pair of line plumes. The continuous line is the corresponding system comprising two axisymmetric plumes. In this case, $\hat{L} = 15$.

as R increases, the descending plume is less diluted with fluid from the upper layer as it reaches the interface. We already have the result that a line plume undergoes less fractional dilution than an axisymmetric plume over the same vertical distance if all other parameters are equal. Hence, the descending line plume will arrive at the interface less diluted than a corresponding axisymmetric plume. Therefore, the density of the lower layer increases by a greater amount due to a line plume. The lower-layer density will therefore $\rightarrow 1$ for a smaller value of R than for a dual line-plume filling-box system. This is the behaviour shown in figure 4.4.

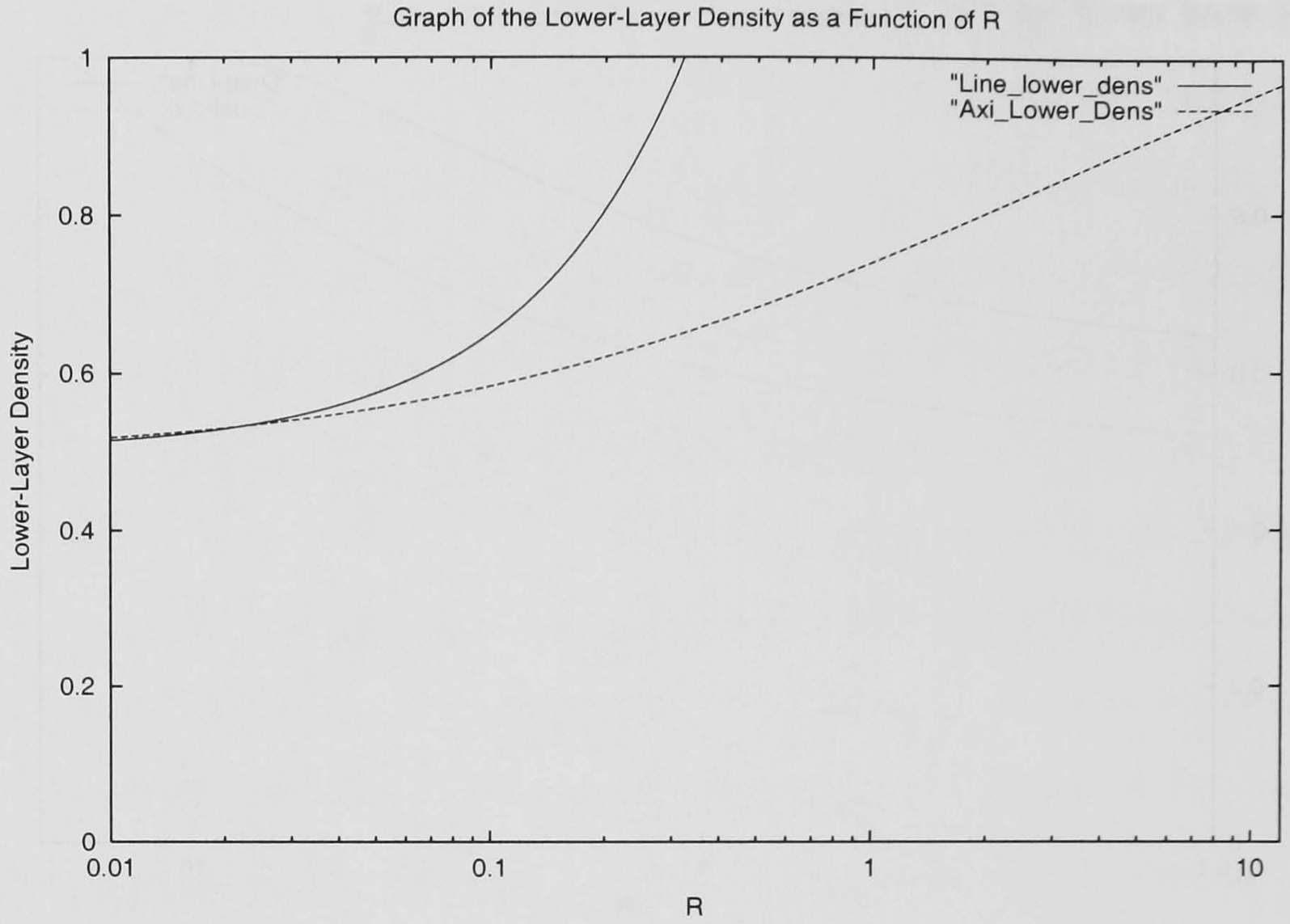

FIGURE 4.3: Density of the lower fluid layer as a function of the normalised mass flux associated with the ascending plume. The *dashed* curve refers to a dual-plume filling-box system driven by a pair of line plumes. The continuous line is the corresponding system comprising two axisymmetric plumes. In this case, $\hat{L} = 15$.

4.2.5 The Equal-Magnitude Case for Varying $\hat{L}$

We now present numerical results corresponding to figures 4.3 and 4.4 of the previous section, but in this case we examine the implications of varying values of $\hat{L}$.

Recall that $\hat{L} = L_i/W_i$, where L_i is the length of the line source and W_i is its respective width. Hence, as $\hat{L} \to 1$, the line source will become progressively more square in shape if the total cross-sectional area is the same in each case.

Therefore, as $\hat{L}$ decreases, we expect that the physical behaviour associated of the resulting flow will change. Principally, this occurs as the source

becomes more square. This suggests the source will produce a more distributed flow. The self-similarity of the line plume will start to break down as this happens. Therefore, the entrainment assumption will no longer be valid. We therefore expect that as $\hat{L}$ decreases, equations (4.15) and (4.16) will present only approximations to a line source. With this caveat, figure 4.4 shows $\hat{h}$ as a function of R for $\hat{L} = 15, 10, 5$ and 1. We note that since $R = S$ in this case, each of the solution curves represent flows that originate from the same initial mass and buoyancy fluxes.

We can see that as $\hat{L}$ decreases, the interface is located closer to the top of the container. This is consistent with the increased distribution of the source. This implies that the plume will entrain progressively less ambient fluid as $\hat{L}$ decreases, and hence arrives at the top of the confined region less diluted. Therefore, the magnitude of the return flow associated with the ascending plume decreases, and the interface is located nearer to H.

Figure 4.5 shows the density associated with the lower fluid layer for the corresponding situation as for figure 4.4 as a function of R. As $\hat{L} \to 1$, the plume will be less diluted. Hence, the descending plume will arrive at the interface relatively unchanged from its input density. Therefore, $\hat{\rho}_l \to 1$ as $\hat{L} \to 1$.

We briefly conclude by considering the limitations of the results in this section. A thorough model of a distributed plume is beyond the scope of the present work. Hence, figures 4.4 and 4.5 represent simple approximations of the behviour of the dual line-plume filling-box as $\hat{L} \to 1$.

4.2.6 The Equal-Magnitude Case: $\hat{L}_R \neq \hat{L}_s$

In this section, we consider the implications upon the dual-plume filling-box system of line sources which have unequal aspect ratios. We take $\hat{L}_R$ and

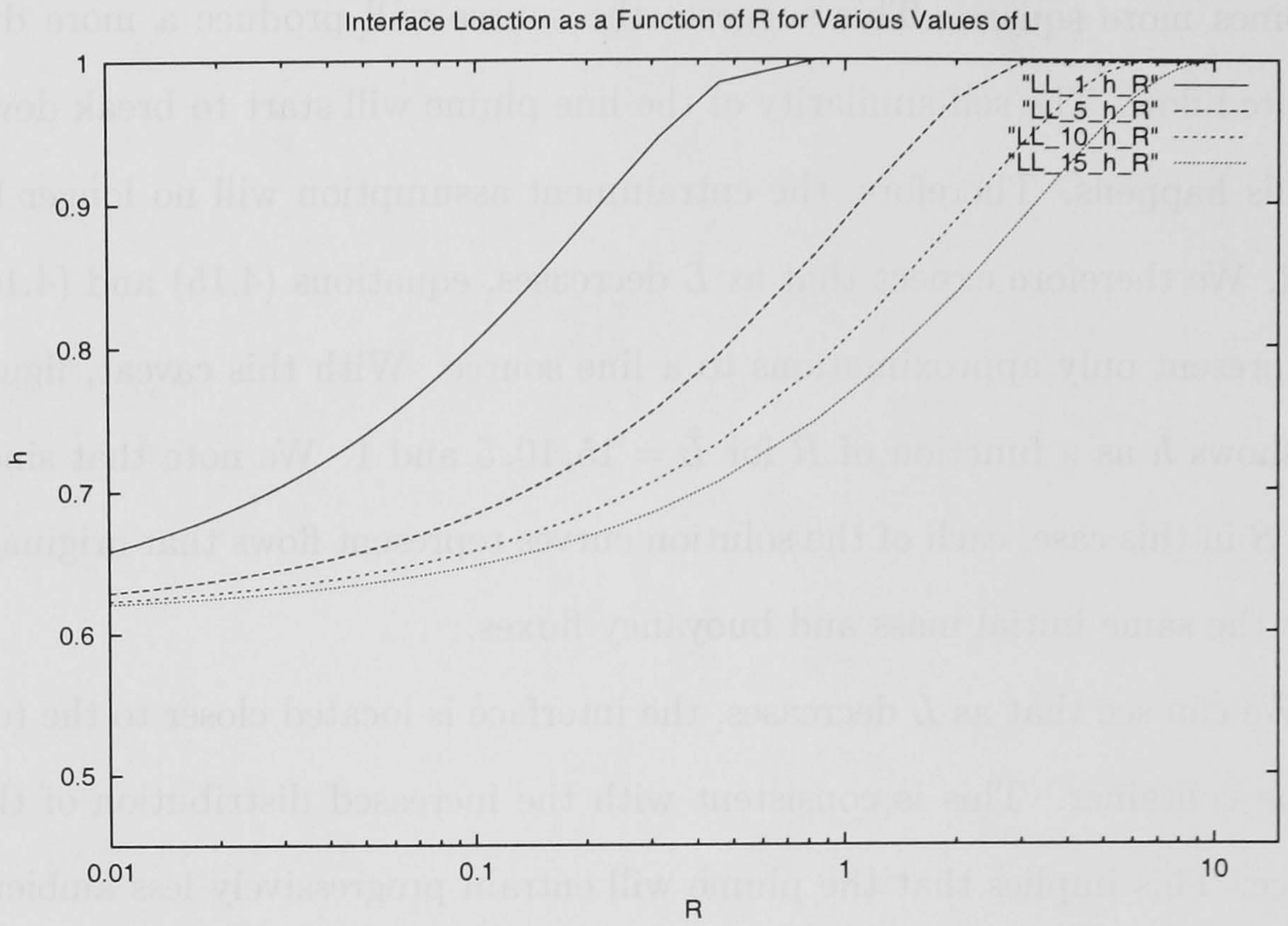

FIGURE 4.4: Location of the fluid interface as a function of the normalised mass flux associated with the ascending plume for a dual-line plume filling-box system. Each of the curves represents a different value of $\hat{L}$.

$\hat{L}_S$ as being the respective aspect ratios of the lower and upper sources. We then incorporate these into the dual-line plume model, and obtain numerical solutions.

Following the derivation in section (4.2), we find that the interface location is given by:

$$\hat{h} = \left[\left(R + \gamma\hat{L}_S\right)^{2/3} - R^{2/3}\right]\left[\left(\frac{R}{R+S}\right)^{1/2}\left(\frac{\gamma\hat{L}_S}{R+\gamma\hat{L}_R}\right)\left(\frac{1}{\hat{L}_R}\right)\right]^{2/3} \tag{4.46}$$

Further, the density of the lower fluid layer is:

$$\hat{\rho}_l = \left(\frac{S}{R+S}\right)\left[\frac{R + (1-\hat{\rho}_u)^{1/2}\left(1-\hat{h}+\hat{h}_u\right)^{3/2}\hat{L}_s}{(1-\hat{\rho}_u)^{1/2}\left(1-\hat{h}+\hat{h}_u\right)^{3/2}\hat{L}_S}\right] \tag{4.47}$$

Figures 4.7 and 4.8 show $\hat{h}$ as a function of R for the case of line sources with unequal lengths.

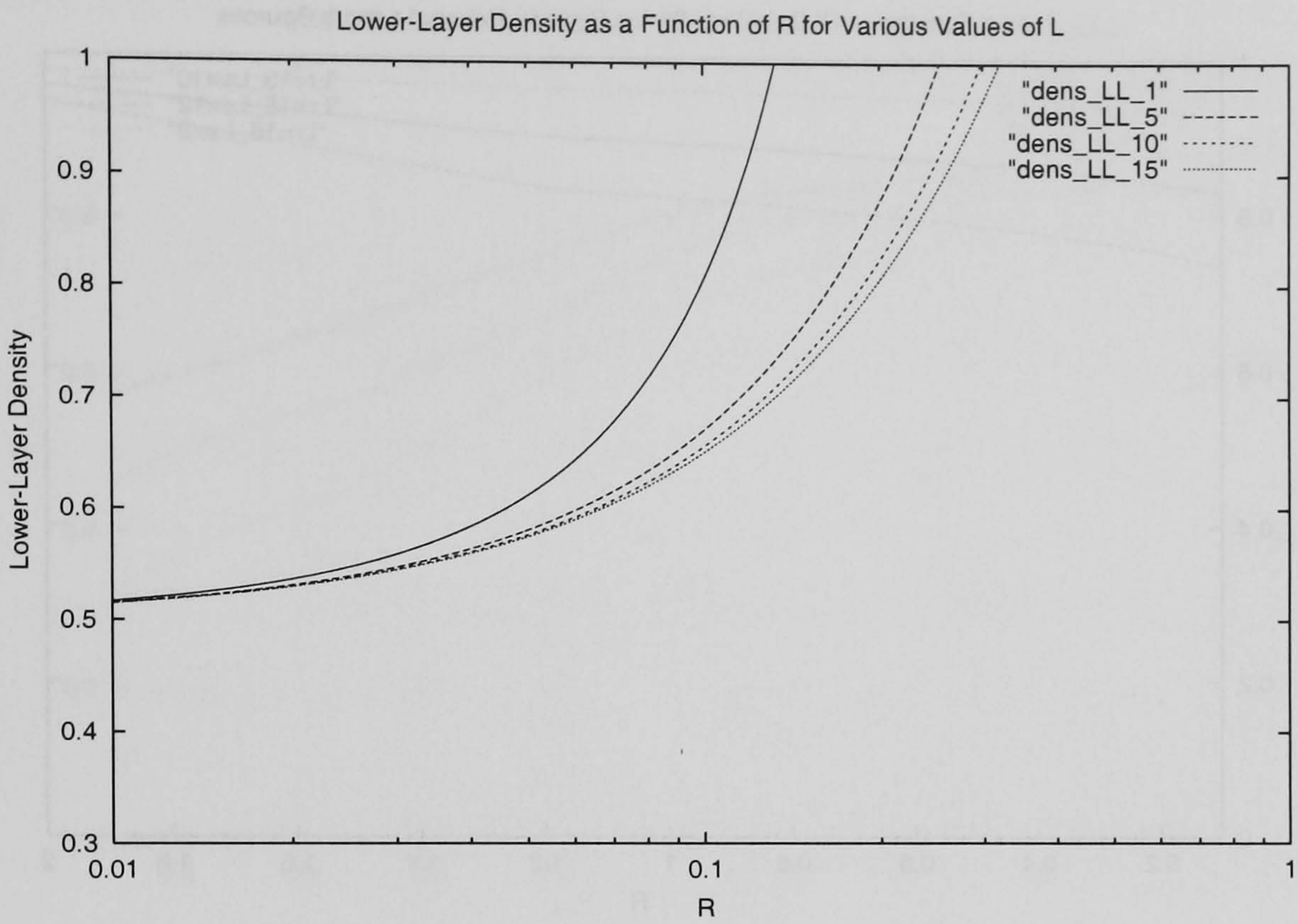

FIGURE 4.5: Density of the lower fluid layer as a function of the normalised mass flux associated with the ascending plume for a dual-plume filling-box system driven by a pair of line plumes. Each of the curves represents a different value of $\hat{L}$.

We see in both figures that reducing the respective value of $\hat{L}$ decreases the fractional dilution of the line plume with respect to the case $\hat{L} = 15$. This is apparent in figure 4.7. The interface is located progressively closer to the top of the container as $\hat{L}_S$ is reduced. We expect the converse to be the case when $\hat{L}_S = 15$, and the values of $\hat{L}_R$ are reduced. This is the behaviour shown in figure 4.8.

4.3 Hybrid Models

In this section, we examine hybrid dual-plume systems, namely a configuration consisting of a line plume and an axisymmetric plume. We derive the model for each system and present the corresponding numerical results

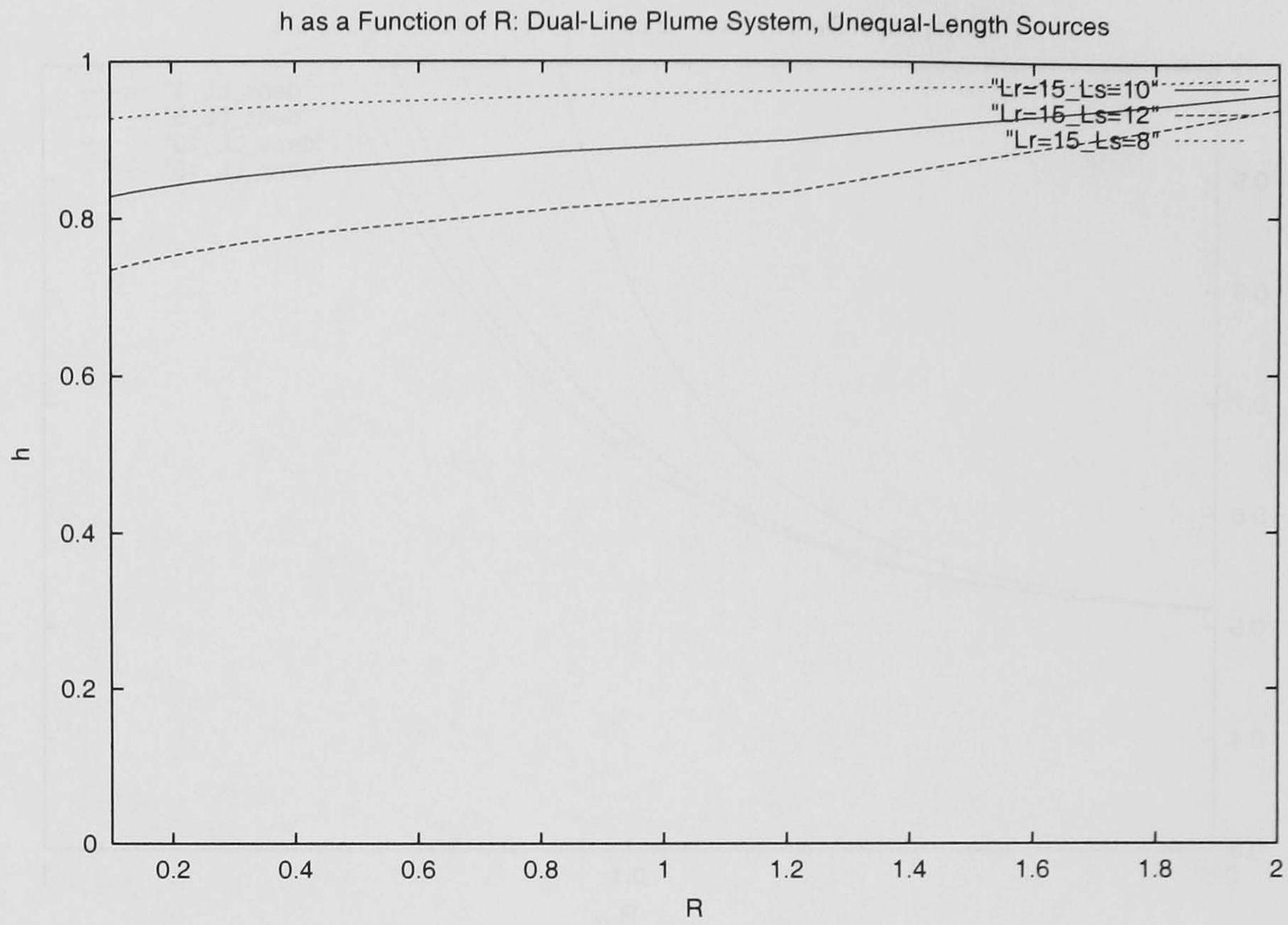

FIGURE 4.6: Interface location as a function of R for $R = S$. In this case, $\hat{L}_R = 15$ and $\hat{L}_S = 12, 10, 8$.

below.

4.3.1 Ascending Line Plume, Descending Axisymmetric Plume

4.3.2 The Model

The total fluid flux associated with the ascending line plume at $\hat{z} = \hat{h}$ is given, in dimensionless form, by

$$\hat{Q}_3 = \hat{\rho}_l^{1/2} \left(\hat{h} + \hat{h}_l \right)^{3/2} \tag{4.48}$$

We may write a similar expression for the net flux associated with the descending axisymmetric plume as it reaches the interface:

$$\hat{Q}_4 = (1 - \hat{\rho}_u)^{1/2} \left(1 - \hat{h} + \hat{h}_u \right)^{5/2} \tag{4.49}$$

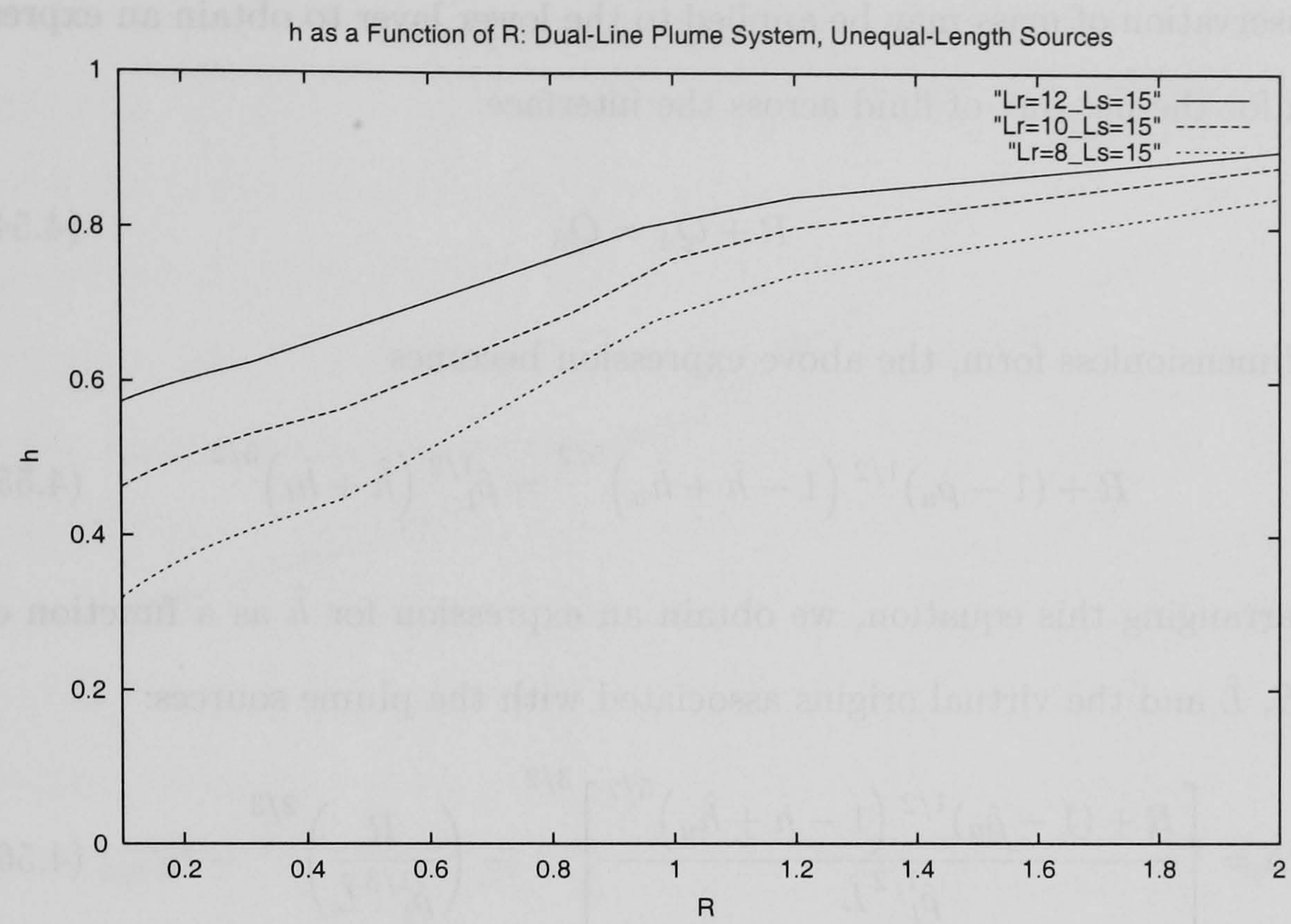

FIGURE 4.7: Interface location as a function of R for $R = S$. In this case, $\hat{L}_S = 15$ and $\hat{L}_R = 12, 10, 8$.

We also have expressions for the dimensionless initial mass fluxes associated with each of the plume sources. For the line plume, this is

$$R = \hat{\rho}_l^{1/3} \hat{h}_l^{3/2} \tag{4.50}$$

and the corresponding expression for the axisymmetric plume

$$S = \left(\frac{R}{R+S} \right)^{1/2} \hat{h}_u^{5/2} \tag{4.51}$$

We may then re-arrange the above two expressions to obtain explicit expressions for each of the virtual origin terms. Firstly, $\hat{h}_l$:

$$\hat{h}_l = \left(\frac{R}{\hat{\rho}_l^{1/3} \hat{L}} \right)^{2/3} \tag{4.52}$$

and the corresponding expression for the upper source

$$\hat{h}_u = \left[S \left(\frac{R+S}{R} \right)^{1/2} \right]^{2/5} \tag{4.53}$$

Conservation of mass may be applied to the lower layer to obtain an expression for the net flux of fluid across the interface:

$$R + Q_4 = Q_3 \tag{4.54}$$

In dimensionless form, the above expression becomes

$$R + (1 - \hat{\rho}_u)^{1/2} \left(1 - \hat{h} + \hat{h}_u\right)^{5/2} = \hat{\rho}_l^{1/2} \left(\hat{h} + \hat{h}_l\right)^{3/2} \tag{4.55}$$

Re-arranging this equation, we obtain an expression for $\hat{h}$ as a function of R, S, $\hat{L}$ and the virtual origins associated with the plume sources:

$$\hat{h} = \left[\frac{R + (1 - \hat{\rho}_u)^{1/2} \left(1 - \hat{h} + \hat{h}_u\right)^{5/2}}{\hat{\rho}_l^{1/2} \hat{L}}\right]^{3/2} - \left(\frac{R}{\hat{\rho}_l^{1/3} \hat{L}}\right)^{2/3} - \hat{h}_l \tag{4.56}$$

Since the descending plume is an axisymmetric plume, the expression for the density of the lower fluid layer is identical to equation (2.45) of Chapter 2. Substituting this expression for $\hat{\rho}_l$ and also $\hat{h}_l$ into equation (4.56) and re-arranging, we obtain:

$$\hat{h} = \left[\frac{\gamma\,(R+\gamma)\,(R+S)}{S}\right]^{3/4} - \left[\left(\frac{R}{\hat{L}}\right)\left(\frac{R+S}{S}\right)\left(\frac{R+\gamma}{\gamma}\right)^{1/3}\right]^{2/3} \tag{4.57}$$

4.3.3 Numerical Results

We now present numerical solutions to equation (4.57), and examine how the density of the lower fluid layer is affected by line sources of various aspect ratios. Figure 4.9 shows the location of the interface as a function of R for the case of a hybrid system driven by an ascending line plume and a descending axisymmetric plume. The corresponding result for the model of Chapter 2 is also presented for comparison.

It is apparent that the the hybrid system consists of two distinct regimes as R increases when compared to the solution of Chapter 2. The first set of

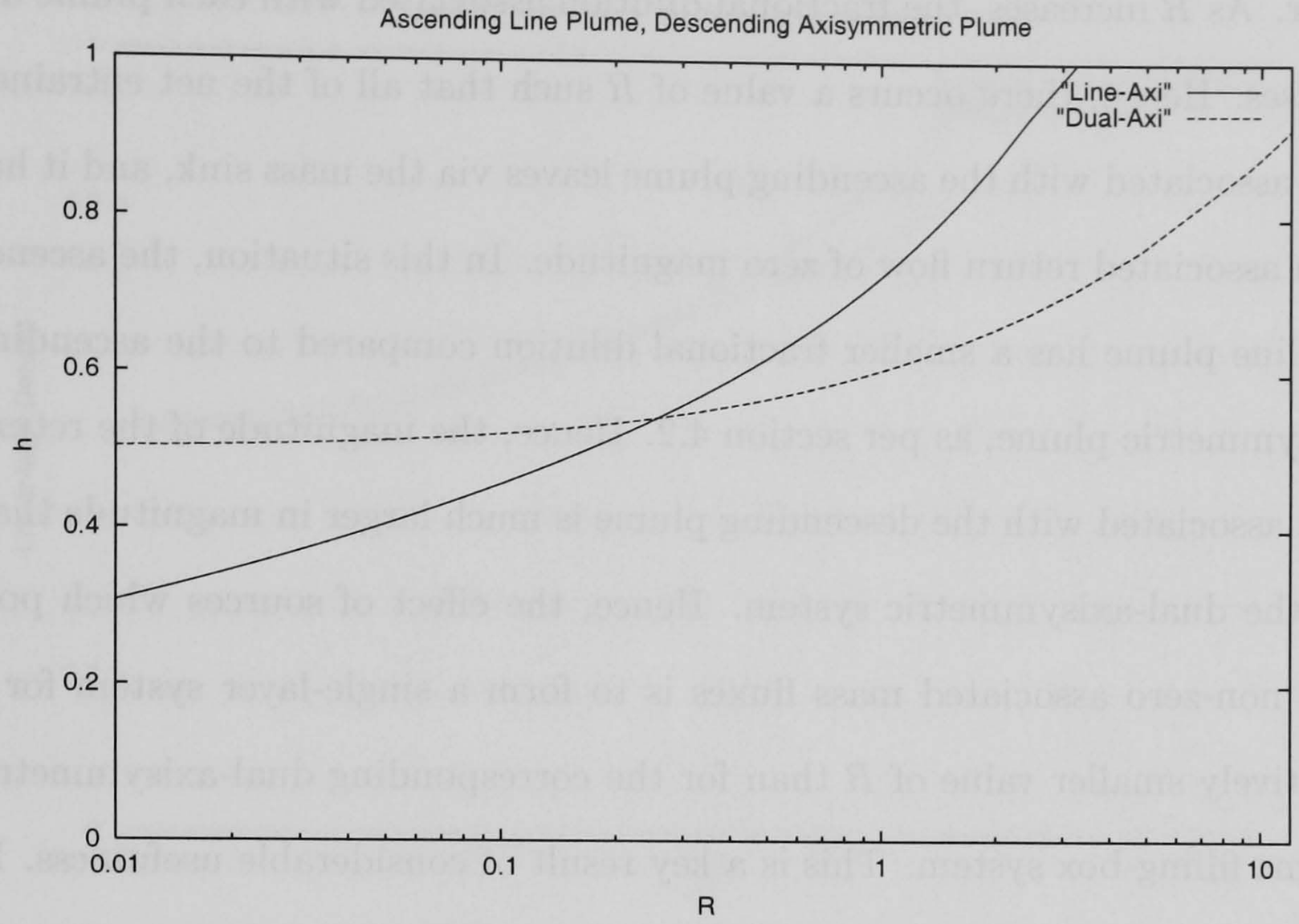

FIGURE 4.8: Location of the fluid interface as a function of the normalised mass flux associated with the ascending plume. The *dashed* curve refers to a dual-plume filling-box system driven by an ascending line plumes and a descending axisymmetric plume. The continuous line is the corresponding system comprising two axisymmetric plumes. In this case, $\hat{L} = 15$.

values to consider is for $R < 0.3$. In this case, the interface is located below the corresponding dual-axisymmetric solution. We explain this as follows.

For a given value of R, we expect that an axisymmetric plume will undergo a greater dilution over a vertical distance $\hat{z}$ than a corresponding line plume. This is true in general. However, in the limit of sources with zero associated mass fluxes, i.e. as $R \to 0$, this is not the case. In this situation, the magnitude of entrainment is greater for the line plume. Hence, as $R \simeq 0.1$, the return flow associated with the line plume is larger in magnitude, and the interface is located below the corresponding dual-axisymmetric solution.

The effects of sources with non-zero associated mass fluxes then become

clear. As R increases, the fractional dilution associated with each plume decreases. Hence, there occurs a value of R such that all of the net entrained flux associated with the ascending plume leaves via the mass sink, and it has a an associated return flow of zero magnitude. In this situation, the ascending line plume has a smaller fractional dilution compared to the ascending axisymmetric plume, as per section 4.2. Hence, the magnitude of the return flow associated with the descending plume is much larger in magnitude than for the dual-axisymmetric system. Hence, the effect of sources which possess non-zero associated mass fluxes is to form a single-layer system for a relatively smaller value of R than for the corresponding dual-axisymmetric plume filling-box system. This is a key result of considerable usefulness. In essence, it states that if the mass fluxes associated with each source is very small, the line plume governs the location of the interface. However, if it is desired to flush all of the upper-layer fluid from the confined region, in the example of a hazardous gas release, the combination of an ascending line plume and a descending axisymmetric plume is more effective than a dual-axisymmetric configuration. Figure 4.10 shows the density of the lower fluid layer as a function of R for the case of an ascending line plume and a descending axisymmetric plume. The corresponding solution from Chapter 2 is reproduced for comparison. We note that for very small values of the mass fluxes associated with the fluid sources, $R \to 0$, the density of the lower fluid layer is approximately the same for both systems. However, for $R \geq 0.3$, $\hat{\rho}_l \to 1$ at relatively smaller values of R for the hybrid system. This is consistent with the solutions presented in figure 4.6. As R increases, the value of H is located closer to the top of the container in the case of the hybrid filling-box. Therefore, the descending axisymmetric plume arrives at the interface less diluted. Consequently, the density of the lower fluid layer

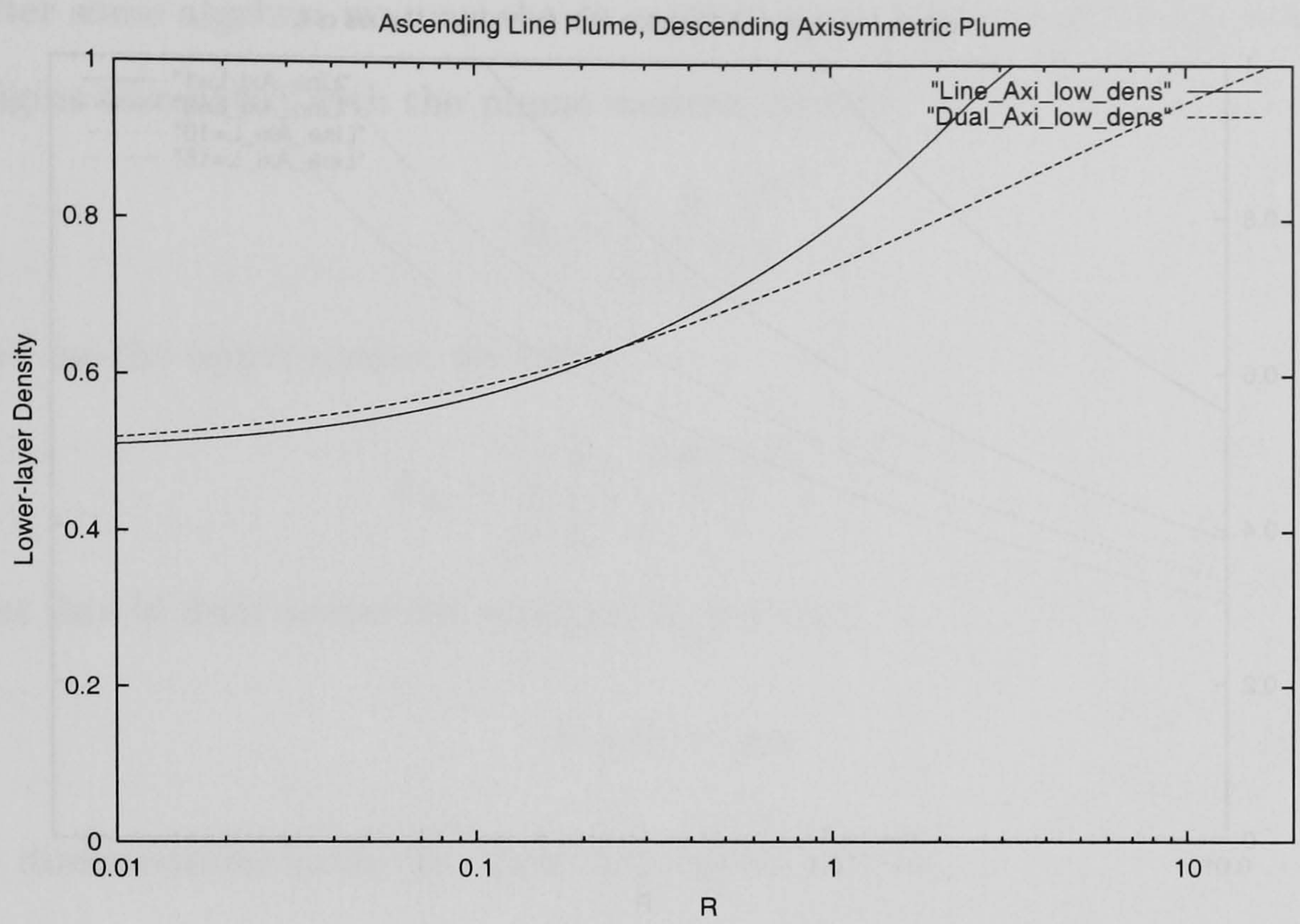

FIGURE 4.9: Density of the lower fluid layer as a function of the normalised mass flux associated with the ascending plume. The *dashed* curve refers to a dual-plume filling-box system driven by an ascending line plumes and a descending axisymmetric plume. The continuous line is the corresponding system comprising two axisymmetric plumes. In this case, $\hat{L} = 15$.

$\rightarrow 1$ for relatively smaller values of R than the dual-axisymmetric filling-box system.

4.3.4 Ascending Axisymmetric Plume, Descending Line Plume

4.3.5 The Model

Finally, we model a dual-plume filling-box system driven by an ascending axisymmetric plume and a descending line plume. The dimensionless net

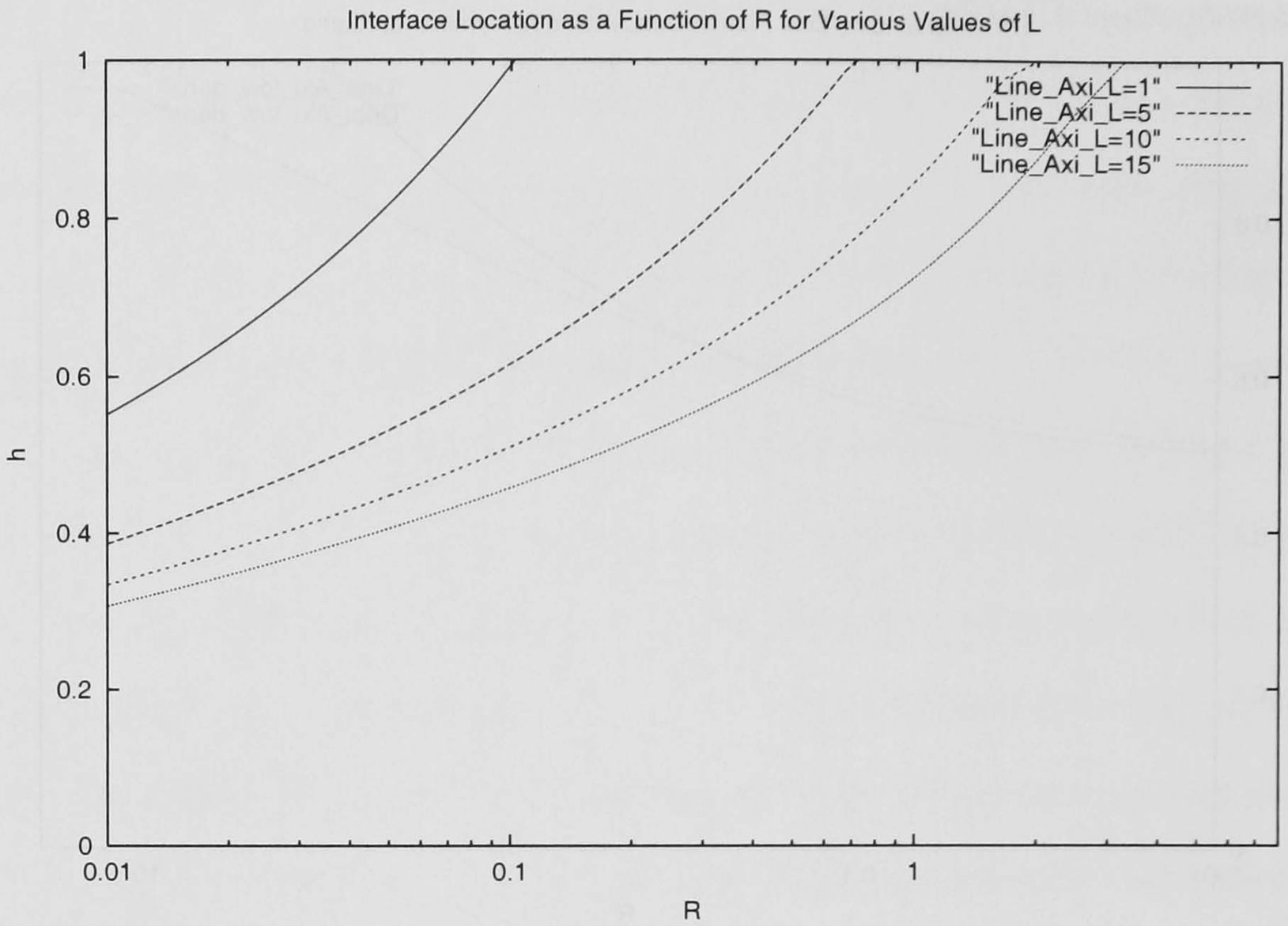

FIGURE 4.10: Location of the fluid interface as a function of the normalised mass flux associated with the ascending plume for a dual-plume filling-box system. The system consists of an ascending line plume and a descending axisymmetric plume. Each of the curves represents a different value of $\hat{L}$.

fluid flux associated with the ascending plume at the interface is given by:

$$\hat{Q}_3 = \hat{\rho}_l^{1/2} \left(\hat{h} + \hat{h}_l\right)^{5/2} \tag{4.58}$$

Correspondingly, for the descending line plume, the net flux at $\hat{z} = \hat{h}$ is

$$\hat{Q}_4 = (1 - \hat{\rho}_u)^{1/2} \left(1 - \hat{h} - \hat{h}_u\right)^{3/2} \hat{L} \tag{4.59}$$

As in the previous section, we may write similar expressions for normalised initial plume mass fluxes:

$$R = \hat{\rho}_l^{1/2} \hat{h}_l^{5/2} \tag{4.60}$$

and

$$S = \left(\frac{R}{R+S}\right)^{1/2} \hat{h}_u^{3/2} \hat{L} \tag{4.61}$$

After some algebra, we may obtain explicit equations for each of the virtual origins associated with the plume sources, namely

$$\hat{h}_l = \left(\frac{R}{\hat{\rho}_l^{1/2}} \right)^{2/5} \tag{4.62}$$

and for the upper source, we have

$$\hat{h}_u = \left[\left(\frac{S}{\hat{L}} \right) \left(\frac{R+S}{S} \right)^{1/2} \right]^{2/3} \tag{4.63}$$

Net flux of fluid across the interface is given by

$$R + Q_4 = Q_3 \tag{4.64}$$

In dimensionless form, the above expression becomes

$$R + (1-\hat{\rho}_u)^{1/2} \left(1 - \hat{h} - \hat{h}_u\right)^{3/2} \hat{L} = \hat{\rho}_l^{1/2} \left(\hat{h} + \hat{h}_l\right)^{5/2} \tag{4.65}$$

Re-arranging, we obtain an equation for $\hat{h}$:

$$\hat{h} = \left[\frac{R + \gamma \hat{L}}{\hat{\rho}_l^{1/2}} \right]^{2/5} - \hat{h}_l \tag{4.66}$$

We also have:

$$\hat{h}_l = \frac{R}{\hat{\rho}_l^{1/2}} \tag{4.67}$$

Since the descending plume is a line plume, the expression for the density of the lower fluid layer is identical to equation (2.45) of Chapter 2. Substituting this expression for $\hat{\rho}_l$ and also $\hat{h}_l$ into equation (4.66) and re-arranging, we obtain:

$$\hat{h} = \left(\frac{R+S}{S} \right)^{1/5} \frac{\left[\left(R + \gamma \hat{L} \right)^{2/5} - R^{2/5} \right] \left(\gamma \hat{L} \right)^{1/5}}{\left(R + \gamma \hat{L} \right)^{1/5}} \tag{4.68}$$

4.3.6 Numerical Results

In this section, we present the numerical results for the hybrid system consisting of an ascending axisymmetric plume and a descending line plume.

Figure 4.12 is a comparison between the hybrid system and the a dual-axisymmetric filling-box. The interface location as a function of R is shown in both cases.

As $R \to 0$, the fractional dilution of the axisymmetric plume is much greater than the corresponding quantity for the line plume. Hence, the return flow associated with the ascending plume is greater in magnitude than than the return flow associated with the descending plume. This is true even though the mass sink is located in the upper fluid layer. As R increases, however, the interface is located for similar values of $\hat{h}$ in both systems. This is because as R increases, the location of the interface is controlled by the fractional dilution associated with the ascending plume. This has been the case for each of the systems that we have examined when $R = S$. Therefore, we expect the difference in $\hat{h}$ between the hybrid model and the system of Chapter 2 to be small. This is the behaviour shown in figure 4.12.

This is, however, an important result. It states that the difference in $\hat{h}$ between the hybrid system and the dual-axisymmetric case is small if the amount of fluid mass flowing through the confined region is relatively large. We expect this not to be the case for the density of the lower fluid layer. however. Figure 4.13 shows the density of the lower fluid layer as a function of R for the case $R = S$. A system consisting of an ascending axisymmetric plume and a descending line plume, and the model of Chapter 2, are shown.

The physical effects of each of the plume flows is apparent in this figure. Firstly, $\hat{\rho}_l \to 1$ for a smaller value of R in the hybrid model than for the dual-axisymmetric case. This arises due to the fractional dilution of the descending line plume being less than the axisymmetric plume in the model of Chapter 2. Hence, the descending plume arrives at the interface undiluted

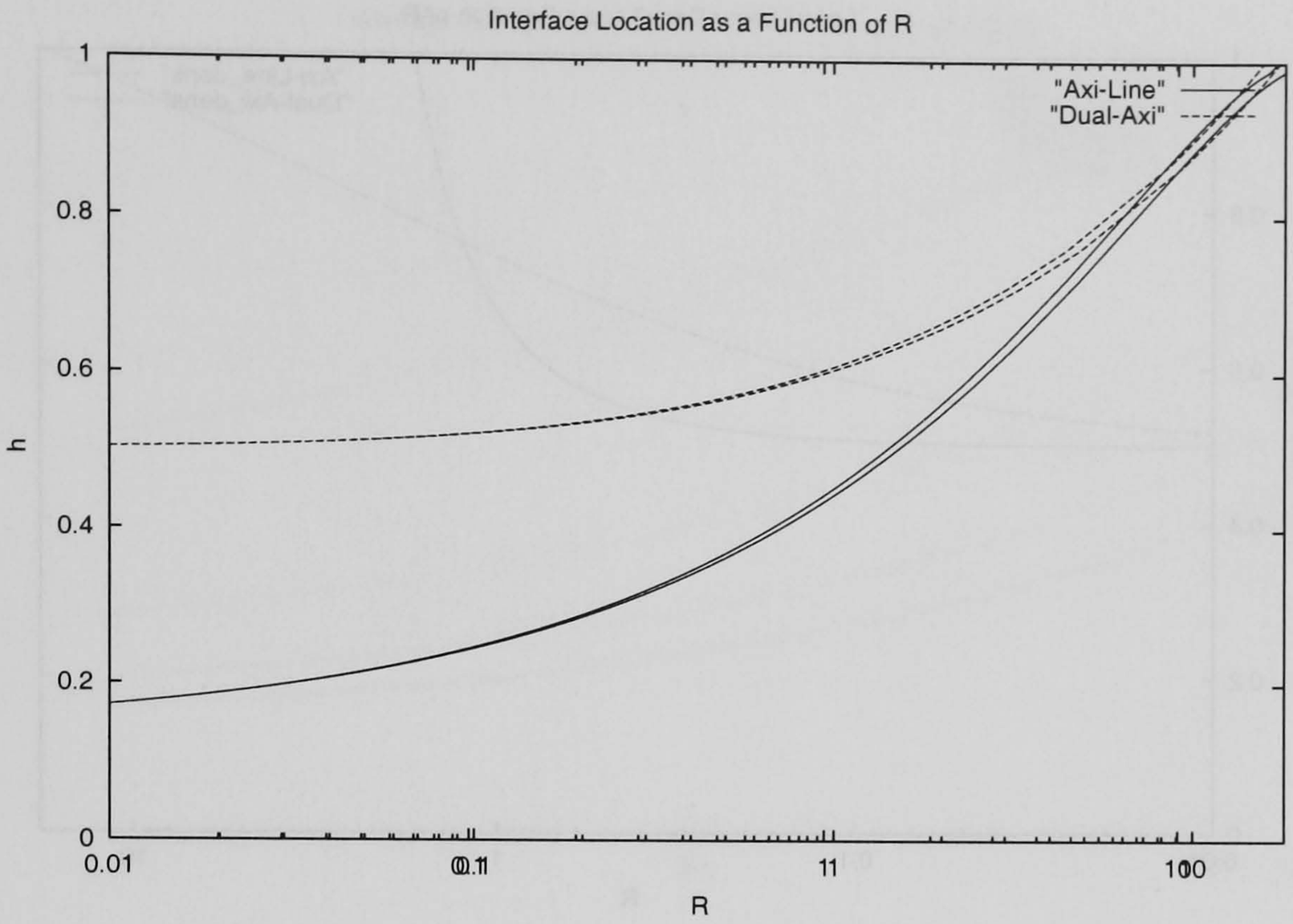

FIGURE 4.11: Location of the fluid interface as a function of the normalised mass flux associated with the ascending plume. The *continuous* curve refers to a dual-plume filling-box system driven by an ascending axisymmetric plumes and a descending line plume. The dashed line is the corresponding system comprising two axisymmetric plumes. In this case, $\hat{L} = 15$.

for a value of R less than in the dual-axisymmetric case. Further, for $R < 0.5$, $\hat{\rho}_l$ is approximately constant. This occurs because the lower fluid layer is relatively deep for $R < 1.0$. The system remains in a stably-stratified configuration, however, and so the descending line plume does not decrease in density below ~ 0.5. This is also because the fractional dilution of the descending plume is less than the corresponding dilution of the axisymmetric plume. Figure 4.13 shows the lower-layer density as a function of R for the case of a hybrid system. The density variation is plotted for different values of $\hat{L}$. As before, we expect the fractional dilution of the line plume to decrease as $\hat{L}$ decreases. This occurs due to reduced entrainment, arising

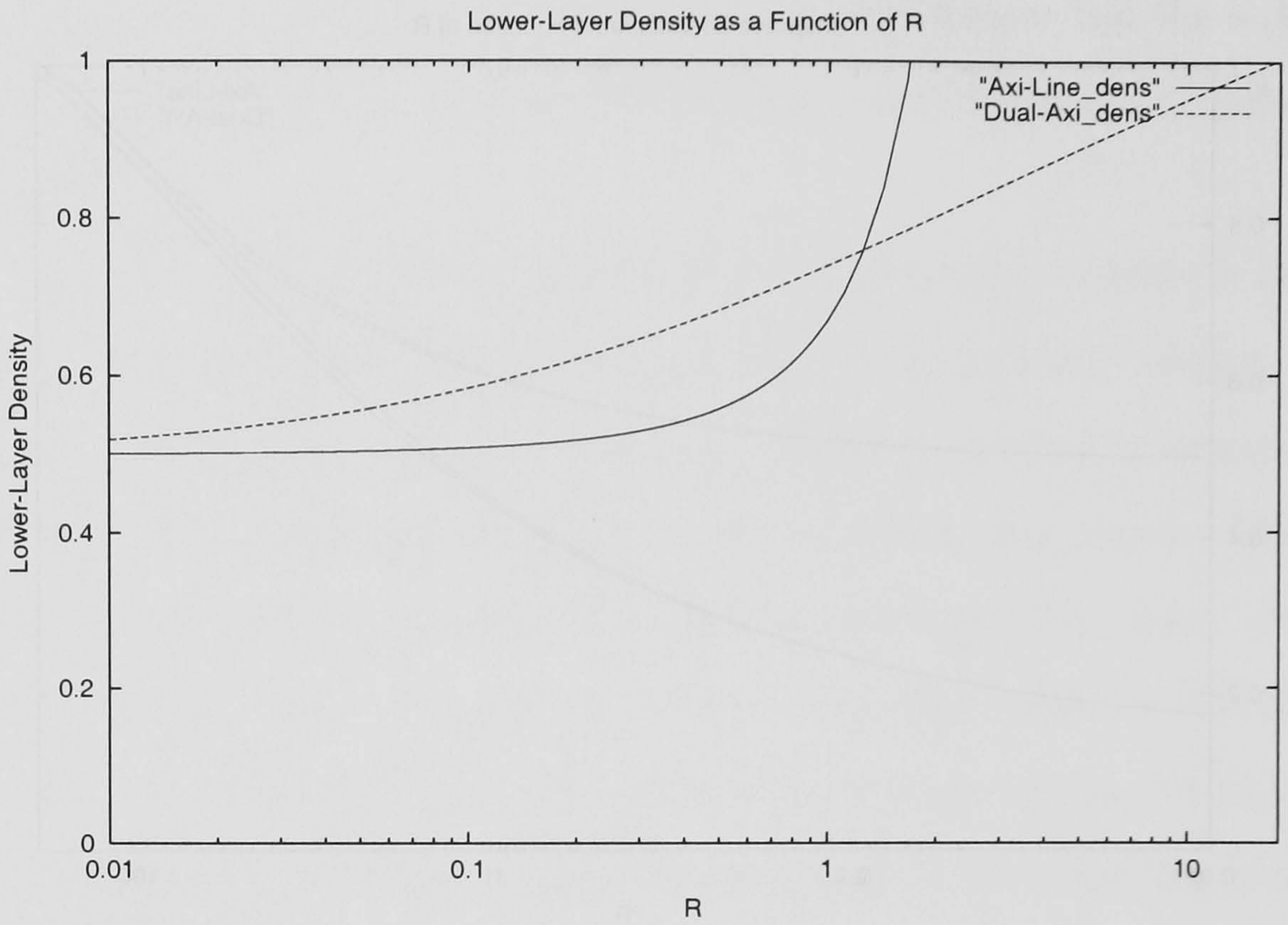

FIGURE 4.12: Density of the lower fluid layer as a function of the normalised mass flux associated with the ascending plume. The *continuous* curve refers to a dual-plume filling-box system driven by an ascending axisymmetric plume and a descending line plume. The dashed line is the corresponding system comprising two axisymmetric plumes. In this case, $\hat{L} = 15$.

because of the distributed source. Hence, we expect that as $\hat{L}$ decreases, the descending line plume will become progressively less diluted. Hence, $\hat{\rho}_l \to 1$ as progressively smaller values of R. This is the behaviour shown in the graph.

4.4 Conclusions

The steady-state dual-plume filling-box model of Chapter 2 has been extended by considering a variety of different source configurations. The principle investigation concerned the effects of a line source which provided a

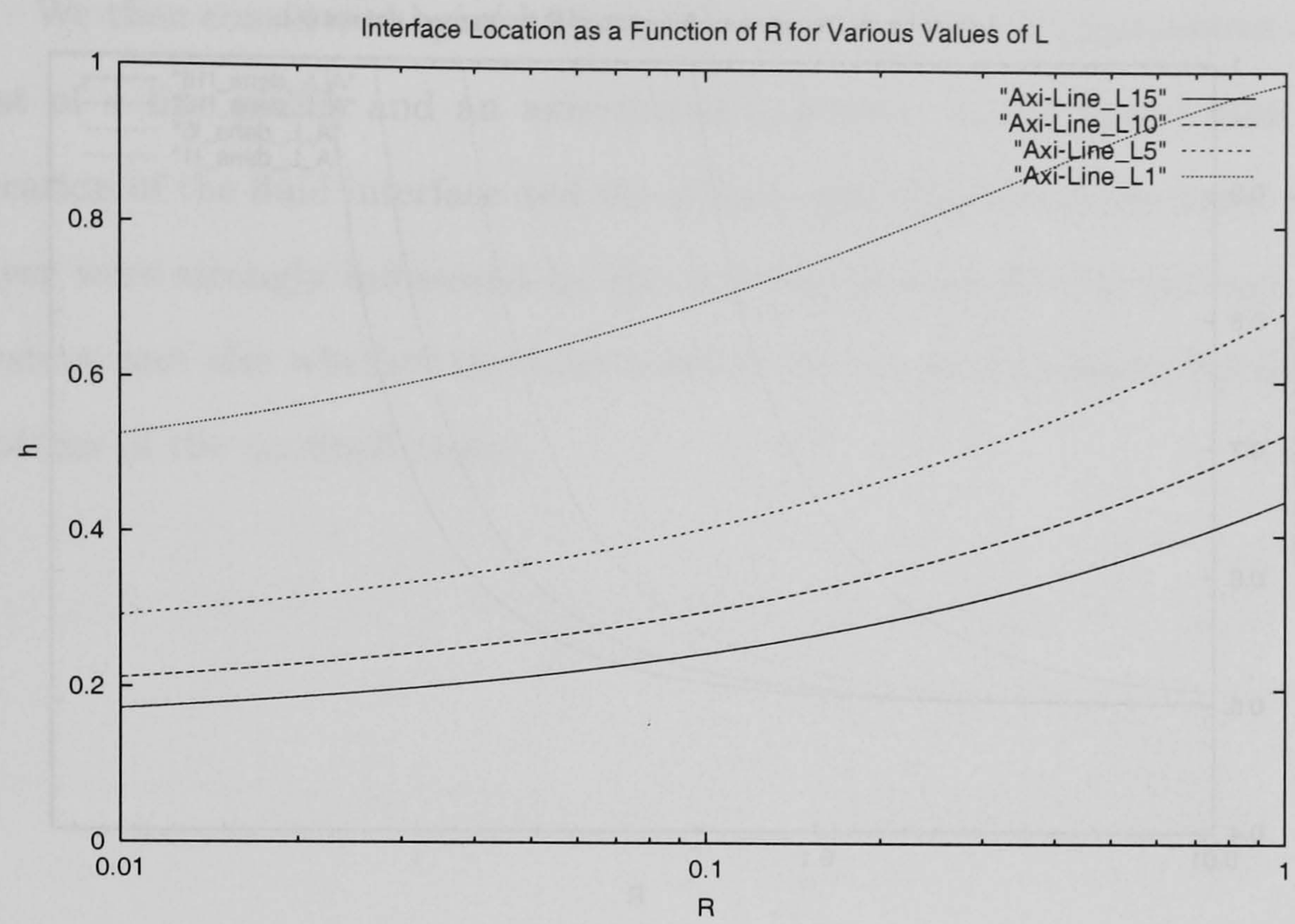

FIGURE 4.13: Location of the fluid interface as a function of the normalised mass flux associated with the ascending plume. The *dashed* curve refers to a dual-plume filling-box system driven by an ascending axisymmetric plumes and a descending line plume. The continuous line is the corresponding system comprising two axisymmetric plumes. In this case, $\hat{L} = 15$.

non-zero associated flux of fluid mass.

A filling-box driven by a line plume had previously been commented upon by Baines & Turner (1969). However, a dual-plume system had not previously been studied. Further, a filling-box flow driven by a line source which supplied fluxes of buoyancy and mass constituted new work.

It was found that the dual-line plume filling-box system had quantitative differences when compared with the dual axisymmetric model of Chapter 2. The system considered two line plumes of equal aspect ratio. The fluid interface between the two well-mixed layers was found to be located closer to the top of the container for the dual line-plume system. This occurred

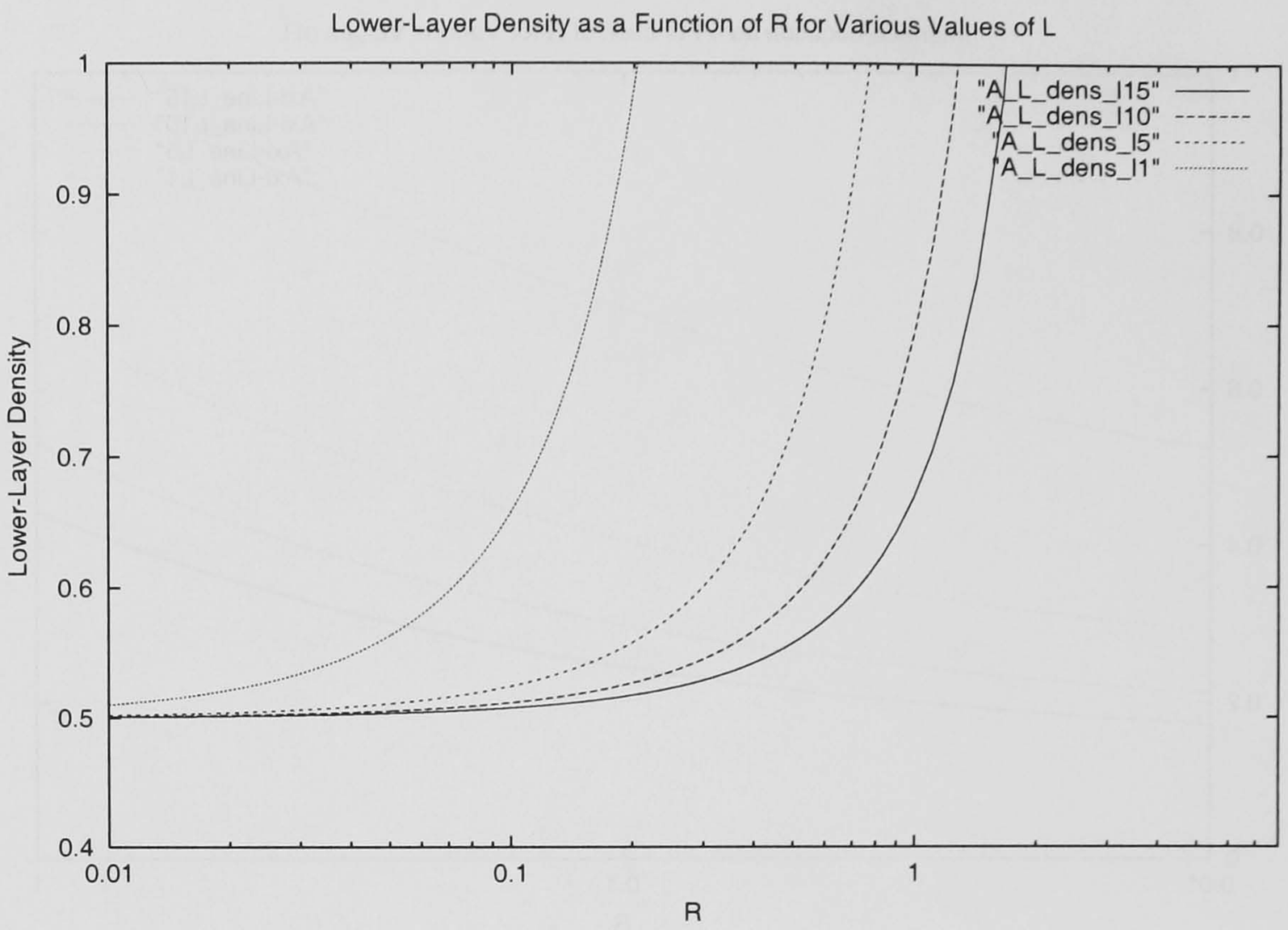

FIGURE 4.14: Density of the lower fluid layer as a function of the normalised mass flux associated with the ascending plume. The *dashed* curve refers to a dual-plume filling-box system driven by an ascending axisymmetric plume and a descending line plume. The continuous line is the corresponding system comprising two axisymmetric plumes. In this case, $\hat{L} = 15$.

because of the reduced fractional dilution of the line plumes compared to the dual-axisymmetric case. Consequently, the $\hat{\rho}_l \to 1$ at a lower value of R.

A simple modification to the model implied that as the aspect ratio of the line source was decreased, the effect was to cause the fluid flow to become distributed over an area. This was implied by the reduction in the fractional dilution of the line plume, which became apparent from comparison of numerical solutions for various values of $\hat{L}$. It was also found that increasing R caused the density of the lower fluid layer to tend to 1 faster in the case of a dual-line source filling-box system.

We then considered hybrid filling-box models. These configurations consist of a line plume and an axisymmetric plume. It was found that the location of the fluid interface and the density associated with the lower fluid layer were strongly influenced by the net flux of mass flowing through the system, and also whether the axisymmetric source was located at the top or bottom of the confined region.

Chapter 5

The Naturally-Ventilated Dual-Plume Filling Box

" (Come in under the shadow of this red rock),

And I will show you something different from either

Your shadow at morning striding behind you

or your shadow at evening rising to meet you..."

– T.S. Eliot, *The Waste Land: I - The Burial of the Dead*

5.1 Introduction

In recent years, there has been a considerable interest in the design of buildings that are *naturally ventilated.* In this process, mechanical air conditioning is replaced in such a manner that the building is ventilated by fluid buoyancy and wind alone. This system has two immediate advantages. First, the cost of installing and maintaining the machinery to drive the air

flow is saved. Secondly, mechanical ventilation systems may compromise air quality by spreading dust, particularly if they are not regularly serviced.

However, natural ventilation has a number of disadvantages. Firstly, dirt and noise from regions external to the building may be introduced into its interior. Secondly, the buoyant flows that drive the ventilation require certain temperature ranges in the external ambient. Hence, the natural ventilation process may not be so effecient in Winter. Finally, natural ventilation is less controllable than mechanical ventilation. Further, buildings which are intended to be naturally-ventilated must be carefully designed if the flows are to be effective.

Since the buoyant flows through interconnected finite-sized regions are liable to be extremely complex, it is of interest to use simple models to aid understanding of natural ventilation flows.

Cooper & Linden (1996) published a study which examined the natural ventilation flow in a confined region. The container was rectangular in shape, and possessed vents in both the upper and lower horizontal boundaries. The fluid flows in the confined region consisted of two turbulent axisymmetric plumes of opposing buoyancy. Cooper & Linden (1996) derived a steady-state model for the system, which predicted the density profile and the location of the fluid interfaces.

However, their model considered plume flows which originated from sources of pure buoyancy alone. One of the principal features of naturally-ventilated systems is the displacement of fluid through a vent to allow fluid with a more desirable temperature, say, to flow into the room. Such displacement ventilation often involves fluid flows with an associated mass flux, for example the inflow of cool air into a hot room.

In this section, therefore, we extend the steady-state system of Chapter 2

to examine the consequences of sources with non-zero associated mass upon a system which may admit naturally-ventilated flows. To facilitate this, we provide a second mass sink located in the lower horizontal boundary. Our principal interest is to obtain some simple conditions with which to predict the net flow of fluid mass through the confined region.

We begin this Chapter in §5.2 by providing a brief overview of the fluid mechanics of the natural ventilation of a finite enclosure. We consider the dynamics of the ventilation process, and how this is driven due to buoyancy forces displacing fluid out of the closed region in section 5.3.

We also arrive, via some simple analysis, at key result. We find that there are two possible flow regimes for the system. Further, we provide a simple limiting argument to predict which of the two states the system will be in.

Proceeding in a similar manner to Chapter 2, we derive models for each of the two ventilation states in 5.3.2 and 5.3.4. One of these models is solved numerically, and the the corresponding results are presented in §5.4. For the other model, we discuss the repercussions of the model in 5.3.3

In the models described above, we assume that the flow of fluid out of the confined region is unimpeded. In actuality, there may be an flow of wind outside the confined region. This external flow may impose a pressure gradient on the fluid leaving the building. We briefly consider this case in 5.5, and derive a simple model to examine the subsequent effects upon the ventilation flow. Finally, some overall conclusions are discussed in §5.6

5.2 Overview of natural ventilation

The ventilation of indoor spaces provides a method to control ambient air quality and achieve thermal comfort for the occupants. The efficient appli-

cation of ventilation is therefore a powerful means to exhaust air pollutants of all forms into the outdoor environment. However, mechanically-driven ventilation systems may be costly in terms of energy usage. In cases where the outdoor conditions are suitable, natural ventilation may prove to be an energy-saving method to reduce the internal cooling load, achieve thermal comfort, and to maintain a satisfactory indoor environment. Air is driven in and out of internal enclosures as a result of pressure differences across the openings in the building, such as windows and doors. These pressure variations arise due to buoyancy forces, which occur due to environmental temperature contrasts.

The inflow and outflow of air through large building openings in natural ventilation is mainly due to the effect of thermal forces. These forces arise due to internal temperature differences, especially under conditions of low ambient wind speeds (Santamouris & Asimakopoulos, 1997). However, in situations where the external atmospheric conditions are significant, the effect of the wind may play a significant rôle in affecting the ventilation dynamics. Frequently, this occurs when the ventilation stack is located upon one side of the building. Such a stack consists of a chimney-like construct for venting relatively hot air out of the building. This implies that in one direction, the wind may suppress the fluid leaving the confined region, while in the other direction, the effect of the wind may be to enhance the ventilating process. A simple example of this is when a window is opened in a relatively warm room. In conditions of low wind, the fluid leaving the container will be driven entirely by displacement ventilation. However, if the direction of exterior wind is towards the window, the effect of the displacement will be reduced. A detailed description of the effects of external wind upon the ventilation process may be found in Hunt & Linden (1996).

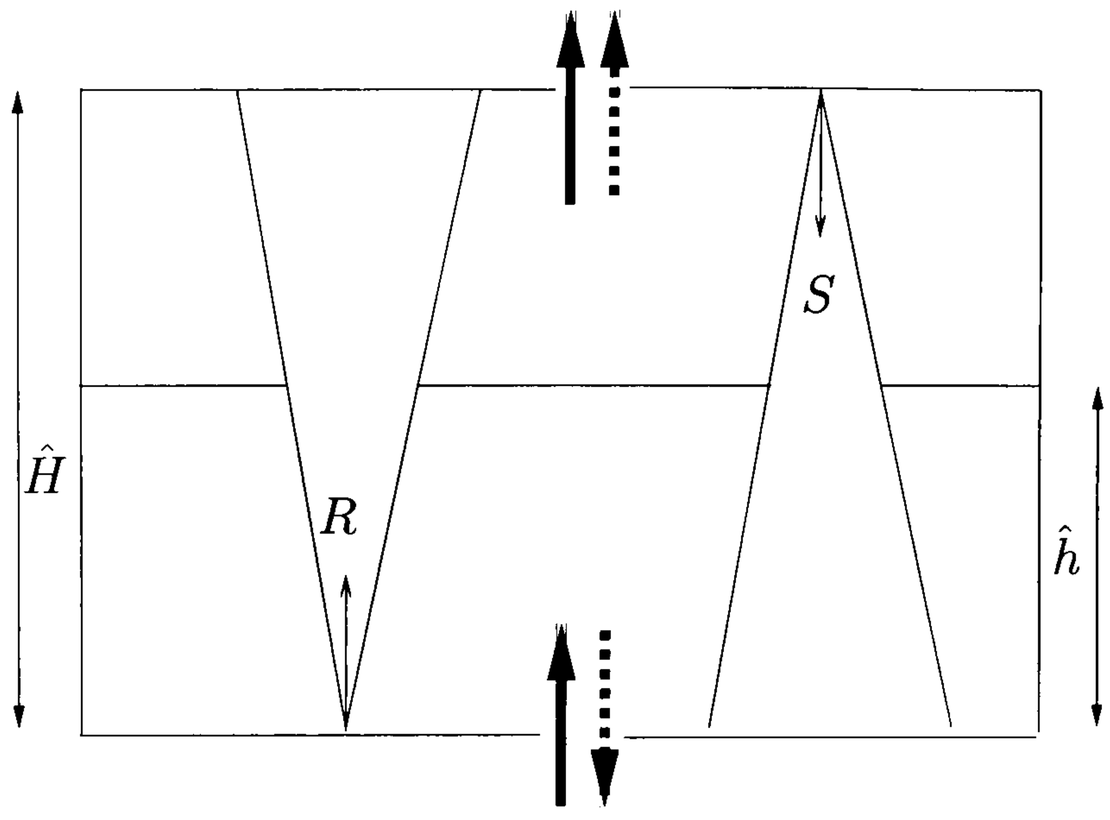

FIGURE 5.1: Illustration of the dual-plume filling-box system subject to natural ventilation. This arises due to the provision of a second mass sink in the lower horizontal boundary. The dashed arrows refer to the non-exchange regime; the unbroken arrows indicate the direction of mass flux in the naturally-ventilated flow case. Each regime is discussed in greater detail in the text.

5.3 Models of Naturally-Ventilated Systems

5.3.1 The Limiting Case

In the current discussion, we simply provide a second mass sink. This second outflow vent is located in the lower horizontal boundary. Hence. if the sources and the initial ambient density are configured appropriately, external fluid will enter the confined region via the lower opening. Fluid mass will hence exit the filling-box via the outflow vent in the upper boundary. The system is then representative of a natural ventilation flow. This is illustrated in figure 5.1.

We expect, however, that this will only be the case for a certain range of R and S. Essentially, we would expect that for very large values of the initial

mass fluxes associated with the fluid sources, fluid in the confined region would leave via *both* mass sinks. Note that in modelling the flow system in this Chapter, we do not explicitly quantify the pressure at each outflow vent. We consider the limiting case, described below, as implicitly representing the pressure gradients at the upper and lower horizontal boundaries. A more complex description of the system is beyond the scope of this Chapter, but would be vital in direct application of the model.

We may apply a simple argument to derive an expression to determine whether the system exhibits an exchange flow. The criteria we require is the limiting case such that fluid mass leaves the confined region via the upper vent *only*. In this situation, all of the buoyancy and mass entering the system via the plume sources leaves through the upper vent. Further, in this situation external fluid will enter the confined region via the lower vent. We refer to this as the *exchange-flow case*.

Let us denote the mass fluxes associated with the plume sources for the model of Chapter 2 as $\overline{Q}_1$ and $\overline{Q}_2$. We use the steady-state model of Chapter 2 as a reference case.

Now, the limiting argument may be described as follows. First, we let Q_1 and Q_2 be the mass fluxes associated with the ascending and descending plumes, respectively, the double-vented dual-plume filling-box system shown in figure 5.1. Now, there exists the possibility that Q_1 and Q_2 take values such that all of the mass flux entering via the sources just leaves through the upper vent. This implies that the system contains pressure gradients such that fluid just enters from the external region via the lower vent.

We then take the new model, hypothetically create a lower opening, and then compare the actual source mass fluxes of that case with those for the canonical model. Hence, we have three flow regimes. The first of these is

the model of Chapter 2, where global mass conservation is given by

$$\overline{Q}_1 + \overline{Q}_2 = Q_u \tag{5.1}$$

where Q_u is the flux of fluid mass leaving the confined region via the upper vent. The global conservation of buoyancy is

$$\overline{Q}_1\rho_1 + \overline{Q}_2\rho_2 = Q_u\rho_u = \left(\overline{Q}_1\rho_1 + \overline{Q}_2\right)\rho_u \tag{5.2}$$

The next possibility is a model which admits an exchange flow. In this situation, global mass conservation is given by

$$Q_1 + Q_2 = Q_u - Q_l \tag{5.3}$$

where Q_l is the mass flux of the fluid entering the region through the outflow vent located in the lower horizontal boundary, Global conservation of buoyancy is given by

$$Q_1\rho_1 + Q_2\rho_2 = Q_u\rho_u - Q_l\rho_{ext} \tag{5.4}$$

where ρ_{ext} is the density of external fluid entering the confined region via the lower vent. Finally, we also have the situation dictated by the non-exchange model, with corresponding global mass conservation according to

$$Q_1 + Q_2 = Q_u + Q_l \tag{5.5}$$

and the global conservation of buoyancy is given by the following relation:

$$Q_1\rho_1 + Q_2\rho_2 = Q_u\rho_u + Q_l\rho_l \tag{5.6}$$

We have now arrived at the key result. The limiting argument above gives two conditions. Firstly, if

$$Q_1 + Q_2 > \overline{Q}_1 + \overline{Q}_2 \tag{5.7}$$

the system is in a non-exchange flow regime. Conversely, if

$$Q_1 + Q_2 < \overline{Q}_1 + \overline{Q}_2 \tag{5.8}$$

there is exchange of ambient fluid through the filling-box region. Therefore, by knowing the values of Q_1 and Q_2, we may use the conditions 5.7 and 5.8 above, together with the model of Chapter 2 to predict the net flow of mass through the system. Even though the limiting argument is very simple, it is a useful result for approximating to leading-order the overall behaviour of the system.

We may primarily associate the mixing ventilation with the buoyancy component of the source, and the displacement ventilation with the component of the source mass flux. We also impose the restriction that all such fluid is incompressible. This is a reasonable assumption given the typical temperature ranges present in building ventilation.

5.3.2 $Q_c > Q_0$: The Non-Exchange Flow System

We model this flow regime by proceeding in a standard manner. We first form global conservation laws. The global conservation of mass is given by the relation

$$Q_1 + Q_2 = Q_u + Q_l \tag{5.9}$$

and, secondly, global buoyancy conservation is specified by

$$Q_1\rho_1 + Q_2\rho_2 = Q_u\rho_u + Q_l\rho_l \tag{5.10}$$

We may now write similar conservation equations for each of the two fluid layers. The upper layer mass conservation is given by the relation

$$Q_3 + Q_2 = Q_4 + Q_u \tag{5.11}$$

while the local buoyancy conservation is described by

$$Q_3\rho_3 + Q_2\rho_2 = Q_4\rho_l + Q_u\rho_u \tag{5.12}$$

For the lower layer, mass conservation yields the expression

$$Q_1 + Q_4 = Q_3 + Q_l \tag{5.13}$$

while conservation of buoyancy results in

$$Q_1\rho_1 + Q_4\rho_l = Q_3\rho_u + Q_l\rho_l \tag{5.14}$$

From (5.11), we have:

$$Q_u = Q_3 + Q_2 - Q_4 \tag{5.15}$$

Substituting into (5.12) and re-arranging, we get

$$Q_4 = \frac{Q_2\left(\rho_2 - \rho_u\right)}{\rho_l - \rho_u} \tag{5.16}$$

upon using the condition that $\rho_3 = \rho_u$. Similarly, (5.13) gives

$$Q_l = Q_1 + Q_4 - Q_3 \tag{5.17}$$

and hence, use of (5.14) yields

$$Q_3 = \frac{Q_1\left(\rho_1 - \rho_l\right)}{\left(\rho_u - \rho_l\right)} \tag{5.18}$$

We now eliminate the venting mass fluxes. Using (5.9) and (5.10) to eliminate Q_u and Q_l:

$$Q_u = \frac{Q_1\rho_1 + Q_2\rho_2 - \rho_l\left(Q_1 + Q_2\right)}{\rho_u - \rho_l} \tag{5.19}$$

$$Q_l = \frac{Q_1\rho_1 + Q_2\rho_2 - \rho_u\left(Q_1 + Q_2\right)}{\rho_l - \rho_u} \tag{5.20}$$

We hence arrive at the system of four equations:

$$Q_3 + Q_2 = Q_4 + \left[\frac{Q_1\rho_1 + Q_2\rho_2 - \left(Q_1 + Q_2\right)\rho_l}{\rho_u - \rho_l}\right] \tag{5.21}$$

$$Q_3\rho_u + Q_2\rho_2 = Q_4\rho_l + \rho_u\left[\frac{Q_1\rho_1 + Q_2\rho_2 - \rho_u\left(Q_1 + Q_2\right)}{\rho_u - \rho_l}\right] \tag{5.22}$$

$$Q_1 + Q_4 = Q_3 + \left[\frac{Q_1\rho_1 + Q_2\rho_2 - \rho_u\left(Q_1 + Q_2\right)}{\rho_l - \rho_u}\right] \tag{5.23}$$

$$Q_1\rho_1 + Q_4\rho_l = Q_3\rho_u + \rho_l\left[\frac{Q_1\rho_1 + Q_2\rho_2 - \rho_u\left(Q_1 + Q_2\right)}{\rho_l - \rho_u}\right] \tag{5.24}$$

We now apply precisely the same scalings as per equations (2.32) – –(2.36) of Chapter 2. Hence, we have $\rho_1 \to 0$, $\rho_2 \to 1$, $Q_1 \to R$ and $Q_2 \to S$. Applying these to parameters, we normalise equations (5.21) – –(5.24), and obtain:

$$\hat{Q}_3 + S = \hat{Q}_4 + \left[\frac{S - (R+S)\,\rho_l}{\hat{\rho_u} - \hat{\rho}_l}\right] \tag{5.25}$$

$$\hat{Q}_3\hat{\rho}_u + S = \hat{Q}_4\hat{\rho}_l + \hat{\rho}_u\left[\frac{S - (R+S)\,\rho_l}{\hat{\rho_u} - \hat{\rho}_l}\right] \tag{5.26}$$

$$R + \hat{Q}_4 = \hat{Q}_3 + \left[\frac{S - (R+S)\,\hat{\rho}_u}{\hat{\rho}_l - \hat{\rho}_u}\right] \tag{5.27}$$

$$\hat{Q}_4\hat{\rho}_l = \hat{Q}_3\hat{\rho}_u + \hat{\rho}_l\left[\frac{S - (R+S)\,\hat{\rho}_u}{\hat{\rho}_l - \hat{\rho}_u}\right] \tag{5.28}$$

Next we apply the scalings to reduce equations (5.27) and (5.28) to dimensionless form. We have:

$$\hat{Q}_4 = \frac{S\left(1 - \hat{\rho}_u\right)}{\hat{\rho}_l - \hat{\rho}_u} \tag{5.29}$$

$$\hat{Q}_3 = -\frac{R\hat{\rho}_l}{\hat{\rho}_u - \hat{\rho}_l} \tag{5.30}$$

Next, we recall the explicit expression for $\hat{Q}_4$ from section 2.3 of Chapter 2, namely

$$\hat{Q}_4 = \left(1 - \hat{\rho}_u\right)^{1/2}\left(1 - \hat{h} + \hat{h}_u\right)^{5/2} \tag{5.31}$$

Equating the above expression with (5.29), and re-arranging, we find that

$$\hat{h} = 1 + \hat{h}_u - \left[\frac{\left(1 - \hat{\rho}_u\right)^{1/2}}{\hat{\rho}_l - \hat{\rho}_u}\right]^{2/5} \tag{5.32}$$

To complete the model, we wish to derive expressions for $\hat{\rho}_u$ and $\hat{\rho}_l$. To continue, we take $R = S$ and normalise equations (5.21) $-$ $-$(5.24) above. We then have:

$$-\frac{R\hat{\rho}_l}{\hat{\rho}_u - \hat{\rho}_l} + R = \frac{R\left(1-\hat{\rho}_u\right)}{\hat{\rho}_l - \hat{\rho}_u} + \frac{R - 2R\hat{\rho}_l}{\hat{\rho}_u - \hat{\rho}_l} \tag{5.33}$$

$$-\frac{R\hat{\rho}_l\hat{\rho}_u}{\hat{\rho}_u - \hat{\rho}_l} + R = \frac{R\left(1-\hat{\rho}_u\right)\hat{\rho}_l}{\hat{\rho}_l - \hat{\rho}_u} + \hat{\rho}_u\left[\frac{R - 2R\hat{\rho}_l}{\hat{\rho}_u - \hat{\rho}_l}\right] \tag{5.34}$$

$$R + \frac{R\left(1-\hat{\rho}_u\right)}{\hat{\rho}_l - \hat{\rho}_u} = -\frac{R\hat{\rho}_l}{\hat{\rho}_u - \hat{\rho}_l} + \left[\frac{R - 2R\hat{\rho}_l}{\hat{\rho}_l - \hat{\rho}_u}\right] \tag{5.35}$$

$$\frac{R\hat{\rho}_l\left(1-\hat{\rho}_u\right)}{\hat{\rho}_l - \hat{\rho}_u} = -\frac{R\hat{\rho}_l\hat{\rho}_u}{\hat{\rho}_u - \hat{\rho}_l} + \hat{\rho}_l\left[\frac{R - 2R\hat{\rho}_l}{\hat{\rho}_l - \hat{\rho}_u}\right] \tag{5.36}$$

Now, we note that when $R = S$, the above set of equations are *independent* of R. Further, simplifying equation (5.33) implies that

$$\hat{\rho}_u + \hat{\rho}_l = 1 \tag{5.37}$$

Further, some algebra upon equation (5.36) yields the result

$$\hat{\rho}_l = \hat{\rho}_u \tag{5.38}$$

Hence, $\hat{\rho}_u = \hat{\rho}_l = 0.5$ by the above two results. This implies that equation (5.32) does not have a physical solution for the location of the interface. We note that examining the case when $R \neq S$ yields similar results.

5.3.3 Discussion of the Non-Exchange Flow System

In deriving the model for the non-exchange flow case, we have applied the same assumptions as per Chapter 2. One of these stated that the equilibrium configuration of the dual-plume system consisted of two well-mixed layers. Theoretical and numerical calculations subsequently indicated that the system may actually consist of a single fluid layer. However, this eventuality is a key result in the theory, and did not in fact violate any of the assumptions used to derive the model.

However, the non-exchange configuration presents a different circumstance. Here, the assumption of a two-layered system is incorrect. There are no values of the initial mass fluxes associated with the fluid sources that form a two-layer system. We note at this point that the global conservation laws are still valid, however.

There are two broad circumstances which may account for this behaviour. The first is to consider that the non-exchange case *always* consists of a single well-mixed fluid layer. This could only be the case if all of the net entrained flux associated with each of the plumes vented from the confined region via the corresponding mass sink. In other words, the total flux of fluid associated with the ascending plume at a vertical distance $z = H$ would leave the confined region via the upper outflow vent. This would also be the exact case for the descending plume.

However, this prospect seems unlikely. It is plausible for specific initial conditions, but unfeasible for all values of R and S. Suppose $R = 10S$. This would immediately imply that the fractional dilutions associated with each plume are different in magnitude. Further, we would expect that $\hat{D}_S >> \hat{D}_R$. Hence, the return flow associated with the descending plume would be much greater in magnitude than the corresponding return flow for the ascending plume. This is not a sufficient condition for the net entrained fluid associated with both plumes to completely vent from the confined region. This follows from the equation for global conservation of mass, namely

$$Q_1 + Q_2 = Q_u + Q_l \tag{5.39}$$

A more physically-reasonable explanation is that the system consists of precisely *three* distinct fluid layers. This represents a substantial result in itself. The central layer comprises unmixed ambient fluid. In this situation, the significant amount of the net entrained fluid associated with each plume

vents via the corresponding mass sink. However, there is still a return flow associated with each of the plumes. The equilibrium steady-state is the situation for which the return flows do not meet at some point in the confined region. Instead, the magnitude of fluid vented via the mass sink is large enough that the fronts eventually come to rest. This leaves the central fluid layer effectively comprised of unmixed ambient fluid.

A priori, we would expect that for the case $R = S$, the depth of the upper and lower fluid layers would be governed by the magnitude of the mass fluxes associated with the fluid sources. Hence, as R and S increase, the fractional dilution associated with each of the plumes would decrease. The magnitude of the return flows would therefore also decrease. Consequently, the upper and lower layers would decrease in depth, leaving a large central region of unmixed fluid. This may be a desirable occurence in certain industrial processes, for example separation of fluids after flowing through a neutral agent.

However, to model the three-layer system and perform a set of experiments that verify its configuration is beyond the scope of the present work. Hence, we now examine the case for which $Q_c < Q_0$.

5.3.4 $Q_c < Q_0$: The Exchange-Flow System

We begin with the expressions for global conservation of mass,

$$Q_1 + Q_2 = Q_u - Q_l \tag{5.40}$$

and global conservation of buoyancy

$$Q_1\rho_1 + Q_2\rho_2 + Q_l\rho_{ext} = Q_u\rho_u \tag{5.41}$$

As previously, we consider the local conservation laws as they relate to each of the fluid layers. For the upper layer, conservation of mass gives:

$$Q_3 + Q_2 = Q_4 + Q_u \tag{5.42}$$

while buoyancy conservation yields

$$Q_3\rho_u + Q_2\rho_2 = Q_4\rho_l + Q_u\rho_u \tag{5.43}$$

Similarly, we have conservation relations for the lower fluid layer. Firstly, mass conservation:

$$Q_1 + Q_4 + Q_l = Q_3 \tag{5.44}$$

and finally buoyancy conservation:

$$Q_1\rho_1 + Q_4\rho_l + Q_l\rho_{ext} = Q_3\rho_u \tag{5.45}$$

Equation (5.40) implies that

$$Q_u = Q_1 + Q_2 + Q_l \tag{5.46}$$

and hence we may use this relation to eliminate Q_u from the consequent expressions. Next, we form (5.43) $-$ (5.42) $\cdot\,\rho_u$ to give

$$Q_2\left(\rho_2 - \rho_u\right) = Q_4\left(\rho_l - \rho_u\right) \tag{5.47}$$

Using (5.40) and (5.41):

$$Q_l = \frac{Q_1\rho_1 + Q_2\rho_2 - \left(Q_1 + Q_2\right)\rho_u}{\left(\rho_u - \rho_l\right)} \tag{5.48}$$

Further, equation (5.41) implies that

$$Q_3 = \frac{Q_1\left(\rho_1 - \rho_l\right) + Q_l\left(\rho_{ext} - \rho_1\right)}{\rho_u - \rho_{ext}} \tag{5.49}$$

Combining these two relations:

$$Q_3 = \frac{Q_1\left(\rho_1 - \rho_l\right)}{\left(\rho_u - \rho_l\right)} + \left(\rho_{ext} - \rho_1\right)\left[\frac{Q_1\rho_1 + Q_2\rho_2 - \left(Q_1 + Q_2\right)\rho_u}{\rho_u - \rho_{ext}}\right] \tag{5.50}$$

Equation (5.42) implies that

$$Q_u = Q_3 + Q_2 - Q_4 \tag{5.51}$$

And so

$$Q_u = \frac{Q_1(\rho_1 - \rho_l) + Q_2(\rho_{ext} - \rho_1)}{\rho_u - \rho_l} + Q_2 - \frac{Q_2(\rho_2 - \rho_u)}{\rho_l - \rho_u} \tag{5.52}$$

Hence, we now have expressions for Q_3, Q_4, Q_u and Q_l in terms of Q_1, Q_2, ρ_u, ρ_l and ρ_{ext}. Scaling as per section X, these equations have the following dimensionless forms:

$$\hat{Q}_4 = \frac{S(1 - \hat{\rho}_u)}{(\hat{\rho}_l - \hat{\rho}_u)} \tag{5.53}$$

$$\hat{Q}_3 = \hat{\rho}_{ext}\left[\frac{S - (R+S)\hat{\rho}_u}{\hat{\rho}_u - \hat{\rho}_{ext}}\right] - \frac{R\hat{\rho}_l}{\hat{\rho}_u - \hat{\rho}_l} \tag{5.54}$$

$$\hat{Q}_l = \frac{S - (R+S)\hat{\rho}_u}{\hat{\rho}_u - \hat{\rho}_l} \tag{5.55}$$

$$\hat{Q}_u = S - \frac{S - (R+S)\hat{\rho}_u}{\hat{\rho}_u - \hat{\rho}_l} - \frac{R\hat{\rho}_l + S\hat{\rho}_{ext}}{\hat{\rho}_u - \hat{\rho}_l} \tag{5.56}$$

Further, the normalised form of equation (5.43) gives

$$\hat{Q}_3\hat{\rho}_u + S = \hat{Q}_4\hat{\rho}_l + \hat{Q}_u\hat{\rho}_u \tag{5.57}$$

Substituting for $\hat{Q}_3$, $\hat{Q}_4$ and $\hat{Q}_u$ into the above expression, and re-arranging, gives:

$$\hat{\rho}_u\hat{\rho}_{ext}S - \frac{(R+S)\hat{\rho}_u^2\hat{\rho}_{ext}}{\hat{\rho}_u - \hat{\rho}_{ext}} = -\frac{S\hat{\rho}_u\hat{\rho}_{ext}}{\hat{\rho}_u - \hat{\rho}_l} \tag{5.58}$$

Some further algebra then yields

$$\hat{\rho}_l = \frac{\left[\frac{(R+S)\hat{\rho}_u\hat{\rho}_{ext}}{\hat{\rho}_u - \hat{\rho}_{ext}} - S\hat{\rho}_u\hat{\rho}_{ext}\right]}{\left[\frac{\hat{\rho}_u^2\hat{\rho}_{ext}}{\hat{\rho}_u - \hat{\rho}_{ext}} - \hat{\rho}_u\hat{\rho}_{ext}S\right]} \tag{5.59}$$

Next, we take the dimensionless form of (5.44), and substitute for $\hat{Q}_4$, $\hat{Q}_l$ and $\hat{Q}_3$ to give

$$R + \frac{S(1 - \hat{\rho}_u)}{\hat{\rho}_l - \hat{\rho}_u} + \frac{S - (R+S)\hat{\rho}_u}{\hat{\rho}_u - \hat{\rho}_l} = \hat{\rho}_{ext}\left[\frac{S - (R+S)\hat{\rho}_u}{\hat{\rho}_u - \hat{\rho}_{ext}}\right] - \frac{R\hat{\rho}_l}{\hat{\rho}_u - \hat{\rho}_l} \tag{5.60}$$

Re-arrangement of the above expression eventually yields

$$\hat{\rho}_u = \frac{\rho_{ext}\,(1+S)}{S+(R+S)\,\hat{\rho}_{ext}} \tag{5.61}$$

In a similar manner to the non-exchange case, we recall equation (2.12) from Chapter 2:

$$\hat{Q}_4 = (1-\hat{\rho}_u)^{1/2}\left(1-\hat{h}+\hat{H}_u\right)^{5/2} \tag{5.62}$$

Combining this with equation (5.55) results in an expression for the location of the fluid interface:

$$\hat{h} = 1-\left[\frac{S\,(1-\hat{\rho}_u)^{1/2}}{\hat{\rho}_l-\hat{\rho}_u}\right]^{2/5}+\hat{h}_u \tag{5.63}$$

If we take $R = S$, then the equations reduce to the following forms:

$$\hat{\rho}_u = \frac{(1+R)\,\hat{\rho}_{ext}}{R\,(1+2\hat{\rho}_{ext})} \tag{5.64}$$

$$\hat{\rho}_l = \frac{R\,(2-\hat{\rho}_u+\hat{\rho}_{ext})}{\hat{\rho}_u\,(1-R)+R\hat{\rho}_{ext}} \tag{5.65}$$

5.4 Numerical Results for the Exchange-Flow Case

We now examine the numerical solutions for the exchange-flow system. Figure 5.3 shows the densities associated with each of the fluid layers for the two cases of $\hat{\rho}_{ext} = 0.1, 0.3$, with $R = S$. We may immediately see that, in both cases, there exist values of R such that the system is unstably stratified. For $\hat{\rho}_{ext} = 0.1$, the system is just in stable stratification for $R \simeq 1.9$. The corresponding value is $R \simeq 3.8$ for the case $\hat{\rho}_{ext} = 0.3$.

Even though the model represents only a simple picture of what occurs at the lower vent, this does not compromise the validity of the result. We explain this as follows. When the double-vented system admits exchange flows, there is an inflow of fluid mass via the lower orifice. This fluid is

relatively light compared with the density of the lower fluid layer. Further, it is implicitly assumed that the cross-sectional area of each vent is much greater than the cross-sectional area of each plume source. The simplest way to model the flow in via the vent, therefore, has been utilised in the model. However, the simple model is still physically reasonable.

We now elaborate upon the result. When $R \to 0$, $\hat{\rho}_l \to 0$ and $\hat{\rho}_u \to 1$. Hence, the density contrast between the two layers is greatest when the source mass fluxes are small. This occurs because the inflow via the lower vent decreases the density of the lower fluid layer. Therefore, the density of the lower fluid layer decreases. This occurs even though the descending plume continues to supply relatively dense fluid.

Consequently, the ascending plume experiences a much smaller increase in density as it propagates through the lower layer. As it reaches the interface, it is much lighter than in the single-vent case. The density of the upper fluid layer therefore tends towards the input density of the ascending plume.

However, for values of $R > 2.0$, the system becomes stably stratified when $\hat{\rho}_{ext} = 0.1$. Hence, we may state a key result: the principle effect of increasing the total mass flux entering the exchange-flow system is to stabilise the density stratification.

The controlling factor for this is the fractional dilution associated with the descending plume. As R increases, the fractional dilution $\hat{D}_S$ of the descending plume will decrease. Hence, the descending plume arrives at the interface progressively less diluted. Now, global mass conservation dictates that fluid mass is lost via the upper vent only. Hence, all of the net entrained flux associated with the relatively dense descending plume arrives in the lower fluid layer. This is greater in magnitude than the inflow of light fluid

via the lower aperture. Hence, we expect as R increases, the density of the lower fluid layer will rapidly tend towards the input density of the descending plume. Further, the larger the magnitude of $\hat{\rho}_{ext}$, the greater the stability of the system. This is the behaviour shown in figure 5.3.

Further, figure 5.2 indicates that the location of the interface is sensitive to the total flux of mass entering the system. Further, we see that in the exchange-flow case, the filling-box system always comprises two layers. However, as R increases, the lower layer becomes very deep. This is due to the net entrained flux associated with the ascending plume leaving via the upper mass sink. However, the steep gradients in figure 5.2 also occur because of the fluid mass *entering* the confined region via the lower aperture. This additional mass flux will effectively enhance the magnitude of the return flow associated with the descending plume. Hence, the increase in $\hat{h}$ is much greater with increasing R than in the model of Chapter 2. This influx of mass via the lower orifice also explains why the system always comprises two fluid layers.

To predict when the exchange-flow system is stably stratified, we may use a simple argument. Suppose that the minimum value of R required to obtain a stable stratification is denoted R_0. This value occurs at the limiting case when $\hat{\rho}_u = \hat{\rho}_l$. Hence, we may eliminate the upper- and lower-layer densities and subsequently combine equations (5.64) and (5.64). Proceeding in this manner, we obtain, after some algebra, a cubic in R_0:

$$R_0^3\left[2\hat{\rho}_{ext}^3 - 6\hat{\rho}_{ext}^2 - 7\hat{\rho}_{ext} - 2\right] + R_0^2\left[-2\hat{\rho}_{ext}^3 - 2\hat{\rho}_{ext}^2\right] + R_0\left[\hat{\rho}_{ext}^2\right] + \left[\hat{\rho}_{ext}\right] = 0 \tag{5.66}$$

The cubic is plotted over the range of interest for $\hat{\rho}_{ext} = 0.1$ and 0.3 in figure 5.4. We see that the predictions for the minimum value of R required to produce a stably-stratified system are in good agreement with the numerical

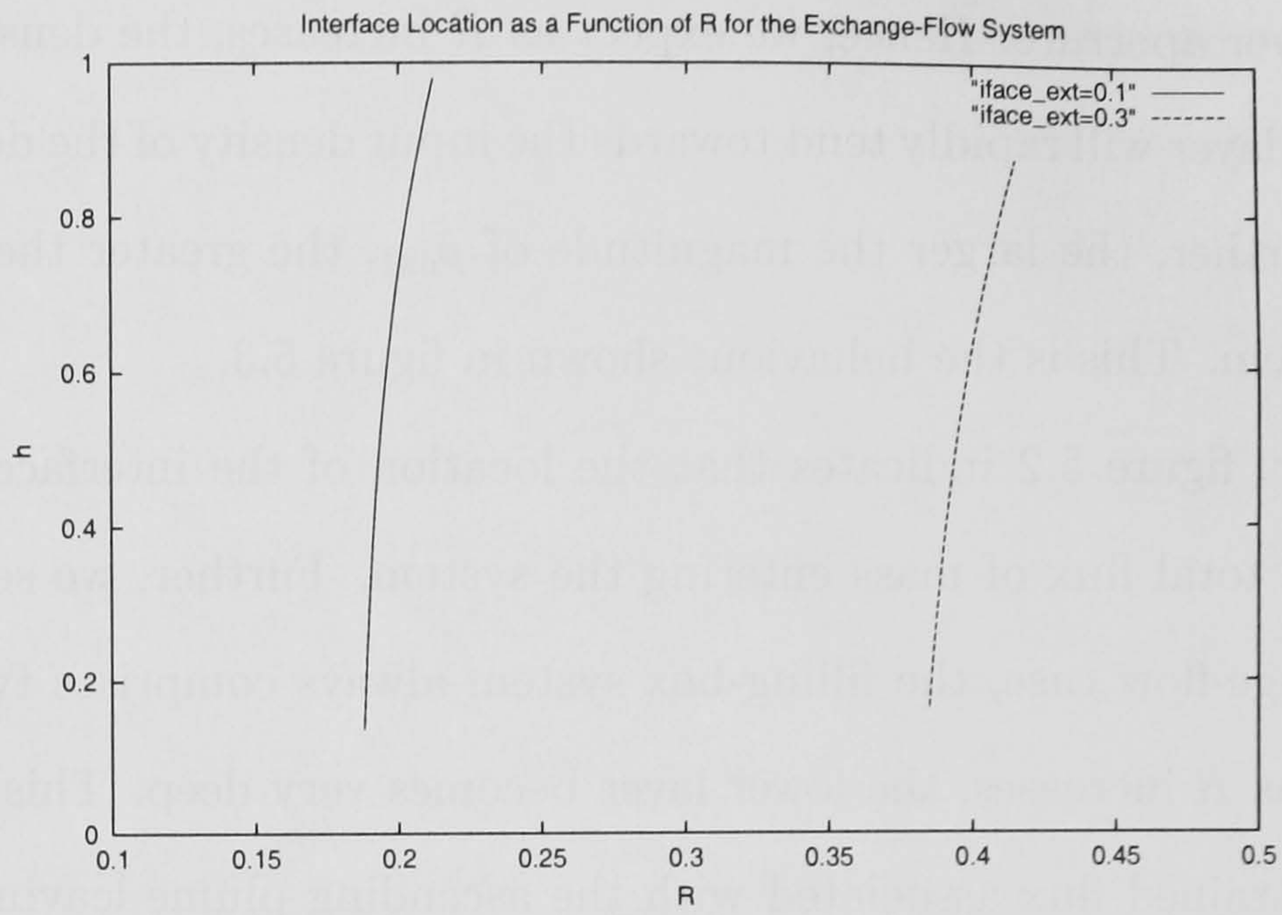

FIGURE 5.2: Graph of interface location as a function of R for the equal-magnitude naturally-ventilated exchange case.

results presented in figure 5.3. Hence, equation (5.66) represents a very useful, simple method to predict when the exchange-flow system will be in a stable configuration.

5.5 The Effect of External Wind Upon Displacement Ventilation

So far in this Chapter, we have made the assumption that the external ambient fluid does not affect flow into or out of the confined region.

However, suppose that the building was ventilated on a windy day. Motion of this type in the external ambient may affect the fluid flows occurring inside the building. There are two principle cases. Firstly, the external wind may act to assist the flux of fluid entering the building. If the lower vent is located at the bottom of one of the vertical boundaries, for example a door, the effect of the wind will be to increase the flow of relatively cold fluid into

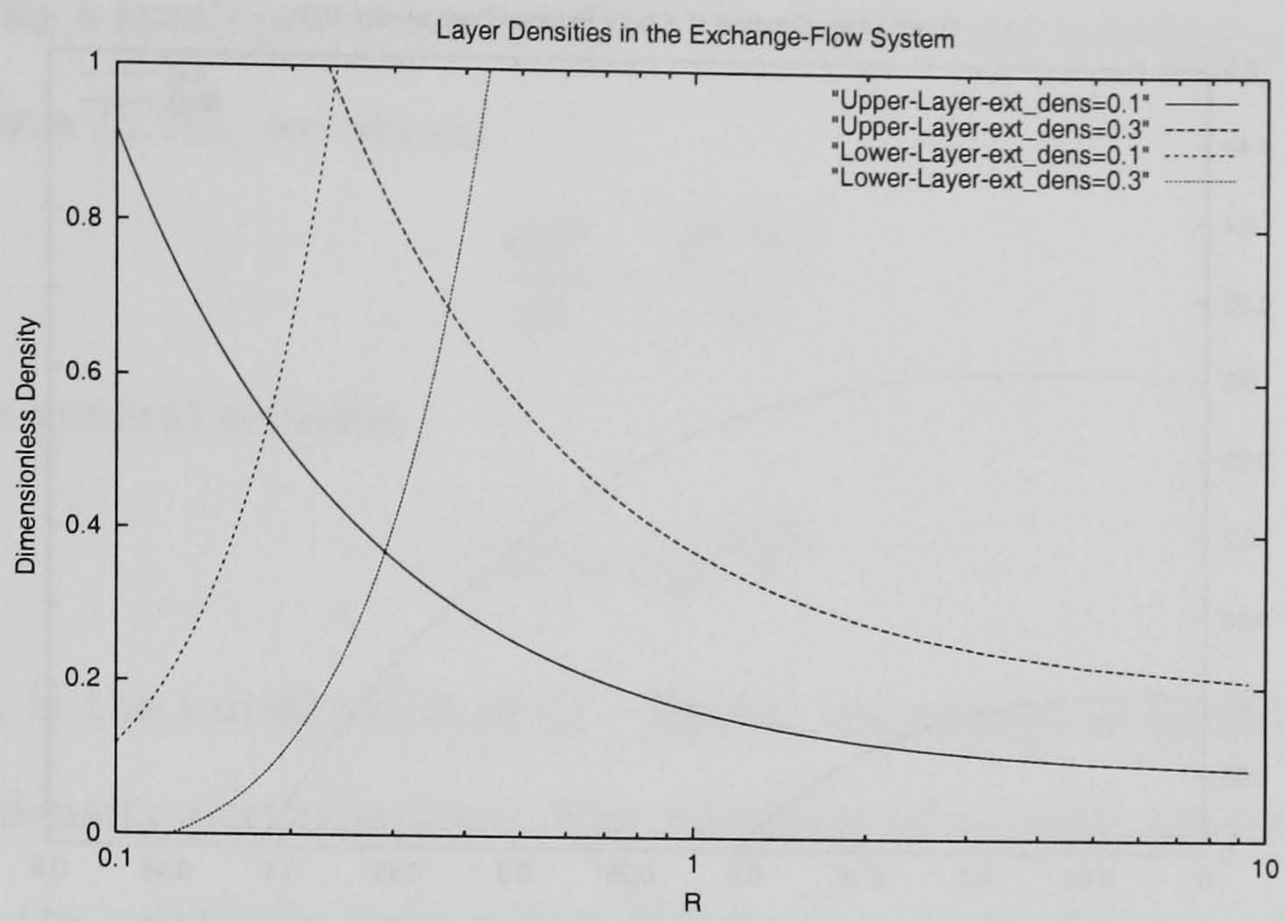

FIGURE 5.3: Graph of density variation as a function of R for the equal-magnitude naturally-ventilated exchange case.

the confined region. Mass conservation therefore dictates that the flow of relatively light fluid out of the upper vent will therefore increase. Hence, the flux of mass through the lower opening is now given by

$$Q_l = A_l \left(\frac{\Delta p_l}{\rho_l} + g_l' h \right)^{1/2} \tag{5.67}$$

where Δp_l is the pressure gradient arising due to the wind external to the confined region at the lower opening, which has an area A_l.

The second, more complicated situation occurs when the pressure due to the wind opposes the direction of the displacement ventilation flow. In this case, fluid leaving via the upper vent may encounter a strong breeze. This has the effect of opposing the flux of mass leaving via the vent.

If the external force due to the wind is sufficiently large, it may exceed the magnitude of the the buoyant force driving fluid out of the confined region. Should this situation occur, the direction of the displacement flow may be reversed. Hence, relatively dense fluid enters the warm upper layer via the top vent, and relatively warm fluid enters the dense lower layer via

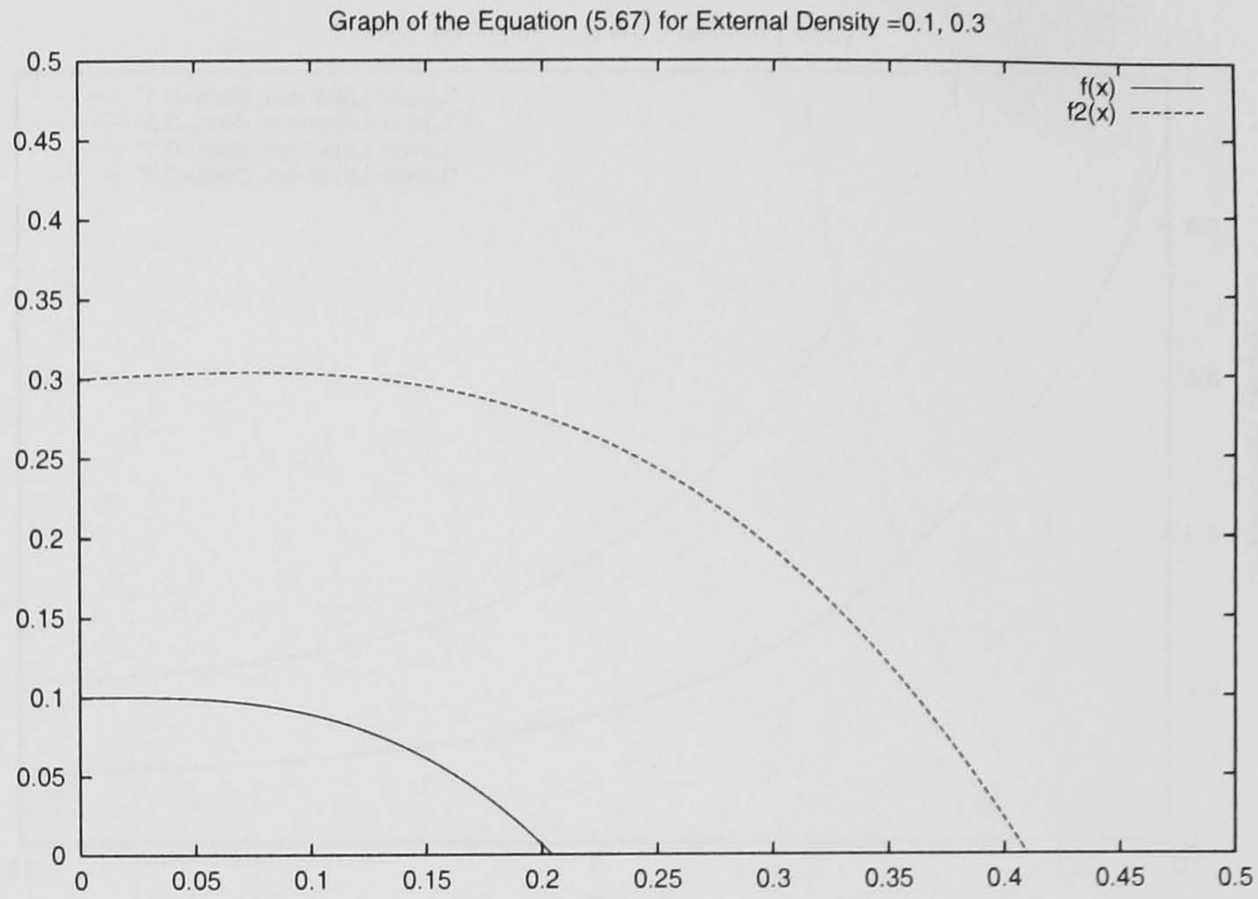

FIGURE 5.4: Graph of density variation as a function of R for the equal-magnitude naturally-ventilated exchange case.

the vent located in the base of the room. Each of these auxiliary flows may have relatively small mass fluxes when compared with the plume sources, but they may possess relatively strong fluxes of buoyancy.

We may model, to leading order, this situation by assuming that density in the room increases according to

$$H\frac{\mathrm{d}g'}{\mathrm{d}t} = g'Q_w \tag{5.68}$$

where

$$Q_w = A^*\left(\frac{\Delta p}{\rho} - g'H\right)^{1/2} \tag{5.69}$$

We may examine the implications of this model by undertaking some elementary stability analysis. Re-writing equation (5.68) as:

$$\frac{\mathrm{d}g'}{\mathrm{d}t} = \frac{g'}{\alpha}\left(\beta - Hg'\right)^{1/2} \tag{5.70}$$

where $\alpha = A^*/H$ and $\beta = \Delta P/\rho$ We may find the equilibrium points of this O.D.E by considering the steady solutions:

$$g' = 0, \quad g' = \frac{\beta}{H} \tag{5.71}$$

Introducing a small perturbation G to the equilibrium solution and linearising equation (5.70), we obtain

$$\frac{\mathrm{d}G'}{\mathrm{d}t} = \frac{\beta^{1/2}G'}{\alpha} \tag{5.72}$$

which has general solution

$$G' = G'_0 e^{\frac{\beta^{1/2}t}{\alpha}} \tag{5.73}$$

where G'_0 is the initial value of G'. Hence, the system is linearly unstable to small density perturbations. The intrusion of a small amount of dense fluid into the relatively light upper will cause a large density contrast that will is unbounded as time increases. This directly implies instability and overturning of the stratification.

However, we note that the nonlinearity in equation (5.70) is sufficient to cause the right-hand side of the ordinary differential equation to change sign, provided that

$$\frac{Hg'^3}{\alpha^2} > \frac{g'^2\beta}{\alpha} \tag{5.74}$$

which is a physically reasonable possibility. Hence, we need to continue the analysis beyond considering the linear case. Further, we note that linear instability is a sufficient condition for instability, but linear or marginal stability is only a necessary condition for stability. Hence, we proceed by considering the including the nonlinear terms in (5.70). In a typical stability calculation, this is often extremely complicated. However, in the present case, the analysis is relatively straightforward. Hence, we first note that equation (5.70) is separable and has a closed-form solution given by

$$G' = \frac{1}{H}\left(\beta - \beta^{1/2}\left[\tanh\left(\frac{-\beta^{1/2}t}{2\alpha}\right)\right]^2\right) \tag{5.75}$$

This function is plotted in figure 5.5. Now, the function $y = \tanh(t)$ has asymptotes $y = \pm 1$. Consequently, since we are only concerned with the

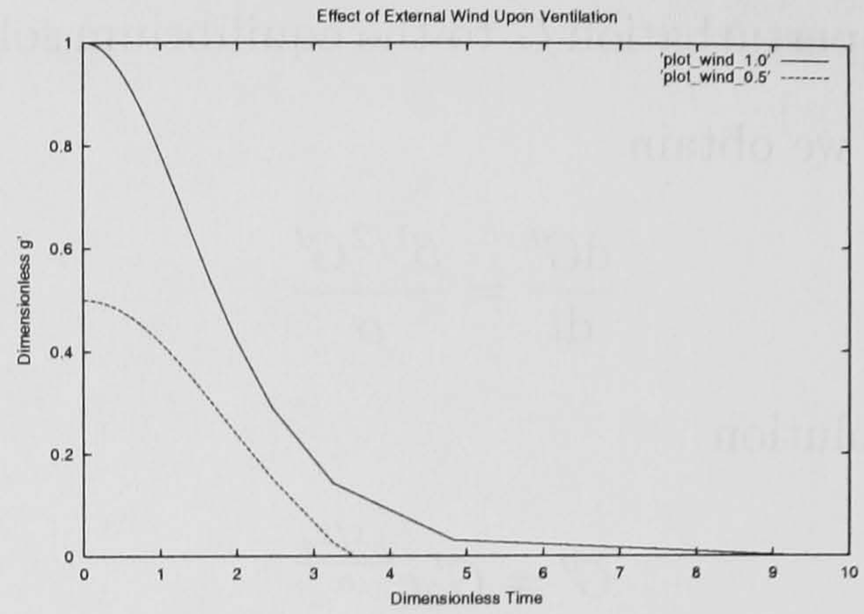

FIGURE 5.5: Graph showing the behaviour of the density distribution as influenced by the effect of external wind. The upper curve represents $\beta = 1.0$, while the lower curve is for $\beta = 0.5$

behaviour of the solution for $t > 0$, we take the negative root of $\beta^{1/2}$. Hence, the function asymptotes to $+1$ as $t \to \infty$, and so the large-time asymptotic behaviour of the solution is

$$G' \sim \frac{1}{H}\left(\beta + \beta^{1/2}\right) \tag{5.76}$$

Since α, $\beta > 0$, the nonlinearity implies that there is a stable configuration that may be attained. Therefore, the stable state is dependent upon the imposed pressure due to the external wind. Hence, there is a value of G' for which the effect of the wind is to mix intruding fluid into each of the stratified layers in such a manner that they remain in a stable stratification. Effectively, each layer experiences a change in density due to the intruding fluid which is less than the density transported into the layer by the relevant plume. Assuming that each layer remains well-mixed, the stability condition implies that

$$\Delta\rho_{wind} < \Delta\rho_{plume} \tag{5.77}$$

Consequently, the system remains in a stable two-layer configuration because of the well-mixed constraint governing the density of each layer.

Hence, $\rho_l > \rho_u$, as before.

5.6 Conclusions

In this chapter, we have presented and discussed new steady-state models for natural ventilation based upon a dual-plume filling-box system. Our aim has to been to complement and extend the current models of natural ventilation of buildings. Typically, the physics of such flows are very complex. Therefore, simple models may offer both useful insight and also important results.

The models derived in this section arise from a limiting case. This argument, based upon comparison with the steady-state model derived in Chapter 2, identifies two possible flow regimes. Firstly, the non-exchange flow case, whereby fluid leaves the confined region via both apertures, was discussed. The key result in this case was a departure from a two-layer system. Although modelling this case was beyond the scope of the present work, reasons for considering the system to consist of *three* fluid layers were discussed. It was shown, however, that the system cannot comprise two layers for any values of R and S. The infeasibility of a single-layer configuration was also discussed.

The second regime represented the more typical natural-ventilation process. In this exchange-flow case, fluid exited the confined region via the upper orifice, and relatively light ambient fluid entered the container via the lower aperture. There were two key results in the case $R = S$. Firstly, the system was unstably stratified when the mass fluxes associated with the sources was small. The second result indicated that increasing the mass fluxes associated with the fluid sources stabilised the system. Further, the mass flux entering via the lower vent caused the interface to be located close

to the upper boundary in the case of a stably-stratified system. Finally, a simple argument yielded a cubic equation that predicted the values of R that would ensure the system was stably stratified.

In the final section, the effect of an imposed pressure gradient upon the filling-box system were investigated. The pressure manifested due to the effect of an external flow in the ambient fluid outside the filling-box region. This represented the effect of wind upon the naturally-ventilated system. It was assumed that the imposed pressure was constant, and hence it may be taken in steady-state to assume that the pressure was due to a time-averaged, and hence steady, effect of the wind.

Two possibilities were described for this this situation. Firstly, the effect of the wind was be to enhance the displacement ventilation flow through the system. This occurred if the direction of the imposed pressure acted in the same direction as the naturally- ventilated flow of fluid through the system. A simple expression for the additional flux of fluid through the container was assumed. In the second case, the wind acted in the opposite sense. and it was found that the system may not attain a steady-state configuration due to the effect of relative dense fluid entering the upper layer via the vent in the top boundary. A simple stability analysis was performed to derive some conditions for which the system may attain a stably-stratified configuration were discussed. a

Part IV

The Unsteady Dual-Plume Filling-Box Model

Chapter 6

Transient Dynamics: Theory and Experiment

"Look back on Time, with kindly eyes –

He doubtless did his best –

How softly sinks that trembling Sun

In Human Nature's West."

– Emily Dickinson

6.1 Introduction

In Chapter 2, we presented a model for the steady-state equilibrium configuration of the dual-plume filling box system. Numerical solutions of the model, confirmed by experimental and theoretical analysis, indicated that the steady-state of the system consisted of either two distinct well-mixed fluid layers separated by a well-defined interface, or a single well-mixed fluid

layer. The initial conditions for which the latter circumstance arose were identified.

In general, however, the equilibrium state consists of a two-layer stratification. Experimental observations indicate that this is the result of where the fronts associated with two distinct filling-box flows meet (please refer to Chapter 3 for a discussion of this). In the pre-equilibrium phase of the system, there exist three separate fluid layers. In addition to the filling-box fronts, each associated with a return flow due to one of the plumes, there is a central region of unmixed ambient fluid. This gradually diminishes in depth as the two fronts advect through the container.

It may be seen from the brief description given above that the time regime over which the system converges to steady-state equilibrium involves some complex, non-trivial fluid dynamics. This is because in addition to the propagation of the two fronts, the density of the mixed regions also evolves as a function of time towards their steady-state values.

Our aim in this Chapter then is to examine the time-dependent, *transient* evolution of the dual-plume filling-box system from its initial conditions towards its eventual steady-state equilibrium. There are several reasons for doing this. The first reason is that the time-dependent dual-plume filling-box system has not previously been studied. Secondly, in addition to this, the effect of sources which possess non-zero associated mass fluxes upon the evolution of the transient system is also new work. It is not straightforward to estimate precisely what effects the addition of mass into the system will have. Thirdly, the transient system has several useful applications, particularly in conjunction with the steady-state model of Chapter 2. For example, in the context of ventilating a room, the steady-state model allows a prediction of the final temperature distribution. However, the transient model

allows evaluation of the time it takes to reach the equilibrium temperatures.

We model the convergence process from first principles in §6.2, and show that when the time-dependent terms vanish, the model reduces to the steady-state equations derived in Chapter 2. In §6.3, we describe the implementation of a numerical method to calculate the evolution of the time-dependent density profile. The method is based upon a technique originally due to Germeles (1975). Numerical results obtained by this method are then presented. The solutions are compared with experimentally -obtained transient data corresponding to the displaced-source configuration of Chapter 3. Next, in 6.5, we discuss a phenomenon that occurs for certain sets of initial conditions, and describe how this affects the numerical routine. In §6.7, we return to an issue briefly discussed in chapter 2, namely the effect of locating the mass vent below the ceiling of the container. However, we analyse the effects of this configuration upon the transient stage. We conclude this chapter in §6.8.

6.2 Derivation of the Transient Equations

We now proceed to derive a model of the transient time regime for the dual-plume filling box. We begin with global conservation of mass for the system, which remains unchanged from the model of Chapter 2. The same definitions apply, which we repeat here for clarity. The vertical distance of the interface from the lower boundary is h, the height of the confined region is H, and the virtual origins associated with the plume sources are denoted by h_u and h_l for the ascending and descending plume respectively. Therefore:

$$Q_0 = Q_1 + Q_2 \tag{6.1}$$

Conservation of mass for the lower layer takes the form

$$\frac{\mathrm{d}h}{\mathrm{d}t} = \frac{(Q_1 + Q_4 - Q_3)}{A} \tag{6.2}$$

and, similarly, mass conservation for the upper fluid layer is given by

$$\frac{\mathrm{d}\,(H-h)}{\mathrm{d}t} = \frac{Q_2 + Q_3 - Q_0 - Q_4}{A} \tag{6.3}$$

where A is the uniform cross-sectional area of the container. Hence, generalisation of the model to containers of different shape is straightforward (c.f. Baines & Turner, 1969) by specifying the functional form of A

Conservation of buoyancy follows from the mass conservation relations described above. Thus, for the lower fluid layer, we have

$$\rho_l \frac{\mathrm{d}h}{\mathrm{d}t} = \frac{(Q_1\rho_1 + Q_4\rho_4 - Q_3\rho_3)}{A} \tag{6.4}$$

and for the upper layer, buoyancy conservation is given by

$$\rho_u \frac{\mathrm{d}\,(H-h)}{\mathrm{d}t} = \frac{Q_2\rho_2 + Q_3\rho_3 - Q_0\rho_u - Q_4\rho_4}{A} \tag{6.5}$$

We note here that in the initial stages of evolution, the system comprises three distinct fluid layers. The top and bottom layers are associated with the filling-box flows arising from each of the turbulent plumes. The central layer consists of unmixed ambient fluid. This layer reduces in depth until the fronts associated with each of the filling box flows meet. Further, we assume that the top and bottom layers consist of fluid that is well-mixed to leading order. We now need to obtain expressions for the rate of change of density of each fluid layer as a function of time. We proceed as follows.

We consider the effect of a small vertical increase δh in the location of the fluid interface. We propose that this occurs due to an increase in the volume of the lower layer via the entrainment flux associated with the descending

plume. This consequently changes the density of the lower fluid layer due to the influx of fluid of contrasting density via the plume. We have

$$\begin{aligned}[(\rho_u + \delta\rho_u)(H - h + \delta(H - h))] - [\rho_l h + \rho_u \delta(H - h)] \\ = \frac{-Q_0\rho_u\delta t + Q_1\rho_1\delta t - Q_3\rho_3\delta t + Q_4\rho_4\delta t}{A}\end{aligned} \tag{6.6}$$

Hence, in the limit $\delta t \to 0$, we obtain

$$\begin{aligned}(H - h)\frac{\mathrm{d}\rho_u}{\mathrm{d}t} + (\rho_l - \rho_u)\frac{\mathrm{d}(H - h)}{\mathrm{d}t} \\ = \frac{Q_2\rho_2 + Q_3\rho_3 - Q_0\rho_u - Q_4\rho_l}{A}\end{aligned} \tag{6.7}$$

and, similarly, we have:

$$\begin{aligned}[(\rho_l + \delta\rho_l)(h + \delta h)] - [\rho_u(H - h) + \rho_l\delta h] \\ = \frac{Q_1\rho_1\delta t - Q_3\rho_3\delta t - Q_0\rho_u\delta t + Q_4\rho_l\delta t}{A}\end{aligned} \tag{6.8}$$

$$h\frac{\mathrm{d}\rho_l}{\mathrm{d}t} + (\rho_u - \rho_l)\frac{\mathrm{d}h}{\mathrm{d}t} = \frac{Q_3\rho_l + Q_2\rho_2 - Q_4\rho_4}{A} \tag{6.9}$$

Using the equation for the conservation of mass in the upper layer in equation (6.8) and re-arranging gives:

$$\frac{\mathrm{d}\rho_u}{\mathrm{d}t} = \frac{1}{(H - h)A}\left[Q_2\rho_2 - Q_0\rho_u + Q_3\rho_3 - Q_4\rho_4 - (\rho_l - \rho_u)(Q_2 + Q_3 - Q_0 - Q_4)\right] \tag{6.10}$$

Using the equation for the conservation of mass in the lower layer in equation (6.12) and re-arranging gives:

$$\frac{\mathrm{d}\rho_l}{\mathrm{d}t} = \frac{1}{hA}\left[Q_1\rho_1 + Q_4\rho_4 - Q_3 - (\rho_u - \rho_l)(Q_1 + Q_4 - Q_3)\right] \tag{6.11}$$

The third equation occurs directly from the consideration of conservation of mass in the lower fluid layer, and has the form

$$\frac{\mathrm{d}h}{\mathrm{d}t} = \frac{Q_1 + Q_4 - Q_3}{A} \tag{6.12}$$

We now proceed to apply the scalings (2.32) – –(2.33) in chapter 2 to normalise the expressions (6.12) – –(6.14). This is useful for illustrating and identifying key properties of the transient system. Applying these scalings and re-arranging the equations, we arrive at a set of three nonlinear first-order ordinary differential equations, namely:

$$\frac{\mathrm{d}\hat{\rho}_u}{\mathrm{d}\hat{t}} = \frac{1}{1-\hat{h}}\left[S-(R+S)\,\hat{\rho}_u+\hat{\rho}_l^{1/2}\hat{\rho}_3\left(\hat{h}+\hat{h}_l\right)^{5/2}-(1-\hat{\rho}_u)^{1/2}\,\hat{\rho}_4\left(1-\hat{h}+\hat{h}_u\right)^{5/2}\right.$$
$$\left.-(\hat{\rho}_l-\hat{\rho}_u)\left(S+\hat{\rho}^{1/2}\left(\hat{h}+\hat{h}_l\right)^{5/2}-(R+S)-(1-\hat{\rho}_u)^{1/2}\left(1-\hat{h}+\hat{h}_u\right)^{5/2}\right)\right] \quad (6.13)$$

$$\frac{\mathrm{d}\hat{\rho}_l}{\mathrm{d}\hat{t}} = \frac{1}{\hat{h}}\left[(1-\hat{\rho}_u)^{1/2}\,\hat{\rho}_4\left(1-\hat{h}+\hat{h}_u\right)^{5/2}-(\hat{\rho}_l-\hat{\rho}_u)\right. \quad (6.14)$$
$$\left.\left(S+\hat{\rho}_l^{5/2}-(R+S)-(1-\hat{\rho}_u)^{1/2}\left(1-\hat{h}+\hat{u}\right)^{5/2}\right)\right]$$

$$\frac{\mathrm{d}\hat{h}}{\mathrm{d}\hat{t}} = R+(1-\hat{\rho}_u)^{\frac{1}{2}}\left(1-\hat{h}+\hat{h}_u\right)^{\frac{5}{2}}-\hat{\rho}_l^{1/2}\left(\hat{h}+\hat{h}_l\right)^{5/2} \quad (6.15)$$

We now proceed to show that the equations for the transient case reduce to the steady-state equations when the time-dependent terms vanish. In this situation, equation (6.18) becomes:

$$R+(1-\hat{\rho})^{1/2}\left(1-\hat{h}+\hat{h}_u\right)^{5/2}=\hat{\rho}_l^{1/2}\left(\hat{h}+\hat{h}_l\right)^{5/2} \quad (6.16)$$

which is identical to equation (2.43) of chapter 2. It is this relation that forms the basis of the steady-state expression for the location of the fluid interface as a function of the mass fluxes associated with the plume sources. The time-independent form of equation (6.14) is

$$Q_1\rho_1+Q_4\rho_4-Q_3\rho_3-\rho_u\left(Q_1+Q_4-Q_3\right)+\rho_l\left(Q_1+q_4-Q_3\right)=0 \quad (6.17)$$

Re-arranging and solving for ρ_l yields

$$\rho_l=\frac{\rho_u Q_1+\rho_u Q_4-Q_1\rho_1}{2Q_4+Q_1-Q_3} \quad (6.18)$$

Upon using the relation

$$Q_4 = Q_1 - Q_3 \tag{6.19}$$

and transforming to dimensionless form, we arrive at

$$\hat{\rho}_l = \frac{\hat{\rho}_u \left(\hat{Q}_1 + \hat{Q}_4\right)}{\hat{Q}_4} \tag{6.20}$$

which is identical to the expression for the steady-state density associated with the lower fluid layer. Finally, the upper-layer density is given by an identical expression to the steady-state case. Global conservation of mass remains unchanged, namely

$$Q_1\rho_1 + Q_2\rho_2 = Q_0\rho_u \tag{6.21}$$

and also

$$Q_1 + Q_2 = Q_0 \tag{6.22}$$

Hence, in dimensionless form, the density associated with the upper fluid layer is given by:

$$\hat{\rho}_u = \frac{S}{R+S} \tag{6.23}$$

This is also identical to the corresponding equation 2.44 in chapter 2.

Therefore, we conclude that the transient equations reduce to the steady-state model of Chapter 2.

6.3 The Numerical Method

We now wish to numerically solve the system of equations (6.16) $-$ $-$(6.18) to obtain the location of the first fronts and the evolution of the mixed regions, both as functions of time. To achieve this we implement a numerical technique based upon a method due to Germeles (1975) to evaluate the

ambient density profile for a single-plume filling-box system. We describe the model for this case in §6.3.1.

Germeles' method was applied to the problem in which the source possessed a non-zero associated mass flux. In §6.3.2, we discuss the extension and subsequent application of the technique to the transient dual-plume filling-box system, with sources which possess non-zero associated mass fluxes.

6.3.1 Theory for the Single-Plume Case

The similarity solution of the plume equations (1.6)-(1.8) yields an expression for the volume flux of the plume as a function of vertical distance from the plume source. In the case of an unstratified environment, this is given by

$$Q = \lambda B_0^{1/3} (z + z_0)^{5/3} \tag{6.24}$$

where the empirical constant $\lambda \sim 0.15$ and z_0 is the length of the virtual origin associated with the plume source. Dimensional analysis gives the velocity of the return flow as

$$w = \frac{\mathrm{d}z}{\mathrm{d}t} = \frac{\lambda B_0^{1/3} (z + z_0)^{5/3}}{A} \tag{6.25}$$

where A is the cross-sectional area of the container, which is assumed to be much greater than the effective cross-sectional area of the plume for all values of $\hat{z}$. This is a principle requirement for the plume to possess a self-similar form, since the flow is not impeded by the boundaries of the confined region. The location of the first front as a function of time is therefore given by solution of (6.28), namely:

$$z = -z_0 + \left(\frac{1}{H^{2/3}} + \frac{2\lambda B_0^{1/3} t}{3A} \right)^{-3/2} \tag{6.26}$$

Hence, for a container of vertical height H and cross-sectional area A, the filling box time scales as

$$\tau \sim \frac{3A}{2\lambda B_0^{1/3}} \left[\left(z_0^{-2/3} \right) - H^{-2/3} \right] \tag{6.27}$$

In the limit $z_0 \to 0$, the first front takes an infinite time to reach the bottom of the container. This is because the limit represents a source of buoyancy with zero associated mass flux.

The density evolution of the mixed region produced above the first front due to the propagation of the plume is given by solution of the advection equation

$$\frac{\partial \rho_a(t,z)}{\partial \mathrm{t}} + w(z) \frac{\partial \rho_a(t,z)}{\partial \mathrm{z}} = 0 \tag{6.28}$$

The advection equation (6.31) represents a conservative system, comprising surfaces of constant density propagating with velocity w. This is readily apparent upon application of the method of characteristics. An effective technique is to therefore utilise an adaptive grid in which the grid points move with the surfaces of constant density. This method is implemented in two stages. Firstly, the plume equations are integrated from the source to the top of the container. Upon successive time steps, a new grid point is added to the topmost grid point of the domain. Secondly, the grid points from the previous time step are then moved downwards. The density profile in the environment may then be evaluated in the region above the first front.

6.3.2 The Dual-Plume Filling-Box

We now apply the method to the dual-plume filling-box system. The dimensionless equation describing the evolution of the density in the system is unchanged from §3.1, namely:

$$\frac{\partial \hat{\rho}_a}{\partial t} + \hat{u} \frac{\partial \hat{\rho}_a}{\partial x} = 0 \tag{6.29}$$

To calculate the ambient density profile as a function of time, we firstly utilise a fixed step-size fourth-order Runge-Kutta method to numerically integrate the plume equations from the horizontal boundaries of the confined region at $\hat{z} = 0$ and $\hat{z} = 1$. The plume equations are re-cast in the following form:

$$\frac{\mathrm{d}\hat{Q}}{\mathrm{d}\hat{z}} = 2\epsilon\hat{M}^{1/4} \tag{6.30}$$

$$\frac{\mathrm{d}\hat{M}}{\mathrm{d}\hat{z}} = 2\left(\hat{\rho}_a - \hat{B}\right)\hat{g}'\hat{Q}^2 \tag{6.31}$$

$$\frac{\mathrm{d}\hat{B}}{\mathrm{d}\hat{z}} = 2\epsilon\hat{\rho}_a\hat{M}^{1/4} \tag{6.32}$$

which are equivalent to equations (1.6), (1.7) and (1.8) of chapter 1. Re-writing the equations in this form makes explicit the fact that the density evolution of the two mixed layers are functions of the buoyancy fluxes associated with the the plume flows. Worster & Huppert (1983) used an approximate analytic expression to evaluate the buoyancy flux, although their method introduced small errors into the calculation. A similar technique will be described later as an means of error checking.

Initially, the location of the two fronts are set at $\hat{z} = 0$ and $\hat{z} = 1$ for the filling-box flows associated with the descending and ascending plumes respectively. The plume equations representing the ascending plume are integrated from $\hat{z} = 0$ to $\hat{z} = 1$, and the fluxes of mass, momentum and buoyancy at the top grid point $n = 100$ are evaluated. Similarly, the descending plume equations are integrated from $\hat{z} = 1$ down to $\hat{z} = 0$ and the fluxes associated with the downward-propagating plume are evaluated at the lower boundary. A key step in the application of the method is that the velocity of the two fronts are effectively independent of each other, and so a non-uniform time-scale is employed in each time step. This is defined

as

$$\mathrm{d}\hat{t} = \frac{\mathrm{d}\hat{z}}{\hat{A}\Delta\hat{Q}_T} \tag{6.33}$$

where $\Delta\hat{Q}_T$ is the total entrained volume flux associated with the plume that originates from the source which possesses the greater associated mass flux. The values of the density profile in the room and the location of the two fronts are then stored in two arrays. The velocity of each front is evaluated according to:

$$\frac{\mathrm{d}\hat{z}}{\mathrm{d}\hat{t}} = \frac{\hat{Q}_n}{\hat{A}} \tag{6.34}$$

where $\hat{Q}_n$ is the normalised volume flux of the plume flow at grid location n, and the fronts are moved up or down, respectively, a distance dependent upon their respective velocity and the magnitude of the time step. However, there are now points in both the density array and the front arrays which are consequently unknown. Linear interpolation is used to approximate these values. The interpolated values are compared with an approximate analytic solution. The interpolated values are then updated into the arrays representing the front location and the density profile. The calculation is compared with the analytical prediction as an error-check. If the error attains an unacceptable magnitude, the step is re-calculated by dividing the previous time-step up into sub-arrays of smaller resolution. This is not an adaptive technique *per se,* but an additional calculation to remove error. If the error is still relatively large after this re-calculation, an error message is flagged and the numerical routine terminates. The overall time is updated by the amount $\mathrm{d}\hat{t}$, and the process is repeated. Hence, the density profile and location of the two fronts is evaluated as a function of time over a total time T.

6.4 Results

In this section, we present some theoretical, numerical and experimental results for the time-dependent dual-plume filling-box system. Firstly, in section 6.4.1, we compare numerical results for the location of the filling-box fronts as functions of time with experimental data.

Next, in section 6.4.2, we investigate the time-dependent density evolution of the two mixed regions in the filling-box system. We present some numerical for the density evolution as a function of time. These are compared with a simple theoretical model for the time-dependent mean density profile.

We then proceed by comparing the numerical results to experimentally-obtained data for the density evolution of the system. The theoretical model is also discussed further.

6.4.1 Time-Dependent Progression of the Filling-Box Fronts

We apply the numerical technique described in section 6.3.2 to evaluate the progression of the two filling-box fronts as functions of time. The technique was applied for two cases: firstly, $z_u = 1\,\text{cm}$ and $z_l = 2\,\text{cm}$, and also for the configuration such that $z_u = 4\,\text{cm}$ and $z_l = 2\,\text{cm}$. The results are shown in figures 6.1 and 6.2.

In both cases, the numerical results are in good agreement with experimental data. The overall trend of the experimental results are well-represented by the numerical solutions. However, it may be seen that there is some scatter associated with the experimental data, which at some points is distant from the numerical results.

This is the result of error in measuring the precise location of each of the filling-box fronts. Although assumed to be sharp density jumps in theory, in

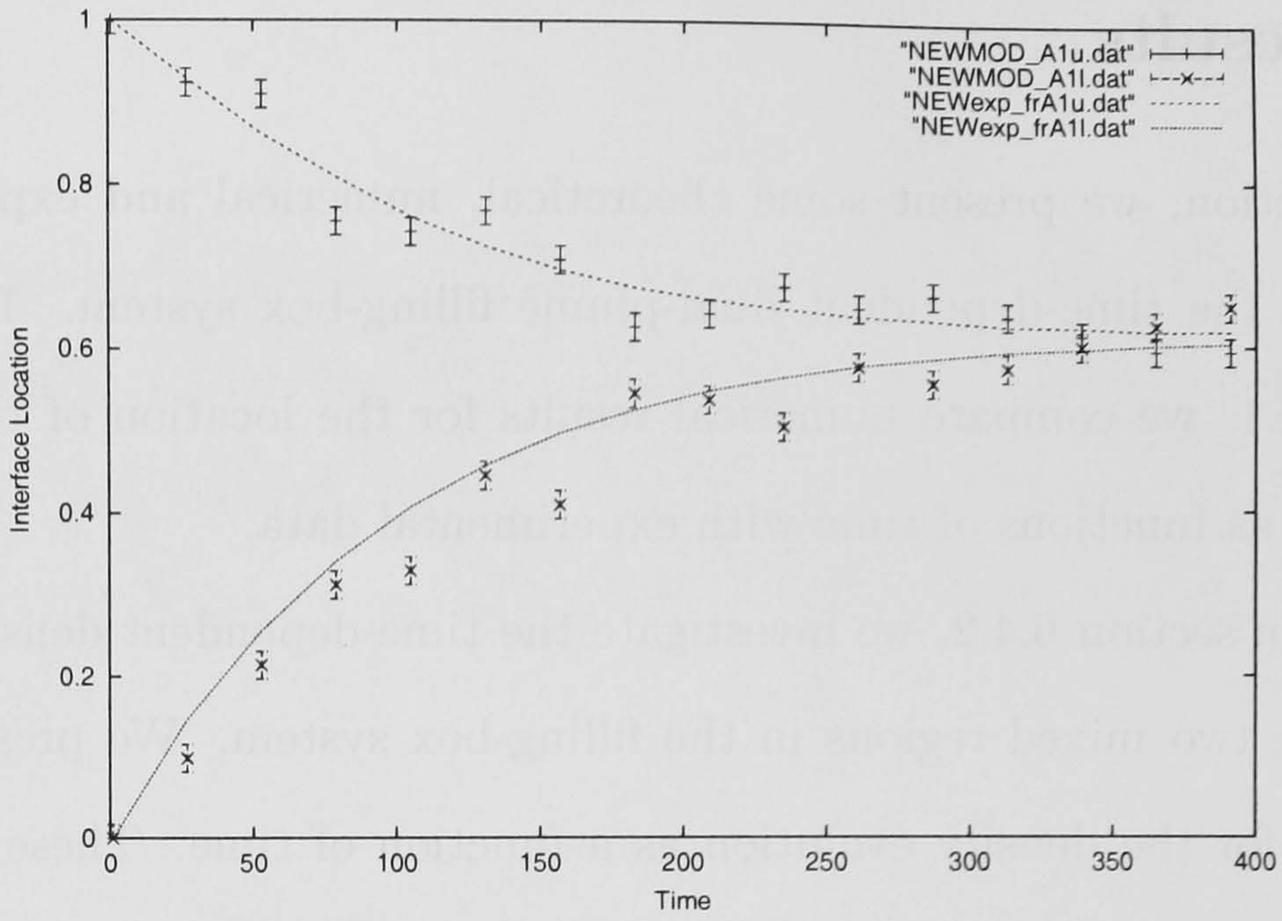

FIGURE 6.1: Comparison between theory and experiment for the propagation of the two fronts associated with the plume return flows. The experimental data is for upper and lower source displacements of 1cm and 2cm respectively. The numerical solution was obtained by assuming equivalent upper and lower virtual origin terms.

actuality the fronts themselves have a depth of a few millimetres. Further error was also due to external vibration, which tended to disrupt the location of the interface by a few millimeters. This is a frequent occurence when performing experiments with stratified fluids, due to the sensitivity of the experimental system to external vibration. This could have been rectified by performing the experiments in a room with a concrete floor, for example.

To minimise random error, a transparent grid was attached to the front of the tank. This was generated by direct manipulation of a PostScript file, and resulted in an accurate grid of 1cm by 1cm. This was found to be of assistance in obtaining much of the experimental data. Further, the fronts were measured at several points along their length and an average value taken.

In conclusion, the agreement between experimental data and numerical

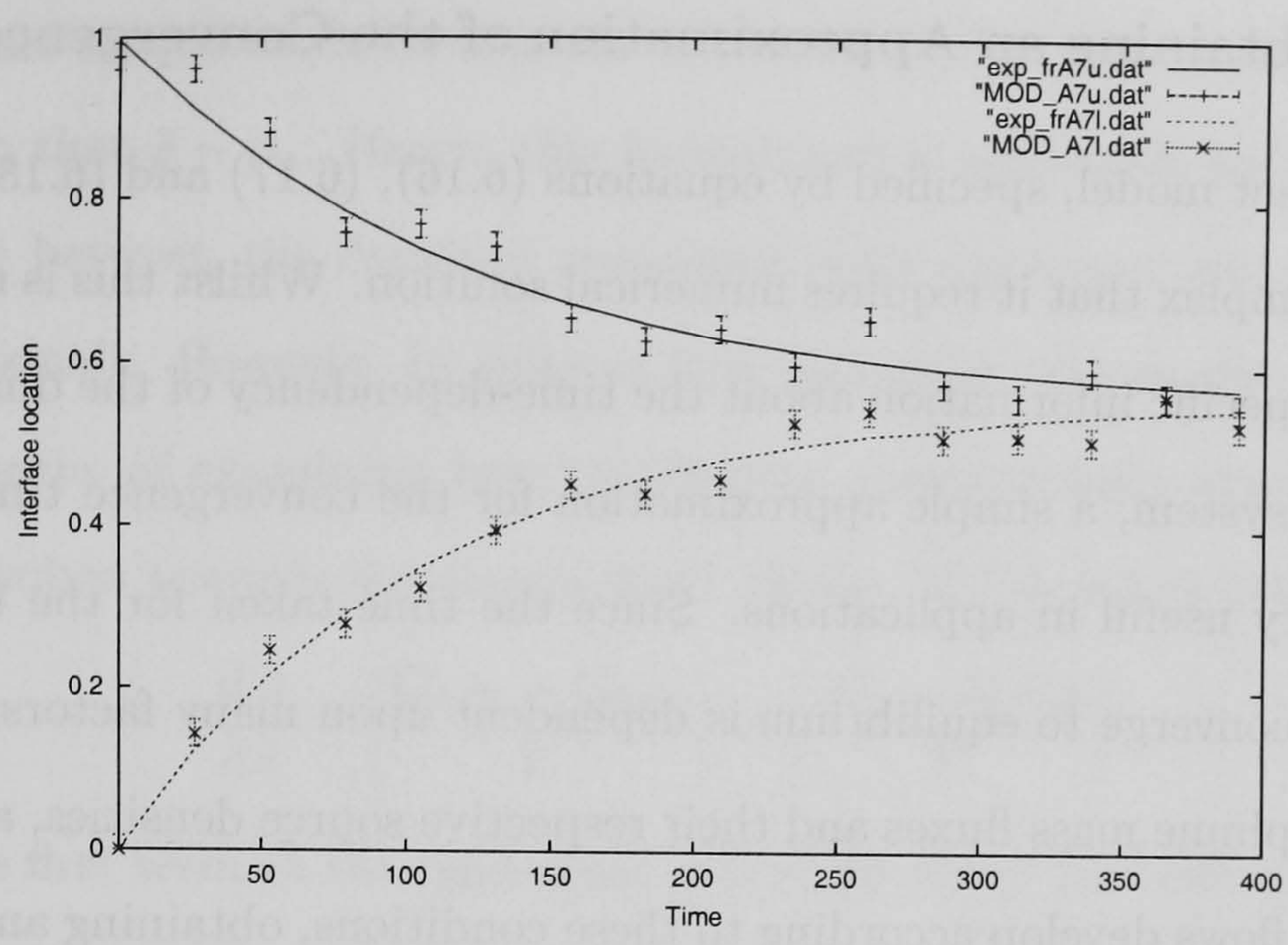

Figure 6.2: Comparison between theory and experiment for the propagation of the two fronts associated with the plume return flows. The experimental data is for upper and lower source displacements of 4cm and 2cm respectively. The numerical solution was obtained by assuming equivalent upper and lower virtual origin terms.

solution is good, with the data in acceptable overall correlation with the numerical results.

6.4.2 The Time-Dependent Density Profile

In this section, we present experimental data for the time-dependent density evolution of the dual-plume filling-box system. The experiments were performed using the displaced-source configuration used in Chapter 3. Further, $R = S$ in all cases. We then compare the experimental data to numerical results for the density profile.

It is also of interest to consider a simple theoretical model for the time-dependent evolution of the density profile. We begin by presenting some numerical results and comparing these with the mean-density model.

6.4.3 Obtaining an Approximation of the Convergence Time

The transient model, specified by equations (6.16), (6.17) and (6.18), is sufficiently complex that it requires numerical solution. Whilst this is desirable to obtain specific information about the time-dependency of the dual-plume filling-box system, a simple approximation for the convergence time would also be very useful in applications. Since the time taken for the transient system to converge to equilibrium is dependent upon many factors, such as the initial plume mass fluxes and their respective source densities, and since the plume flows develop according to these conditions, obtaining an approximation for the convergence time from dimensional analysis is not possible. It is therefore useful to be able to estimate T from another method.

In this section, therefore, we present a simple model for the evolution of the mean fluid density within the confined region. This allows us to obtain an approximate scale for the time taken for the system to converge to equilibrium. We firstly define $\bar{\rho}$ as the mean density profile of the ambient fluid in the confined region. We may then propose a simple model for the evolution of $\bar{\rho}$ as a function of time:

$$\frac{\mathrm{d}\left[\bar{\rho}\left(t\right)V\right]}{\mathrm{d}\,t} = \left[\rho_1\left(t\right) - \bar{\rho}\left(t\right)\right]Q_1 + \left[\rho_2\left(t\right) - \bar{\rho}\left(t\right)\right]Q_2 \tag{6.35}$$

where V is the total volume of fluid in the confined region. Consequently, there exists a value of $\rho_2 - \bar{\rho}$ and also a value of $\rho_1 - \bar{\rho}$ such that these parameters are independent of t. These are the steady-state values to which the system converges. We therefore have:

$$(\rho_1 - \bar{\rho})Q_1 + (\rho_2 - \bar{\rho})Q_2 = 0 \tag{6.36}$$

and hence:

$$\bar{\rho} = \frac{Q_1\rho_1 + Q_2\rho_2}{Q_1 + Q_2} \tag{6.37}$$

and so this simple model tracks the evolution of the mean density until a time such that $\bar{\rho} \sim \rho_u$. Hence, this formulation is applicable only when the difference between the densities associated with the upper and lower fluid layers is small. However, in spite of this limitation, the model provides a simple means of examining how the density approximately changes as the system evolves towards the steady-state values. We therefore have

$$\frac{\mathrm{d}\,\bar{\rho}}{\mathrm{d}\,t} = \left[\frac{Q_1\rho_1 + Q_2\rho_2}{V}\right] - \left[\frac{(Q_1 + Q_2)\,\bar{\rho}}{V}\right] \tag{6.38}$$

where the first term on the right-hand side of the above expression represents the total density flux of fluid entering via the sources in unit time and the second term on the right-hand side represents the mean flux of ambient fluid leaving the confined region via the mass sink in unit time. This follows from the global conservation of mass relation, namely that $Q_{out} = Q_1 + Q_2$. We proceed by re-writing 6.41 in terms of an appropriate integrating factor,

$$\frac{\mathrm{d}}{\mathrm{d}\,t}\left[\bar{\rho}\exp\left(\frac{Q_1 + Q_2}{V}\right)t\right] = \left(\frac{\rho_1 Q_1 + \rho_2 Q_2}{V}\right)\exp\left(\frac{Q_1 + Q_2}{V}t\right) \tag{6.39}$$

and then we arrive at the solution for $\bar{\rho}$:

$$\bar{\rho} = \left(\frac{\rho_1 Q_1 + \rho_2 Q_2}{Q_1 + Q_2}\right) - \left(\frac{\rho_1 Q_1 + \rho_2 Q_2}{Q_1 + Q_2}\right)\exp\left(-\frac{Q_1 + Q_2}{V}t\right) + \bar{\rho}_0\exp\left(-\frac{Q_1 + Q_2}{V}t\right) \tag{6.40}$$

where $\bar{\rho}_0$ is the initial mean density profile, which is equal to the density of the initial ambient fluid. We may normalise this expression as per the scalings of chapter 2 to yield

$$\bar{\rho}' = \left(\frac{S}{R+S}\right)\left[1 - e^{-(R+S)t}\right] + \bar{\rho}'_0 e^{-(R+S)t} \tag{6.41}$$

where an appropriate scale has been chosen so that $V \to 1$. Consequently, the solution implies that, as $t \to \infty$, the mean steady-state density profile is given by:

$$\bar{\rho}' \to \left(\frac{S}{R+S}\right) \tag{6.42}$$

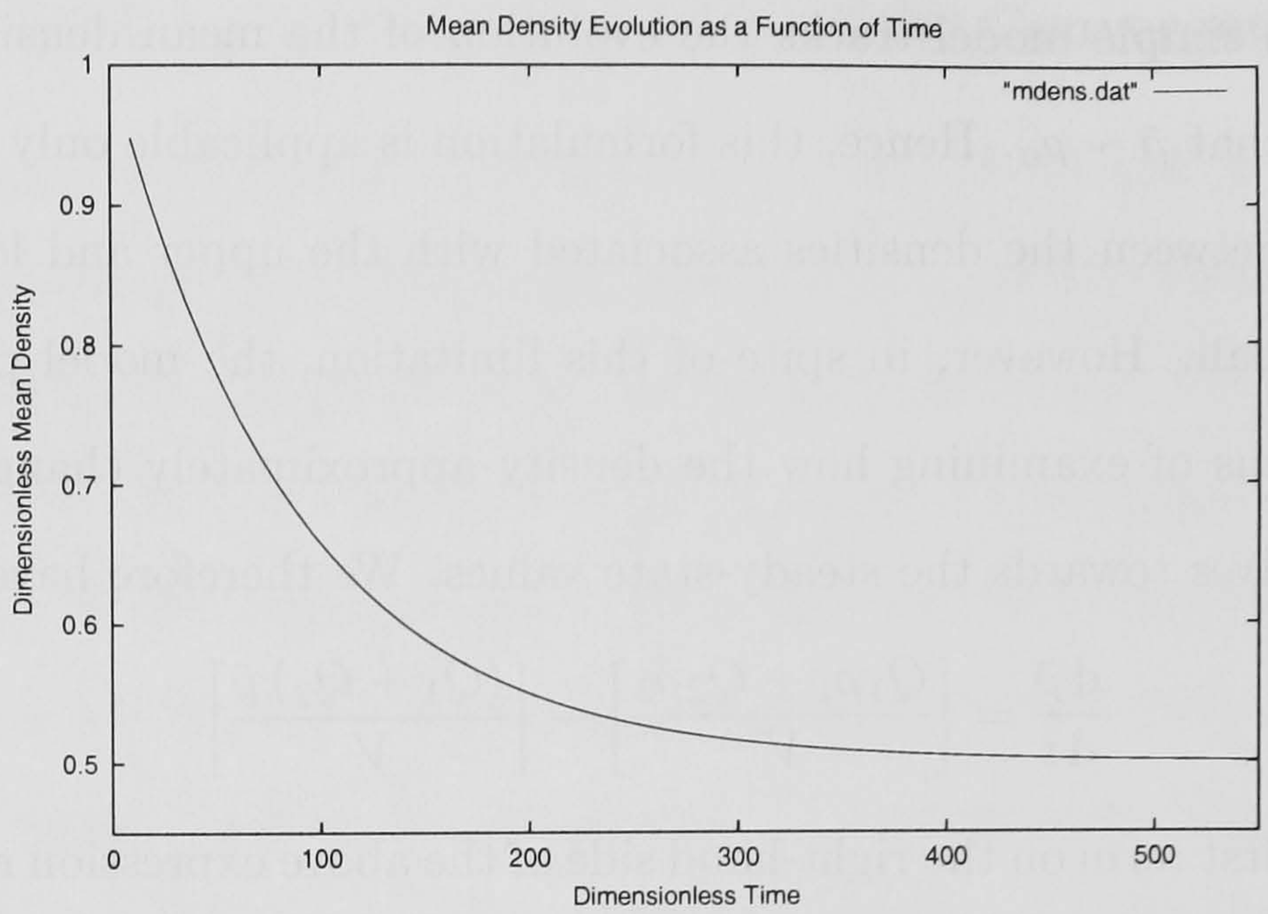

FIGURE 6.3: Mean density evolution as a function of time for the dual-plume filling-box system. The curve represents the the solution of equation 6.43 for $R = S = 0.5$ and an initial ambient density $\overline{\rho}'_0 = 1.0$.

Hence, equation (6.44) may be used to track the mean density evolution from an initial ambient density of $\bar{\rho}'_0$ to the final equilibrium value of $\hat{\rho}_u$. Consequently, this simple model provides only an approximation to the mean density, since it assumes that $\hat{\rho}_l$ is close in value to the upper-layer fluid density.

Figure 6.3 shows the time evolution of the mean density profile by using this model. The ambient fluid has an initial dimensionless density equal to 1.0, and $R = S = 0.5$. The model predicts that the system converges to equilibrium in as dimensionless time $\hat{t} = 400$.

Figure 6.4 shows the density evolution of the dual-plume steady-state system. The figure consists of the normalised relative density as a function of dimensionless height for various normalised times.

The figure shows central unmixed region, consisting of ambient fluid with relative dimensionless density 1.0. This is particularly clear for $\hat{t} = 50$, where

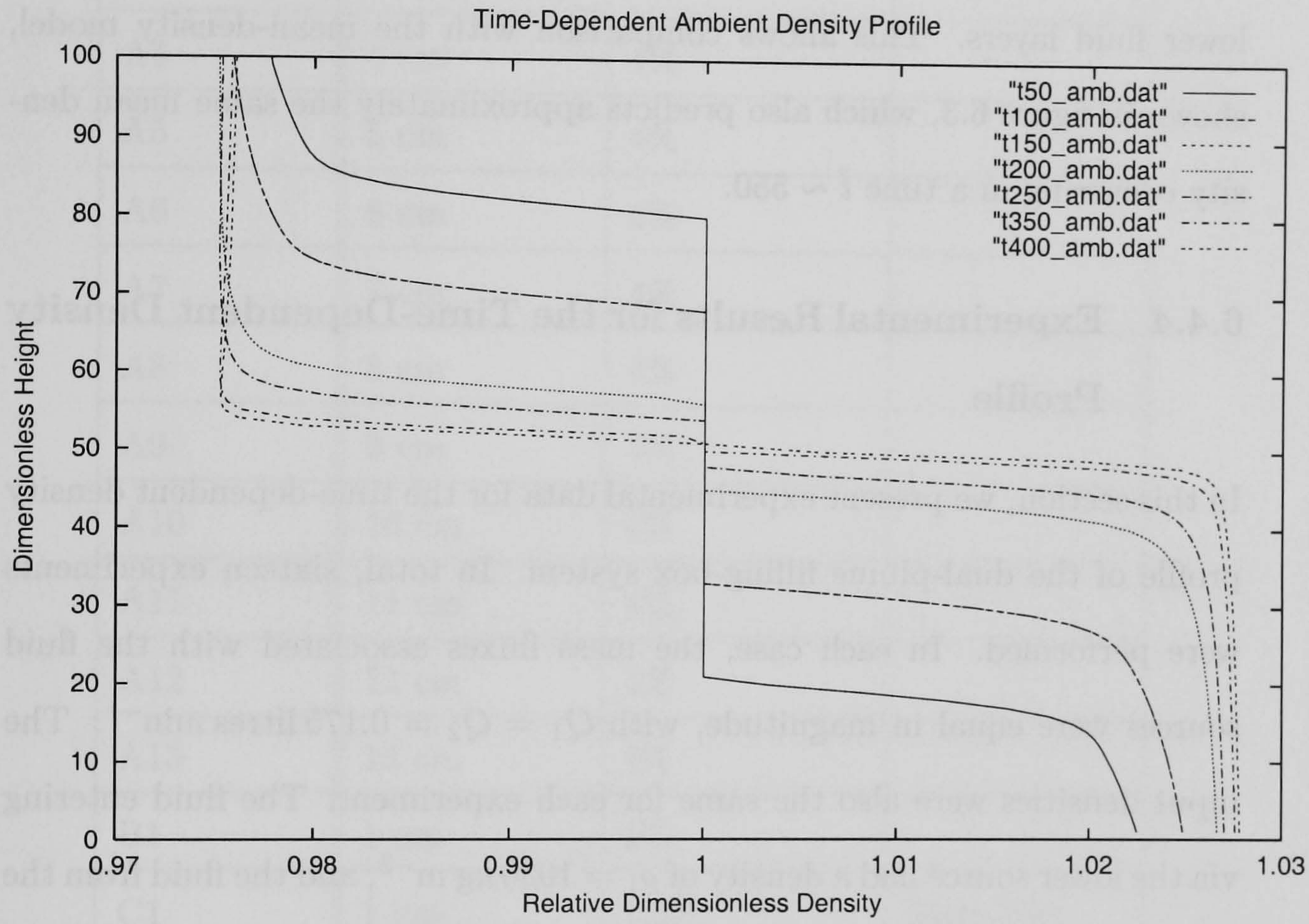

FIGURE 6.4: Results from the application of the numerical technique. Solution curves for the density profile of the ambient fluid are shown as functions of dimensionless height time. The curves represent the state of the system at dimensionless times $\tau = 50, 100, 150, 200, 250, 300, 350, 400$ The plot was obtained for the sources which possessed equal-magnitude associated mass fluxes $R = S = 0.5$. The virtual origin terms were $\hat{h}_u = \hat{h}_l = 1.0/30.0$.

the discontinuity between the unmixed fluid and the two filling-box fronts may be seen. As the dimensionless time increases, the two fronts progress through the confined region, and the density evolves towards its equilibrium values. For the initial conditions specified, convergence to steady-state occurs in $\hat{t} \sim 400$, with a small contrast in density between the upper and lower fluid layers. This allows comparison with the mean-density model, shown in figure 6.3, which also predicts approximately the same mean density occurring in a time $\hat{t} \sim 550$.

6.4.4 Experimental Results for the Time-Dependent Density Profile

In this section, we present experimental data for the time-dependent density profile of the dual-plume filling-box system. In total, sixteen experiments were performed. In each case, the mass fluxes associated with the fluid sources were equal in magnitude, with $Q_1 = Q_2 = 0.175\,\text{litres}\,\text{min}^{-1}$. The input densities were also the same for each experiment. The fluid entering via the lower source had a density of $\rho_1 = 1030\,\text{kg}\,\text{m}^{-3}$, and the fluid from the upper source $\rho_1 = 1050\,\text{kg}\,\text{m}^{-3}$. The ambient fluid had an initial density $\rho_0 = 1040\,\text{kg}\,\text{m}^{-3}$. These values give a mass flux scale as $Q_p = 4.47 \times 10^{-6}\,\text{m}^3\,\text{s}^{-1}$. Applying these scale, we have $R = S = 0.653$.

The upper source displacement was varied in the experiments. Further. the value of the initial ambient density was changed to ensure that convergence to equilibrium occurred over a different timescale. Finally, two of the experiments were repeated with the mass sink located in the floor of the tank. The purpose of this was to verify that the system has the form specified by equations (2.52) – –(2.54) in Chapter 2.

Experiment	Upper source displacement	Initial ambient density	Notes
A1	1 cm	4%	
A2	2 cm	4%	
A3	3 cm	4%	
A4	4 cm	4%	
A5	5 cm	4%	
A6	6 cm	4%	
A7	7 cm	4%	
A8	8 cm	4%	
A9	9 cm	4%	
A10	10 cm	4%	
A11	11 cm	4%	
A12	12 cm	4%	
A13	13 cm	4%	
B1	1 cm	1%	
C1	1 cm	1.5%	Mass sink in lower layer
CC1	12 cm	1.5%	Mass sink in lower layer

Figure 6.5 shows the time-dependent density profile obtained from experiment A1. The density profile is plotted at regular dimensionless time intervals $\hat{T}$, a parameter normalised by scaling with the filling-box time τ. The system converges to a two-layer configuration. Each fluid layer is well-mixed. The density of the upper layer to converges to the predicted steady-state value $\hat{\rho}_u = 0.5$. This value arises from the fact that $R = S$. We note that

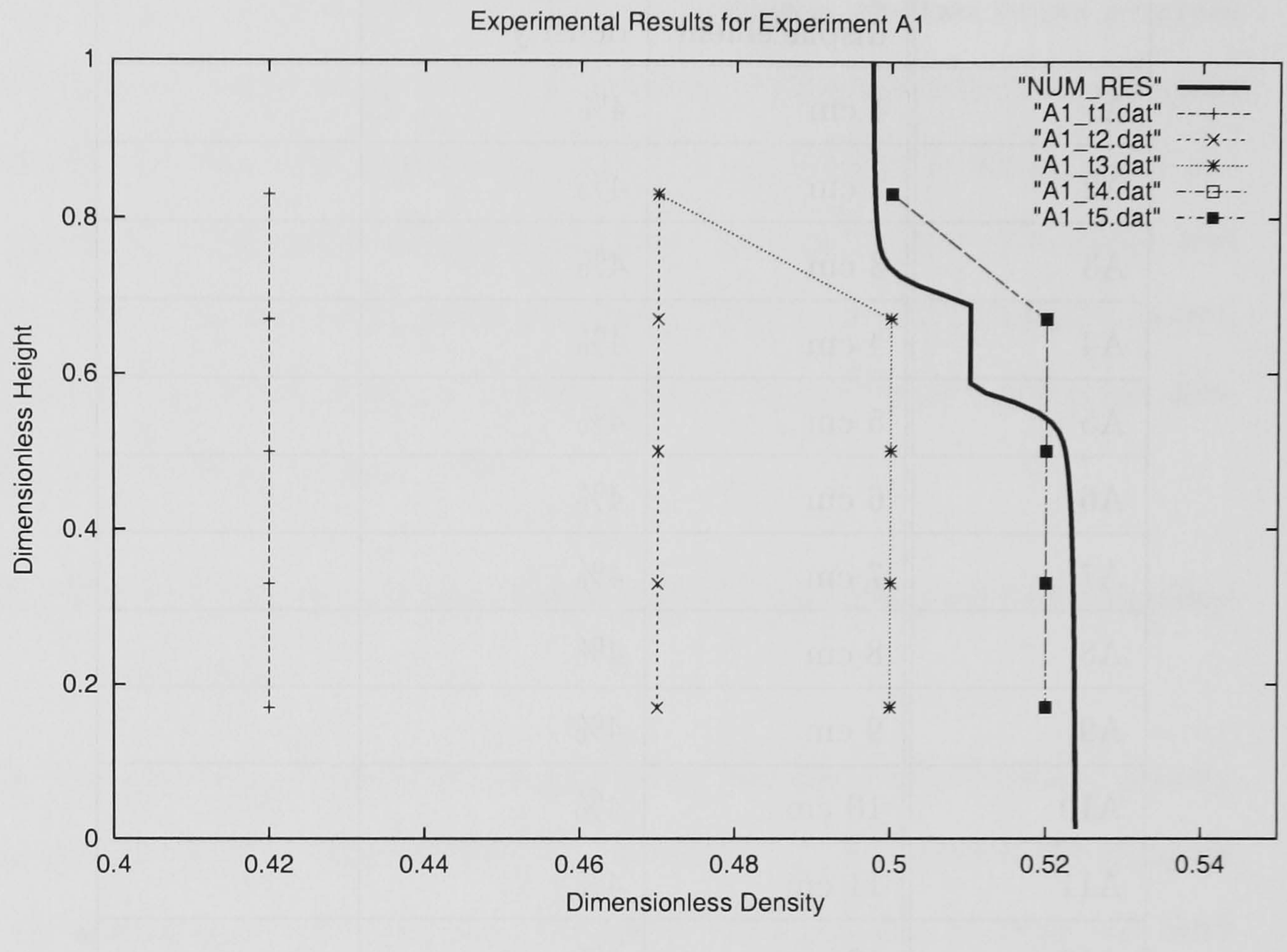

FIGURE 6.5: Time-dependent density profile of experiment A1 and corresponding numerical solutions for the density profile as functions of dimensionless time and height. The solid line represents the numerical solution for a corresponding dimensionless time $\tau = 400$.

the densities for times $\hat{T} = t_4$ and $\hat{T} = t_5$ are identical. We may conclude that the system has therefore reached equilibrium.

The bold line is the numerical solution for the density profile corresponding to $\hat{T} = t_3$. The location of the fluid interface is reasonably well-predicted by the numerical solution, but there is a margin of error in the values of the upper and lower-layer densities. In actuality, the numerical solution has converged faster than the experimental density profile, but is in good agreement with the final steady-state values.

Figure 6.6 is the experimentally-obtained time-dependent density profile

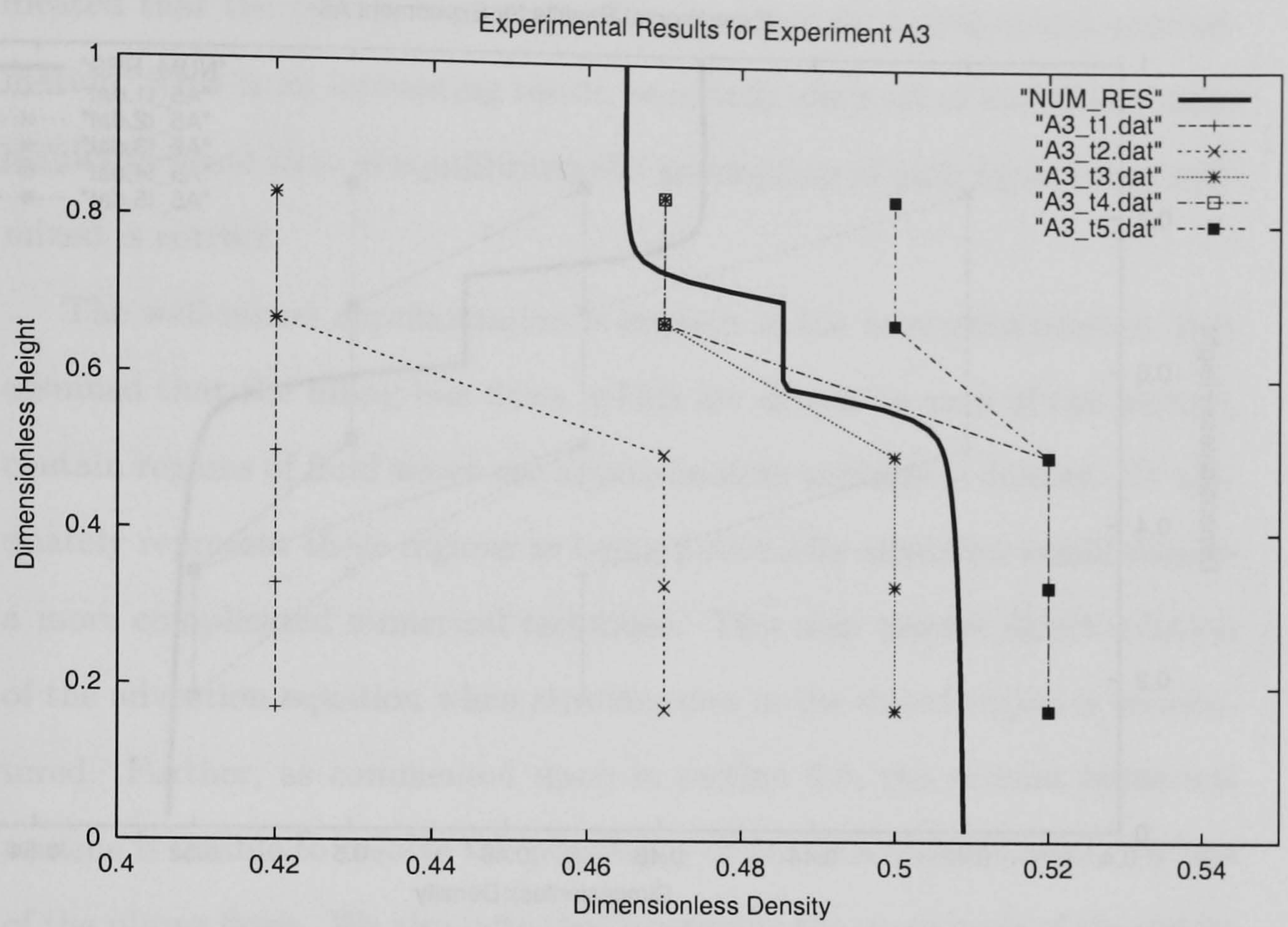

FIGURE 6.6: Time-dependent density profile of experiment A3 and corresponding numerical solutions for the density profile as functions of dimensionless time and height. The solid line represents the numerical solution for a corresponding dimensionless time $\tau = 300$.

corresponding to experiment A3. A key point to note is that above and below the interface location the fluid layers are well-mixed. However, the data for measurements located in the region of the interface, at $\hat{z} \simeq 0.5$ and $\hat{z} \simeq 0.65$ shows a slight density gradient. However, the agreement between the numerical solution and the experimental data is again reasonable. Figure 6.7 shows the time-dependent density profile obtained from experiment A5. It is clear in this figure that there are gradients in the density profile. The numerical solution, however, still predicts two distinct layers separated by a density discontinuity. There is considerable disagreement between the

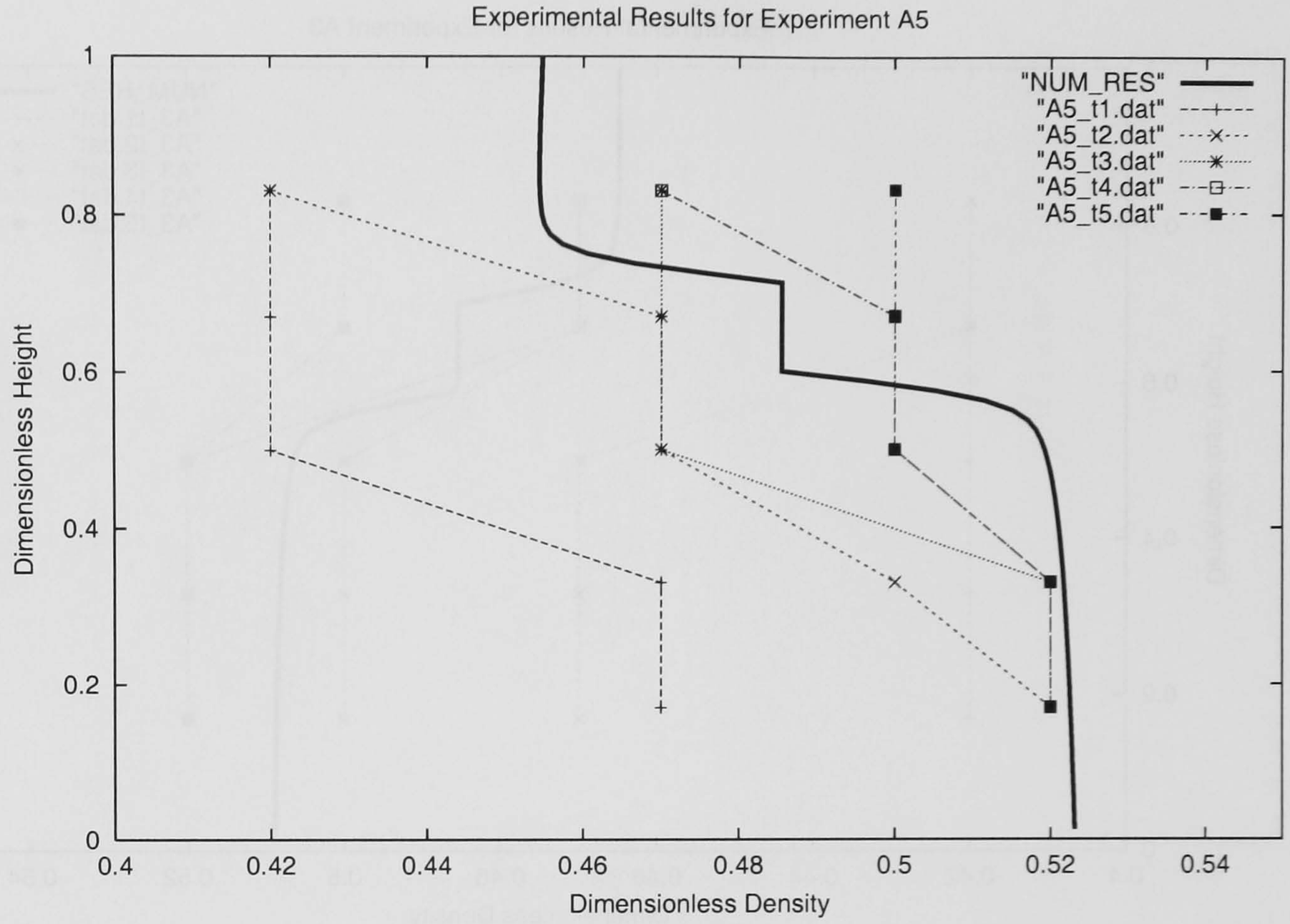

FIGURE 6.7: Time-dependent density profile of experiment A5 and corresponding numerical solutions for the density profile as functions of dimensionless time and height. Note the slight stratification present in the density profile. The solid line represents the numerical solution for a corresponding dimensionless time $\tau = 350$.

numerical solution and the experimental data for $\hat{T} = t_4$. However, the system still converges to equilibrium with the predicted values of the upper and lower layer fluid densities. Further experimental work indicated two key points. Firstly, for all the experiments performed throughout the course of the work, the dual-plume filling-box system eventually converged to steady-state. The equilibrium values of the upper-layer density were particularly convenient to compare with the experimental values, and the predictions were in excellent agreement with the empirical results.

The second point concerns the well-mixed approximation. As the mag-

nitude of the upper-source displacement was increased, the experiments indicated that the system was not well-represented by a well-mixed approximation. This is an interesting result, especially since all of the steady-state results indicate that in equilibrium the assumption of each layer being well-mixed is correct.

The well-mixed approximation is implicit in the numerical routine. It is assumed that the filling-box flows, which are driven by each of the plumes, contain regions of fluid which are approximately uniform in density. To adequately represent these regions as being potentially stratified would require a more complicated numerical technique. This may involve direct solution of the advection equation when stratification in the mixed region is encountered. Further, as commented upon in section 6.5, the present numerical routine is unable to resolve the possibility of fountain-like behaviour by one of the plume flows. We also note that increasing the magnitude of the source displacements seems to increase the occurrence of density gradients. However, experimental observations suggest that increasing the source displacements alone does not produce a density profile exhibiting density gradients more severe than that seen in figure 6.7 for experiment A5.

In concluding this section, it is seen that for relatively small source displacements the numerical routine is in good agreement with the experimental values of the density profile. There is some discrepancy, however, between the empirical and numerical density profiles in terms of the density as a function of time. However, the same program produces very good overall agreement with the location of the filling-box fronts as a function of time.

6.5 Dynamics associated with the propagation of a turbulent fountain

It was seen in sections 6.3 and 6.4 that the results of the numerical method are in good agreement with experimental data for the lower-layer density and the location of the fluid interface. However, all of these results relate to the case for which $R = S$. If we recall the parameter $R* = R/(R+S)$, defined in Chapter 2, we find that the numerical routine is insufficient to evaluate cases for which $R \to 0$ or $R* \to 1$. In this section, we explain the limitations of the numerical technique with reference to experimental observations.

Let us consider the case $R* \simeq 0.1$. In this situation, the mass flux associated with the upper source is relatively large. Suppose further that the input density of the descending plume is also relatively large, for example an aqueous saline solution of 5% concentration compared to an ambient with 1%. Since S is large, the fractional dilution associated with the plume is small, and it arrives at the lower boundary relatively undiluted. Hence, within a short time of commencing the experiment, we expect that a layer of dense fluid would form at the lower boundary of the confined region.

For certain values of R, the ascending plume would entrain a relatively large amount of the dense fluid from the lower layer. This was found to be the case when $R* \to 0$. The ascending plume possessed enough initial momentum flux to progress vertically through the container, past the interface. However, at this point, it was actually a negatively buoyant jet. This was apparent with careful observation of the experiments, which were videotaped using a shadowgraph in conjunction with a high-quality video camera. Observations showed the ascending plume did not reach the top of

the container, and distributed a flux of volume over an area as it flowed in the fountain phase. This redistribution of buoyancy significantly changes the dynamics of the filling-box system since it implies that the fountain creates an intermediate-level stratification.

Further, it may also be possible for one of the plumes to become trapped by the resulting stratification (see, for example, Cardoso & Woods, 1993). These physical effects violate one of the fundamental assumptions of the model, namely that each layer is well-mixed to leading order. However, it was found that in every experimental case, the filling-box system eventually adjusted itself so that two approximately well-mixed layers formed and convergence to steady-state was consequently achieved.

During the fountain phase, however, the numerical technique could not resolve the fluid mechanics of the fountain. In these cases, the numerical solutions of the system of differential equations returned function values that could not be resolved by the interpolation method. Although the Runge-Kutta methods are generally viable for differential equations with discontinuities, the adaptive grid method was unable to deal with the distribution of density over an area. Hence, the program based upon the numerical technique simply halted. It did, however, predict approximately when the fountain effect occurred, compared to experimental observation. However, in the form used to obtain the numerical solutions presented in this Chapter, the program would be inappropriate to use as a predictor of the precise initial conditions required to create the fountain effect or its duration.

The relatively dense fluid associated with the plume was distributed over an area rather than being advected to the upper fluid layer. Such a redistribution of relatively dense fluid mass in the upper region of the container was found to significantly influence the transient stage of the dual-

plume filling-box evolution. Essentially, the approximation that the total buoyancy associated with the plume as it crosses the boundary is mixed into the layer that the plume flow terminates in is no longer valid in the case of the fountain flow.

Further, the approximation that each of the two buoyant fluid layers are well-mixed to leading order was also not applicable. This is due to the fact that the redistribution of relatively dense fluid by the fountain creates a stratified region to form in the container. The assumption of a weak stratification is not applicable in this case.

However, extension of the current numerical technique to such cases is quite complex. Quantification of the filling-box processes associated with turbulent fountains represents relatively recent research (see chapter 1 for more details), particularly in the case of initially-stratified ambient fluid. The physics of a system consisting initially of a fountain and a plume, in a dual-source filling-box configuration, have not yet been studied. In the present work, the principal complication added the fountain flow is the distribution of relatively dense fluid over a region with a substantial area. This presents a problem in modelling the resulting flow due to the lack of self-similarity and application of direct scaling techniques. In principle, however, one could progress by extrapolating from the experiments sets of initial conditions which caused the fountain to manifest. These could be used in a more rigorous numerical technique to obtain appropriate solutions of the advection equation (7.31), such as a finite-difference scheme. This approach would be preferably to say, a finite-element technique due to the increased complexity of the latter, or the implementation of a spectral method since such numerical routines do not work well when discontinuities are present.

6.6 Venting Below The Ceiling

In this section, we return to the question posed at the end of chapter 2, namely, what are the effects upon the transient system if the outflow vent is located in one of the vertical boundaries rather than the ceiling of the container? It was concluded that if the steady-state system still comprised two well-mixed fluid layers for the case of a mass sink located upon the a side-wall, the global and local equations for mass and buoyancy conservation were unchanged. The system was therefore identical to the canonical model. Our principal investigation in this section will therefore be to analyse the effect of venting below the ceiling upon the evolution of the transient dual-plume filling-box system.

6.6.1 Theory

Consider first a single-plume filling-box ventilated above the floor. The system is driven by a positively-buoyant ascending plume. A downward-propagating first front arises due to the return flow associated with volume flux of the plume at the top of the confined region.

The return flow experiences a discontinuity upon passing the location of the mass sink. This is apparent upon considering a control volume consisting of a horizontal surface below the ventilation opening, coupled with the upper part of the closed room, above this horizontal surface. Consequently, the net flux through this surface is zero.

We now need to extend the above analysis to the transient dual-plume filling-box system. We firstly consider the case such that the mass sink is located in one of the vertical boundaries. Further, we assume that the vent is located in the upper half of the container, namely at a vertical height greater than $\hat{H}/2$. We may then impose the condition that only the return

flow associated with the ascending plume will experience a discontinuity upon passing the outflow vent. Such a restriction assumes that, in steady-state, the interface will be located below the mass sink. Further, we need only initially concern ourselves with a time-scale $0 < t < T$, where T is the time taken for the two fronts to meet. Taking downward-propagating velocities as being positive, the speed of the first front associated with the ascending plume is given by

$$w = \frac{Q_a}{A} \tag{6.43}$$

where Q_a is the volume flux of the ascending plume at a height $z = H$ and A is the cross-sectional area of the confined region. The above expression is valid only when the return flow is above the mass sink, so is only true initially. When the descending front reaches the location of the mass sink, its velocity is given by

$$w_v = \frac{Q_a - Q_o}{A} \tag{6.44}$$

where global mass conservation gives $Q_o = Q_1 + Q_2$. Hence, the possibility exists that if $Q_a = Q_1 + Q_2$, the front will halt its descent at a vertical height equal to z_o, the location of the outflow vent. In this situation, no such restriction is placed upon the return flow associated with the descending plume, and hence this front will rise to meet the other discontinuity. In this situation, the interface location will be at $z = z_o$. However. the lower fluid layer will end just below the outflow vent so that the system is still asymmetric with regards to the mass sink.

In the case for which $Q_a \neq Q_o$, the descending front continues past the location of the outflow vent. However, the velocity of propagation associated with this return flow will be reduced upon passing the location of the mass sink. Therefore, locating the the outflow vent in the vertical boundary will have the effect of raising the location of the fluid interface. This is

because the reduction in velocity of the descending front will cause it to meet the ascending front further up the container. Therefore, we may form the dimensionless parameter ξ, defined according to

$$\xi = \frac{Q_1 + Q_2}{Q_a} \tag{6.45}$$

to estimate the effect of the sink upon the steady-state flow. Hence, when $\xi = 1$, the interface is located at the mass sink. Typically, however, $\xi < 1$, and hence the smaller the magnitude of the parameter, the less that the interface will be displaced vertically upwards from the canonical case of a vent located in the upper boundary.

In conclusion, the argument presented in chapter 2 is only valid for a relatively small value of ξ. One may not infer by examining the steady-state case the precise effects of venting below the ceiling upon the overall development of the dual-plume filling-box system.

6.7 Conclusions

A model has been derived to describe the evolution of the dual-plume filling-box system from a specified set of initial conditions through its subsequent development to its final steady-state.

The model is numerically solved by an improved method based upon an algorithm first applied by Germeles (1975). The technique involves integrating the plume equations to calculate the magnitudes of the return flows associated with each plume.

The method of characteristics applied to the advection equation allows the density in the well-mixed region behind each front to be evaluated. The dependence of the progression of the two fronts upon the mass fluxes associated with the sources is also examined. The numerical results are in

good agreement with the experimental data for both the location of the fluid interface and the densities associated with each fluid layer.

It was found that the numerical routine was insufficient to resolve the situation whereby one of the plumes acquired the characteristics of a turbulent fountain. The effect of this, deduced from experimental observations, was a redistributed of buoyant fluid over a wide region. This greatly complicated the fluid mechanics of the system. However, it was observed that the dual-plume filling-box did always converge to steady-state equilibrium.

Finally, the effects upon the transient system of venting below the ceiling were discussed. It was found that such a configuration could have a significant effect upon the development of the final equilibrium state. This was principally affected the location of the fluid interface.

Part V

Conclusions

"To keep a drowsy emperor awake;

Or set upon a golden bough to sing

To lords and ladies of Byzantium

Of what is past, or passing, or to come. "

– William Butler Yeats, *Sailing to Byzantium*

The fluid mechanics of a particular class of turbulent buoyant fluid flows propagating in a confined region has been extensively investigated. During the course of the present work, we have examined the consequence of sources which possess non-zero associated fluxes of mass upon the overall dynamics of each system. These effects have shown several novel features which have not been previously investigated.

A model of the filling-box system driven by two plumes of opposite buoyancy was derived for the steady-state regime. The effects of plume sources which feature significant associated fluxes of fluid mass were investigated. The system possessed an internal asymmetry which was dependent upon the vent via which fluid mass flowed out of the confined region. The resulting algebraic equations specifying the dimensionless interface location between the two well-mixed fluid layers, and the density associated with each of these layers, were solved numerically as functions of the source mass fluxes. It was found that for a system with the outflow vent located in the upper fluid layer, the density of the top layer was constant for a given value of the normalised source mass fluxes. It was further shown that the lateral drift associated with the flow of mass through the system has a negligible effect upon the vertical propagation of each of the turbulent plumes. The model was applied to the physical situation of ventilating a confined region

subject to U.K. health and safety guidelines.

The canonical dual-plume filling-box model of chapter 2 was extended to consider plume sources which are effectively two-dimensional. A system that was driven by a combination of two such line plumes was investigated. It was found that the effect of such a system was to translate the solution curves when compared with the canonical model. A further system, consisting of a hybrid combination of a line plume and an axisymmetric plume was then studied. Finally, this system was used to examine and compare the mechanics of entrainment that occur for a line plume and an axisymmetric plume.

Global quantities associated with the system were investigated experimentally in the steady-state regime. The model of chapter 2 was extended to consider sources that were located a vertical distance away from the upper and lower boundaries of the confined region. The numerical method of chapter 2 was extended to investigate the implications of source displacement with regards to the location of the fluid interface and the densities associated with each fluid layer. The numerical solution was seen to be in good agreement with the experimental results. Further, the tendency of the the lower source displacement to greatly influence the system was noted. This was substantiated with the calculations of chapter 6. The additional asymmetry in the source displacements was explained in term of the location of the mass sink.

The canonical model of Chapter 2 was applied directly to the situation of natural ventilation of a confined region. A second mass sink was provided in the lower boundary. A simple model was applied to predict whether there would be an exchange flow with the external ambient fluid, or whether the flux of mass through the system would be one-way. In both cases, the

models were solved to find the steady-state configurations in terms of the mass fluxes associated with the plume sources. In the case of a system which admitted exchange-flow behaviour, it was assumed that the external ambient was quiescent. However, this condition was later relaxed, and a simply model applied to predict the effect of external wind propagating in the opposite direction to the flow of mass via the upper vent. A simple stability calculation was performed to show how the density distribution in the room was affected.

The transient was regime was investigated for the flow configuration presented in chapter 2. It was shown that the time-dependent model reduced to the steady-state system in the limit $t \to \infty$. The model was solved numerically by an extension of a technique which relied upon simple analysis of the advection equation. A simple model for the exponential density distribution was also derived and showed good agreement with experimentally-derived results for the density profile. The convergence to steady-state for all physically-applicable values of the source mass fluxes was also proved. Finally, the influence of the location of the mass sink a vertical distance below the upper boundary upon the subsequent development of the steady-state model was noted and discussed. This was found to be consistent with the experimental and numerical results of Chapter 3.

Part VI

References

BAINES, W.D. 1975 Entrainment by a plume or jet at a density interface. *J. Fluid Mech.* **68**, 309–320.

BAINES, W. D. & TURNER, J. S. 1969 Turbulent buoyant convection from a source in a confined region. *J. Fluid Mech.* **37**, 51–80.

BAINES, W.D., TURNER, J.S., CAMPBELL, I.H. 1990 Turbulent fountains in an open chamber. *J. Fluid Mech.* **212**, 557–592.

BALL, F.K. 1960 Control of inversion height by surface heating. *Q. J. R. Met. Soc.* **86**, 483–494.

BLOOMFIELD, L.J. & KERR, R.C. 1999 Turbulent fountains in a confined stratified environment. *J. Fluid Mech.* **389**, 27–54.

BRYAN, K. 1969 A numerical method for the study of the circulation of the world ocean. *J. Comput. Phys* **4**, 347–371.

COOPER, P. & LINDEN, P. F. 1996 Natural ventilation of an enclosure containing two buoyancy sources. *J. Fluid Mech.* **311**, 177–192.

CARDOSO, S.S.S, & WOODS, A.W. 1993 Mixing by a turbulent plume in a confined stratified region. *J. Fluid Mech.* **250**, 277–305.

DEARDORFF, J.W. 1966 The counter-gradient heat flux in the lower atmosphere and in the laboratory. *J. Atmos. Sci.* **23**, 503–506.

ELLISON, T.H., & TURNER, J.S. 1959 Turbulent entrainment in stratified flow. *J. Fluid Mech.* **6**, 423–448.

GERMELES, A.E. 1975 Forced plumes and mixing of liquids in tanks. *J. Fluid Mech.* **71**, 601–623.

HUNT, G.R. & LINDEN, P.F. 1996 The natural ventilation of an enclosure

by the combined effects of buoyancy and wind. ROOMVENT '96: *The 5th International Conference on Air Distribution in Rooms* **3**, 239–246.

HUPPERT, H.E. & TURNER, J.S. 1981 A laboratory model of a replenished magma chamber. *Earth Planet. Sci. Lett.* **54**, 144–152.

KILLWORTH, P.D. & TURNER, J.S. 1982 Plumes with time-varying buoyancy in a confined region. *Geophys. Astrophys. Fluid Dynamics* **20**, 265–291.

KUMAGAI, M. 1984 Turbulent buoyant convection from a source in a two-layered region. *J. Fluid Mech.* **147**, 105–131.

LINDEN, P. F. 1973 The interaction of a vortex ring with a sharp density interface: a model for turbulent entrainment. *J. Fluid Mech.* **60**, 467–480.

LINDEN, P. F., & COOPER, P. 1996 Multiple sources of buoyancy in a naturally ventilated enclosure. *J. Fluid Mech.* **311**, 177–192.

LINDEN, P. F., LANE-SERFF, G. F., & SMEED, D. A. 1990 Emptying filling boxes: the fluid mechanics of natural ventilation. *J. Fluid Mech.* **212**, 309–335.

MANINS, P.C. 1979 Turbulent buoyant convection from a source in a confined region. *J. Fluid Mech.* **91**, 765–781.

MORTON, B.R., TAYLOR, & G.I., TURNER, J.S. 1956 Turbulent gravitational convection from maintained and instantaneous sources. *Proc. R. Soc. Lond. A* **234**, 1–23.

MORTON, B.R. 1959 Forced Plumes. *J. Fluid Mech.* **5**, 151–163. TURNER, J.S. 1986 Turbulent entrainment: the development of the entrainment assumption, and its application to geophysical flows. *J. Fluid Mech.* **173**,

431–471.

TURNER, J.S. & CAMPBELL, I.H. 1986 Convection and mixing in magma chambers. *Earth Sci. Rev.* **23**, 255–532.

WELLS, M.G., GRIFFITHS, R.W., TURNER, J.S. 1999 Competition between distributed and localized buoyancy fluxes in a confined volume. *J. Fluid Mech.* **391**, 319–336.

WORSTER, M.G., HUPPERT, H.E. 198X Time-dependent density profiles in a filling box. *J. Fluid Mech.* **132**, 457–466.

TURNER, J.S. & GUSTAFSON, L.B. 1978 The flow of hot saline solutions from vents in the sea floor - some implications for exhalative massive sulphide and other ore deposits. *Econ. Geol.* **73**, 1082–1100.